Horizontal Gene Transfer in Bacterial Co-Cultures in Micro-fabricated Environments

by

Cait Costello

A thesis submitted to

The University of Birmingham

For the degree of

DOCTOR OF PHILOSOPHY

School of Chemical Engineering

The University of Birmingham

January 2012

Acknowledgments

There are many people I would like to thank for their help and support during the 3 years of my research and the writing up of my thesis

First of all, I would like to thank my main supervisor, Dr Paula Mendes, for three years of unrelenting support and encouragement during my PhD. Not only did Paula always have the door open any time of the day for a quick chat or to look over data, she also taught me how to be a researcher, taking an interest in my future career as well as teaching me all about the different aspects of research. I consider Paula to be a great role model for the future, and I hope some day to have a career as great as hers.

I would also like to thank my second supervisors, Professor Chris Thomas and Dr Jan Kreft. Their intelligent and constructive comments at group meetings breathed new life into my research when things got tough, and individually I have learnt a lot from both of them, and I hope to take these lessons forward in my future career.

Next I would like to thank Dr Paul Yeung, for taking me under his wing in the lab when I first started, and teaching me with patience once he realised I had very little experience with surface chemistry and miniaturisation techniques, and for being a dear friend.

Many thanks must also go to members of the Mendes group past and present, namely Dr Frankie Rawson, Dr Parvez Iqbal, Dr James Bowen, Scott Charlesworth, Alex Stevenson-Brown, Marzena Allen, Oliver Curnick, Minhaj Lashkor and Alice Pranzetti. Their friendship, advice and support helped me sail through my PhD. Thanks also to the members of Chris Thomas' group in Biosciences, for always helping me out in the times that I worked in their labs

I would also like to thank my past students who have contributed long hours in the lab to help yield the results in this project, namely Victoria Sailsbury, Manoj Dhagra, Ashley Price, Daniel Hammes and Eric Pitheakley.

Thanks t my best friend, Michaela Lock, for her early morning wake-up calls after late nights in the lab, her support and friendship throughout university to the end of my PhD, and for being my rock through hard times.

Finally, I would like to thank my parents Patrick and Marion Costello, for all their sacrifices that have let me be where I am today. Always at the other end of the phone with advice and support (namely financial!), for their lessons throughout life that have helped me enormously in my PhD. I hope I did you proud.

Abstract

In recent years, the majority of research on surface patterning, as a means of precisely controlling cell positioning and adhesion on surfaces, has focused on eukaryotic cells. Such research has led to new insights into cell biology, advances in tissue engineering, and cell motility. In contrast, considerably less work has been reported on tightly-controlled patterning of bacteria, despite its potential in a wide variety of applications, including fabrication of *in vitro* model systems for studies of bacterial processes such as quorum sensing and horizontal gene transfer. We report a rapid and convenient method to generate patterned bacterial co-cultures using surface chemistry to regulate bacterial adhesion and lift-off patterning for controlling cellular positioning at the surface.. A mannoside-terminated SAM formed an adhesive surface for bacterial monolayer formation, allowing fabrication of patterned regions using a subtractive microcontact printing process with a hydrogel stamp. The patterned substrates were subsequently inoculated with a second strain of bacteria from solution which deposited onto the unpatterned regions, forming a robust micropatterned co-culture, providing platforms for spatially controlled studies of conjugation between donor and recipient bacterial cells. Towards this aim, donor cells were transformed with a modified conjugative plasmid that would bind fluorescent molecules and become visible upon entering a recipient cell. We discovered during the course of the project that bacterial co-cultures on metal surfaces exhibit slower growth rates than on semi-solid agar, and as such the time scale required for efficient conjugation lead to photobleaching of fluorescent foci. However, we were able to demonstrate through cultivation techniques that conjugation could occur in these micropatterned co-cultures after three hours.

Contents

Chapter 1: Introduction

Abstract: *This chapter will provide background information to the project in the form of a review of the various principles and mechanisms of conjugation, bacterial adhesion and controlling the spatial arrangement of bacterial cells on the single-cell level. This is then followed by the PhD objectives.*

1.1 Horizontal Gene Transfer

1.1.1 Overview

Horizontal Gene Transfer (HGT) is the non-parent to offspring spread of genetic material from donor and recipient bacterial cells[1]. HGT involves mobile genetic elements (MGE's) including bacterial plasmids, bacteriophages and transposons that can be integrated into the host chromosome, via transduction (bacteriophages), transformation (uptake of 'naked DNA' from the environment) or conjugation (cell to cell).

Transduction (**Fig 1.1 a**) is bacteriophage (virus) mediated lateral transfer of DNA between bacterial cells[2], and is responsible for the acquisition of new genetic traits in many natural systems, including marine and soil environments[3], as well as providing a useful tool for microbial genetics in the lab. Unlike conjugation, it does not require bacterial cell-cell contact. Bacteriophages can infect bacterial cells by injecting their DNA into the cytoplasm. The host's molecular machinery will then replicate the viral DNA, expressing its proteins and reproducing the phage by packaging the DNA into viral capsids, followed by bacterial lysis, releasing the viral progeny, which can subsequently infect other bacterial cells. Transduction can be generalised or specialised; generalised transduction occurs when random fragments of the host chromosome are packaged into viral capsids instead of viral DNA - the resulting phage could infect another bacterial cell, but no replication can occur. However, the DNA from the donor cell

can be integrated into the recipient host genome[4]. Specialised transduction occurs when viral DNA is incorporated into the host chromosome, where it can remain for long periods of time. Upon excision from the host chromosome, a specific part of the bacterial genome can become packaged along with the viral DNA. If the recipient bacterium survives infection, the specific bacterial segment from the donor can be incorporated into its genome, allowing acquisition of new genes[5]. Transduction is a specific process, as bacteriophages have limited host range, yet they are abundant in nature and so are important HGT vehicles.

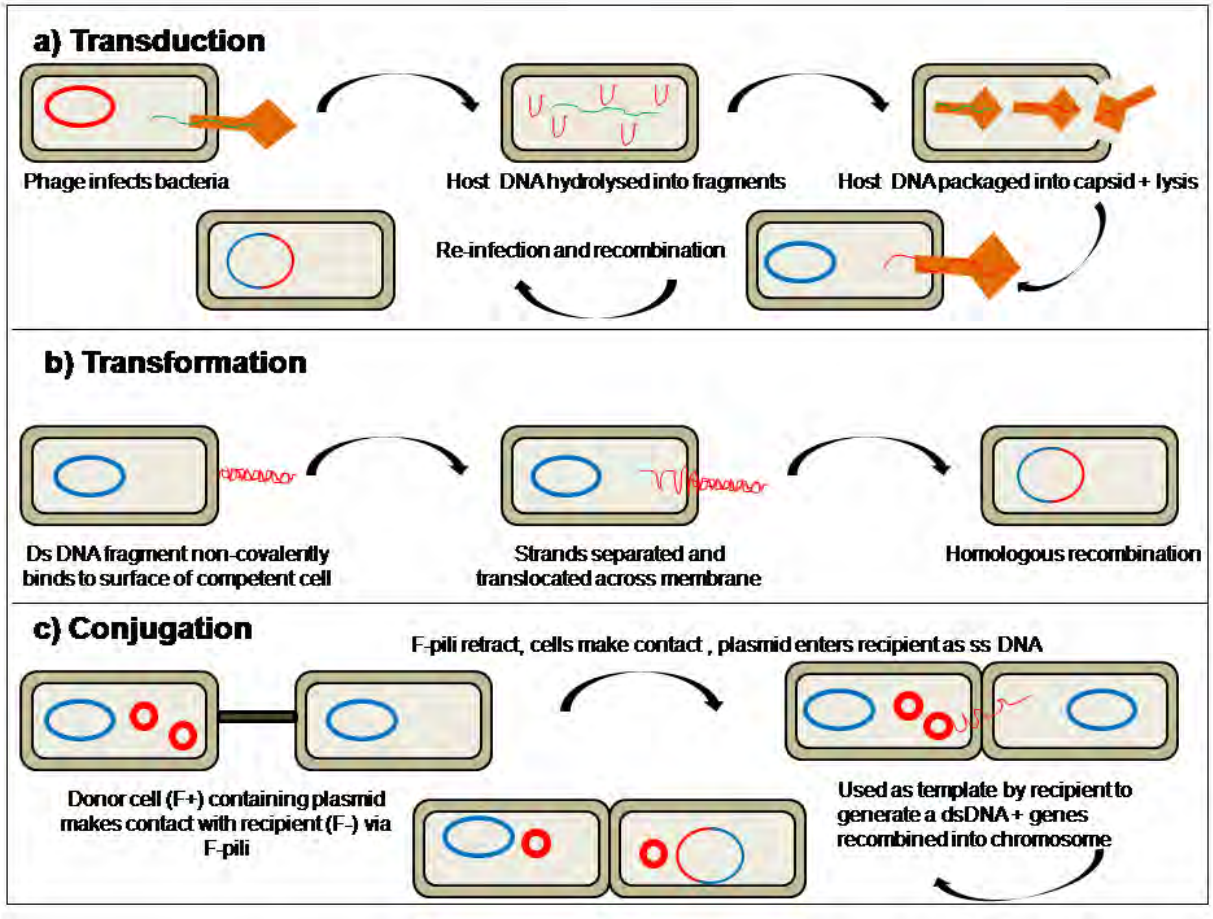

Fig 1.1: Schematic representation of the three mechanisms of HGT

For natural transformation (**Fig 1.1 b**) to occur, bacterial cells must first be in a state of 'competence'[6], and in most naturally competent cells the ability to translocate DNA from the environment is accompanied by extracellular filaments called type-1V pili, and an enzyme called

DNA translocase[7]. Transformation relies on bacterial exposure to extracellular DNA in the environment, which has either been released from dead or decomposing cells through cell lysis[8], or through natural excretion of DNA (found to occur in some species including *Bacillus*[9]). The incoming DNA must cross the outer membrane (in Gram-negative bacteria), the cell wall and the cytoplasmic membrane before being integrated into the bacterial genome in order to persist for future generations. Integration into the host genome is termed "homologous recombination", and the DNA needs to contain regions of between 25 and 200 base pairs (bp) that have similar nucleotide sequences to the host chromosome, which initiate DNA pairing and strand exchange[6]. However, only approximately 1% of bacterial population are naturally competent[6], so to artificially transform cells in the laboratory, biologists use procedures that alter the permeability of the cell membrane (for example, by using calcium or electroporation).

Conjugation (**Fig 1.1 c**), which is the primary focus of this study, is the transfer of genes encoded on a plasmid between donor (F+) and recipient (F-) bacterial cells, also known as a "mating" process or bacterial sex[6].

1.1.2 Conjugation

1.1.2.1 Mechanisms of Conjugation

Conjugation was first discovered by Lederberg and Tatum in 1946, by growing two strains of *E. coli* with different growth requirements on a plate together, selecting for cells that had acquired both growth types. They produced growing colonies at a frequency of 1×10^{-7} CFU/ml, compared with zero colonies when grown separately, suggesting that some recombination of genes had occurred. Subsequent research has revealed that HGT via conjugation requires cell-cell contact between donor and recipient cells[10], mediated by conjugative F-pili[11], and a pore connecting the two cells through which the DNA can pass, although the exact nature of this pore has not yet been determined[6]. The F-pilus, an extracellular filament expressed by the donor cell,

creates a specific contact with one or more recipient cells leading to the formation of a mating pair. Once stabilised, a single strand of DNA is transferred in the 5' to 3' direction, beginning at the nick site of the origin of transfer (*ori*T)[12].

The best-studied bacterial conjugation machinery is also referred to as a type- IV secretion system[13], which is known to be involved in protein secretion in different organisms, but currently knowledge is lacking about the specific mechanisms involved in the plasmid DNA insertion into the recipient cell[14]. Donor cells are either termed F+ or Hrf (high recombination frequency) as they contain the conjugative machinery needed for transfer, and plasmid-free recipient cells are termed F-. Once inside the recipient cell, the DNA is cut by restriction endo-nucleases, replicated into ds-DNA and re-circularised and/or integrated into and recombined with the host chromosome, and they are then termed F+ transconjugants[15].

1.1.2.2 Plasmids

Plasmids are circular MGE's varying in size from 0.85kb to >100kb, with a very compact formation due to super-coiling of the DNA[5] that can replicate independently from the host chromosome, either by rolling circle replication, theta or strand replacement[16]. Plasmids are present in cells with either high or low copy numbers. High copy number plasmids, such as pUC18[17], can replicate even when translation of the host chromosome is not occurring, but they tend to be smaller as plasmids impose a metabolic burden on the cell, so there would be selective pressure in favour of cells that do not possess a plasmid if they were too big. Low copy number plasmids, such as R1, tend to be large and replicate in a similar way to the chromosome by replicating before division, and then partitioning a copy of the plasmid into daughter cells[18].

At a minimum, plasmids must contain an origin of replication, and then carry with them genes that have an essential function (plasmid backbone) or an accessory function. The plasmid

backbone can contain genes coding for replication, copy number, partitioning and genes for transfer. The accessory functions of a plasmid can include genes encoding proteins for antibiotic resistance, or the ability to colonise new environments, which although are not essential for plasmid function, provide enormous advantages to cell survival[13]. In terms of replication, Theta strand replication is the most common mode in gram negative bacteria such as *E. coli* and replication starts at a fixed point (*ori*V and/or r*ep*A) and proceeds in one or both directions around the plasmid until the whole circle is copied[5].

Although many plasmids of the same type can be present in one cell, different plasmids are often incompatible with each other, and are thus termed "incompatibility plasmids", or IncP[19]. The reason is often that a gene from one plasmid encodes a protein that represses the replication of another. For example, some plasmids that use *rep*A in addition to *ori*V as the origin of replication also contain a gene called *cop*B, that codes for a repressor protein of *rep*A to keep plasmid numbers down. However, this also inhibits the replication of related plasmids, meaning they cannot co-exist in the same cell.

Most plasmids have 4-6 base pair (bp) palindrome (same sequence read from 5' to 3' in both strands of DNA) sites for restriction enzymes, also known as restriction endonucleases. Restriction enzymes are proteins produced by bacteria to 'restrict' invasion by foreign DNA, by cutting the foreign DNA into pieces so that it cannot function. There are hundreds of restriction enzymes currently known[20] and most make a cut in the phosphodiester backbone of DNA at a specific position within the recognition site, resulting in a break in the DNA. The enzymes either leave 'blunt ends' by cutting straight down middle, or 'sticky ends', which is an overhanging piece of DNA that can form base pairs with complementary inserts. For example, EcoR1 makes one cut between the G and A in the each of the DNA strands in following DNA sequence:

Cut sites: 5' GAATTC 3'

3' CTTAAG 5'

This leaves an over hanging piece of single stranded DNA which can ligate to another strand of DNA cut with the same enzyme. Restriction endonucleases are used in molecular cloning techniques to swap genes of interest between plasmid types, and also in the so-called molecular 'fingerprinting', where plasmid DNA can be cut into fragments and the bands compared using agarose gel electrophoresis[21].

In terms of HGT, plasmids can be classified into two subtypes: infectious (self-transmissible) and non-infectious plasmids[22]. Self-transmissible plasmids, such as F-plasmids, carry with them the genes required for conjugation, whereas non-infectious plasmids can transfer into a recipient cell only if an infectious plasmid or a transducting phage is present in the same cell.

1.1.2.3 Conjugative Plasmids

Conjugative plasmids spread autonomously since they are equipped with the entire set of genes that are required for plasmid transfer. The best-studied conjugative plasmids are those containing F-like conjugations systems (also known as F-plasmids), and those belonging to the IncP-1 group, including RK2 and R388. Although these plasmids are both self-transmissible, they differ markedly in the organisation of their transfer genes.

F-Plasmids

For conjugative transfer, intercellular contacts are required between the donor and the recipient cells, and when mediated by F-plasmids these contacts are made via conjugative pili (F-pili), also known as the mating pair apparatus[23]. F-plasmids are large (100 kb) and carry their own

origin of transfer, *ori*T as well as *ori*V, and contain a set of genes that code for F-pili within the 33kb *tra* segment.

The exact role of F-pili in the process of HGT has not yet been determined, however recent research, in particular the use of electron cryo microscopy by Wang *et al*., (2009)[24] has yielded greater information about the structure of the protein. Currently we know that F-pili are cylindrical filaments made of a single F-pilin subunit (*tra*A), with an outside diameter of 8 nm and a 2 nm diameter central lumen, although about a dozen or so *tra* gene products are required for assembly[25]. The current view is that F-pilus assembles and extends outward from the membrane, and then the distal subunits attach to protein residues on the recipient cell, retract and bring the cells closer together. Clarke *et.al,* 2008[26] made use of GFP-tagged bacteriophage to target and visualise the retraction and expansion of the conjugative F-pili (**Fig 1.2**), however we still do not know whether F-pili merely act as coupling agents, or whether the plasmid also travels through the lumen to the recipient cell[27].

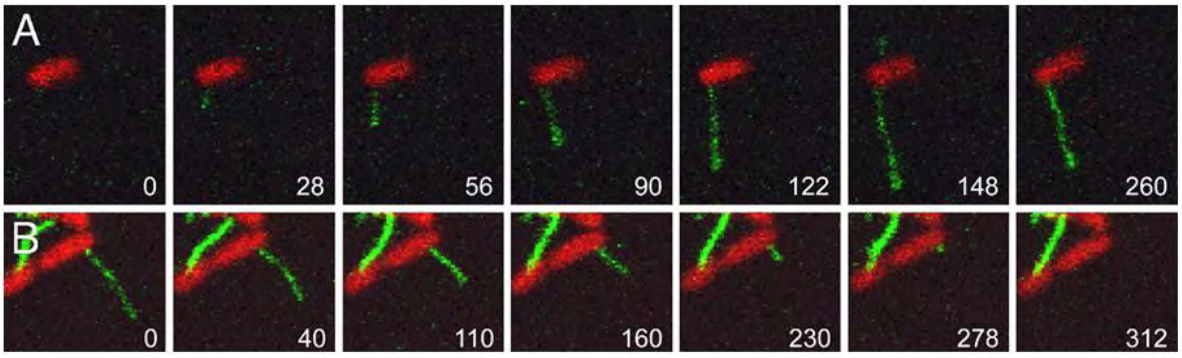

Fig 1.2: Extension and retraction of F-pili[26] GFP-tagged bacteriophage targeting the F-pilus of conjugating donor RFP *E. coli*, showing extension as it reaches to find a recipient over a period of 260 min (A) and retraction once contact has been made over a period of 312 min (B)

Interestingly, Clarke *et al*.,[26] found that pilus extension and retraction occurred independently of the presence of recipients, and that more than one F-pilus could be produced from each cell.

Originally it was thought that donor cells containing similar F-plasmids with similar mating apparatus cannot transfer to each other; a process termed surface exclusion. This is coded for by two genes; *tra*T (10 fold reduction in pili receptiveness), encoding an OM protein that blocks the initial steps in mating-pair formation, and *tra*S (100 fold reduction in pili receptiveness), a protein that sits in the inner membrane which blocks DNA transfer after a mating pair has been established[12]. Surface exclusion is common in conjugation of bacteria, however, inter-plasmid recombination can take place, that can allow the genes from one plasmid to be gained by a related plasmid in a recipient bacterium (forming a co-integrant), proving evidence that surface exclusion is not an absolute barrier, allowing one plasmid to enter a cell that contains a closely-related plasmid[28].

RK2

RK2 is a 60 kb conjugative plasmid that forms the focus of study in this thesis. It has an unusually broad host range among gram-negative bacteria[29], and has a copy number between four and seven per chromosome equivalent in *E. coli*[30]. Plasmid replication has been shown to require two plasmid loci, origin of replication (*oriV*) and the trans-acting *trfA* gene whose product which is essential for replication initiation. Additionally, RK2 has a transfer system with two regions; *Tra*1 with *tra* genes in a 13kb region, and *Tra*2 with *trb* genes in an 11.2 kb region (**Fig 1.3**) which are separated by genes encoding resistance to kanamycin and tetracycline[31].

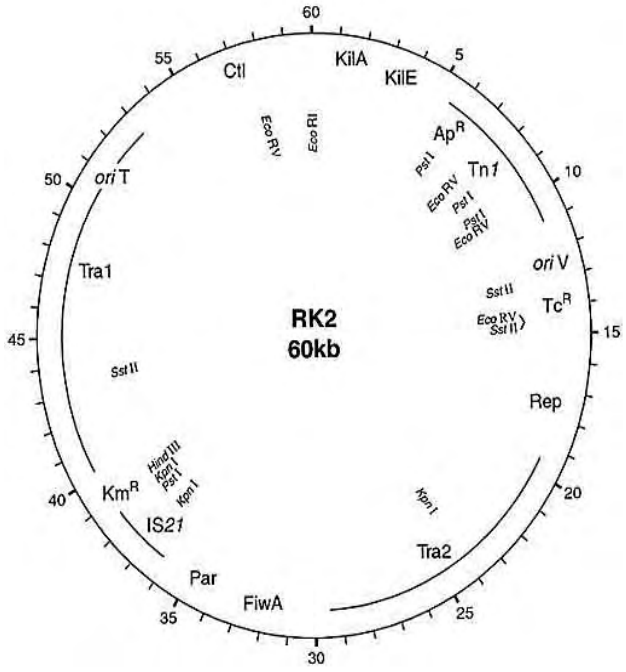

Fig 1.3: Plasmid map of RK2[29] including the *oriT* site and the two separated transfer regions, which all of the genes known to be required for efficient conjugative transfer.

The genes of the *Tra*1 region encode proteins for conjugative transfer and the ten genes of the *Tra*2 region encode the majority of proteins required for conjugative pilus formation (assembly, export and placement). In contrast to the flexible F-pili, the pili from RK2 are thinner and more rigid, and because of this RK2 conjugation has been detected mainly when cells are growing on semi-solid surfaces, unlike F-plasmids which can mate equally well in solid or liquid environments[30]. It is speculated therefore that conjugation requires that the cells carrying RK2 have close cell-cell contact[32]. After initial contact has been established the DNA is thought to be transported in a complex with associated proteins through a channel at the mating bridge between the donor and the recipient cells. Additionally, it has been shown that during conjugation the *Tra*C gene encoding a DNA primase is also transferred to the recipient cell to assist in establishment of the plasmid[33].

1.1.3 Consequences of Conjugation

HGT can have a dramatic effect on both the ecology and evolution of the recipient bacterium, as acquired genes may be advantageous, allowing colonization of otherwise hostile niches and/or improved pathogenicity. For example, studies of Cystic Fibrosis patients by the Hanover Medical School by Klockgether *et al.*,[34] found that 30% of patients were infected with strains of *Pseudomonas aeruginosa* known as "Clone C". It was found that these strains were harbouring a 102kb plasmid called PKLC102, containing virulence genes that resulted in greater morbidity and mortality of the patients[34].

Plasmids can incorporate and deliver genes into the host chromosome by recombination or transposition, and they therefore provide an important dimension to an organism's response to changes in the environment[35]. The most widely studied plasmids are those that carry antibiotic resistance genes, which code for a variety of proteins including beta lactamases that can destroy penicillins. HGT has also been responsible for spreading antibiotic resistance amongst certain strains of bacteria, the acquisition of new secretion systems, iron uptake systems and the ability to utilise novel carbon sources[13]. HGT is an evolutionary process, and could potentially result in the blurring of species boundaries as more genes are passed back and forth and cells become more genetically similar[36].

1.1.4 Detection of HGT

1.1.4.1 Traditional approaches for studying gene transfer events

Some of the first exploratory studies into HGT occurred in soil biofilms, using cells that were dislodged from the natural settings[37]. Early studies focused on determining how environmental factors such as temperature, nutrient availability, moisture etc affect the rate of HGT. Since then, DNA sequencing of whole bacterial genomes has allowed us to compare phylogenetic relationships of genes or proteins that have a similar function between different strains/species of

microorganisms, to determine genetic similarities and therefore the likelihood of a DNA transfer occurrence. For example, it has been discovered that 18% of the extant genome of *E. coli* has been acquired since the divergence from *Salmonella* 100 million years ago[38].

Studies of gene transfer have progressed to determining the population dynamics of transfer events in bacterial communities. Traditional studies have relied on cultivation techniques, where donors, recipients and transconjugants are extracted from their original setting and counted. The use of antibiotic resistance markers and growth factors on plasmids has meant that researchers can select for transconjugants using selective media, creating transconjugant to donor ratios[13].

Gene transfer processes in mammalian organs such the gut have also been studied, using *in vivo* experiments in animals. Bacterial donors and recipients have been cultured *in vitro*, followed by inoculating directly into live animals and then subsequent detection through faecal matter or animal sacrifice[39]. However, in addition to being expensive and unreliable, live animal models make it difficult to observe and document plasmid transfer and gene acquisitions as they occur in real time.

Although the methods above provide useful quantitative information, they do not distinguish between an increased number of transfer events and post-transfer selection (i.e. between initial transconjugants and those that have replicated), and there are many experimental errors and inaccuracies in plating experiments. Additionally, these methods do not tell us what is happening on an individual cell basis – they give population averages, and therefore do not take into account spatial differences present in bacterial environments, which are usually highly variable.

1.1.4.2 Microbial Modelling

Individual based Models (IbMs) such as those designed by Kreft *et al.*, (2006)[40] are in place which allow exploration of bacterial behaviours such as growth and communication, and it would be useful to adapt these models to explore HGT in spatially structured settings. Theoretical microbiology utilises mathematical models (built with data from laboratory testing) and computer software to graphically describe these responses. They are not meant to replace laboratory testing, but rather to provide supplementary information and predictive tools that can be used to guide further exploratory steps into gene transfer events. For example, a current IbM study by Lardon *et.al,* 2011[41] is in development to explain poor plasmid invasion in deep layers of biofilms, and they hypothesized that conjugation was dependent on growth rate of the donor cells. By extending existing IbMs of microbial growth to include the dynamics of plasmid transfer by individual cells they are able to conduct tests of this.

1.1.4.3 Recent advances in studying HGT

New methods have come into development recently for studying HGT without the need for culturing. Reporter-gene technology allows expression of traits that signify the presence of a plasmid in transconjugants. In particular, Scanning Confocal Laser Microscopy (SCLM) in combination with luminescence or fluorescent biomarkers such as the green fluorescent protein (GFP) has heightened our ability to monitor *in situ* conjugation events in a direct and non-disruptive manner. For example, Hausner and Wuertez, 1999, used fluorescent proteins encoded on the conjugative plasmid pRK415 to observe transconjugant formation (**Fig 1.4**). By using plasmids coding for RFP-pRK415, and recipients expressing GFP, they were able to distinguish transconjugants by the colour change[42].

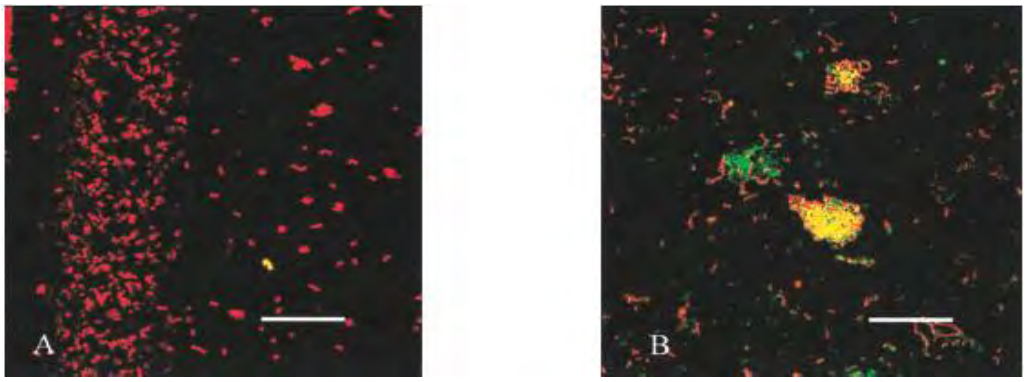

Fig 1.4: Use of whole-cell fluorescence to visualise conjugation: A: donor cells (red) B: donors (red), recipients (green) and transconjugants (yellow – green plus red)[42]

However, this method has its limitations. Once the plasmid enters the recipient cell, the fluorescent proteins would then need to be synthesised and this is dependent on many other factors including metabolic rates, cell fitness, nutrient availability etc. Protein synthesis also takes time, and therefore this method would not allow collection of real-time data. The plasmid may not even be replicated at all, if there is no selective pressure for it to do so.

Therefore, a few groups have used techniques to visualise plasmids via microscopy as they enter recipient cells, by forming fluorescent foci. For example, Babic *et.al.*, 2008[43], used donor plasmids that had been hemimethylated by Dam methylase. A protein called SeqA, which has high affinity for hemimethylated DNA, was tagged with YFP and expressed in the recipient cells. Following conjugation events, the F-plasmids became visible with the YFP-SeqA fusion[43] (**Fig 1.5 a**). Fluorescent foci have also been used to distinguish transfer events in IncP-1 conjugative plasmids. Lawley *et.al.*[44] used the *lacO*/GFP–LacI system introduced by Gordon *et.al.*[45] to label and visualize the plasmid R751 fluorescently during conjugative transfer between live donor and recipient bacteria. A *lacO* cassette, which consisted of 256 tandem repeats of the lactose operator flanked by a kanamycin resistance gene, was introduced into R751. Expression of green fluorescent protein GFP–LacI (encoded by the F- recipient cells) resulted in GFP–LacI

binding to the tandem operators and caused the plasmid to appear as a fluorescent focus that was visualized by fluorescence microscopy[46] (**Fig 1.5 b**).

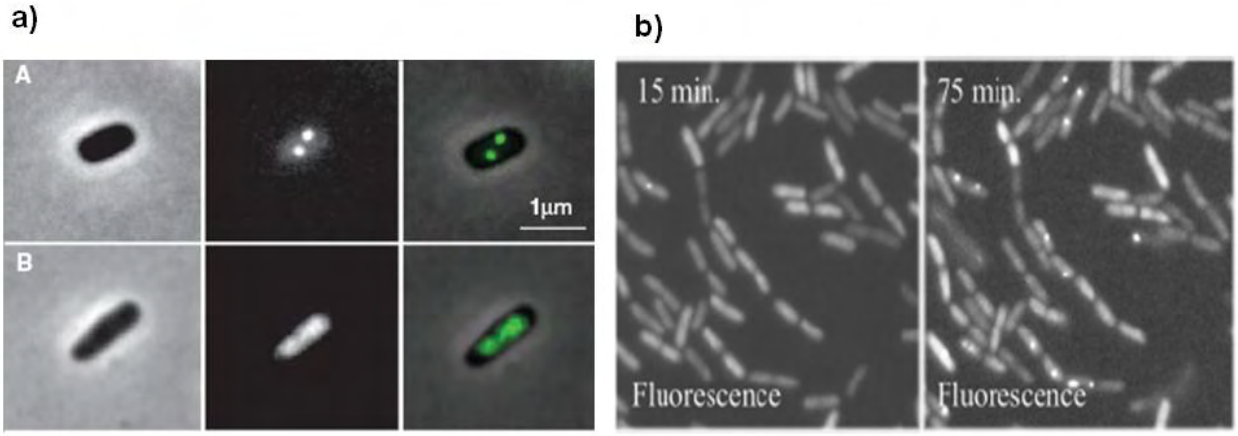

Fig 1.5: Use of fluorescent foci to visualise conjugation: (**a**) Use of SeqA-YFP fusion to show plasmid localisation in Dam-proficient cells (A) and no foci in Dam-deficient cells (B); (**b**) Use of GFP-LacI fusion to visualise plasmids in a timed-dependent study

These methods allow the visualisation of foci regardless of replication, and if replication occurs, it can be quantified by the number of foci present in each cell. The next stage in this development is to use these foci systems to ascertain spatial differences and time scales of plasmid transfer in bacterial cultures. Babic *et al.* (2011) expanded on previous work by using the LacI-GFP fusions to study conjugation in chains of *B. subtilis* growing on agarose blocks[47]. They found that transfer from a donor to a recipient appeared to occur at the cell poles (**Fig 1.6**), or laterally along the surface, and deduced that the high concentration of conjugation proteins at donor cell poles may contribute to this.

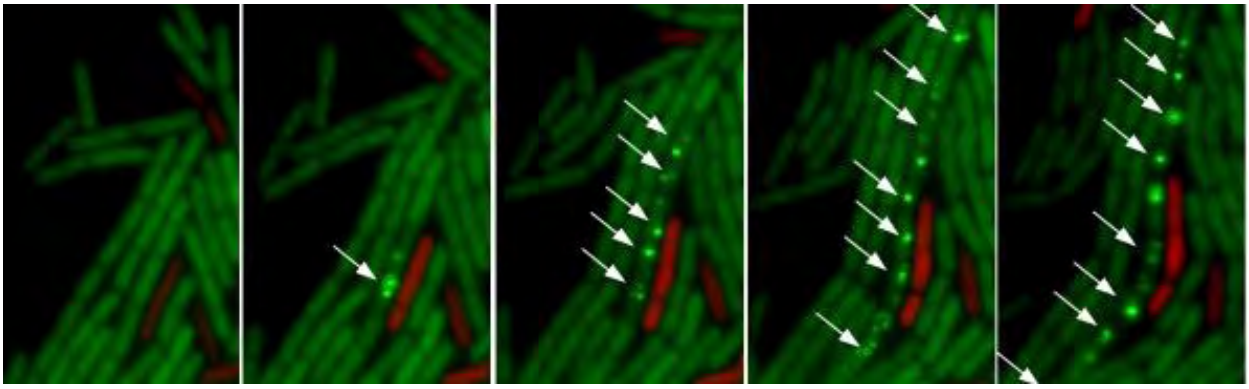

Fig 1.6: Plasmid mobility in bacterial chains: The conjugative plasmid moves from the donor (red) and then spreads preferentially along the recipient cell chain from pole to pole, rather than to neighbouring cells on either cell[47].

One thing that is fundamentally lacking in the current research into HGT is **spatial control** over the cells. Typically, a ratio of modified donors and recipients are inoculated onto a nutritious medium surface, and then plasmid transfer is visualised by microscopy in real time. However, the cells are distributed randomly onto the surface; there is no control over their spatial arrangement in terms of spacing and shape. Having greater control over the position of the donors and recipients would allow us to relate transfer events to the positions of donors and recipients, and it would be easier to distinguish the time it takes for HGT events to occur, the spatial positioning of HGT within the culture as a whole, and the fate of the transferred DNA. In addition, the fact that many bacteria are mobile organisms presents problems for accurately visualising conjugating bacteria. There is therefore a need for a technology that allows for the control of bacterial adhesion, to keep the cells in fixed positions, in conjunction with a patterning technique that would allow spatial positioning.

1.2 Bacterial Adhesion to Surfaces

1.2.1 Overview

Bacteria can exist in nature as free planktonic cells in bulk solution, but the majority prefer to live in surface-associated sessile communities known as biofilms[48]. Biofilms are generally defined as a structured community of microbial cells, enclosed in a secreted polymeric matrix on a surface[49]. Biofilms are ubiquitous; they have been found on almost any surface that is ripe for bacterial colonisation, both in nature and on man-made constructions, including clinically important biomaterials such as contact lenses[50], and materials vital for industry such as industrial marine vessels[51]. **Fig 1.7** shows an overview of the development of a typical biofilm:

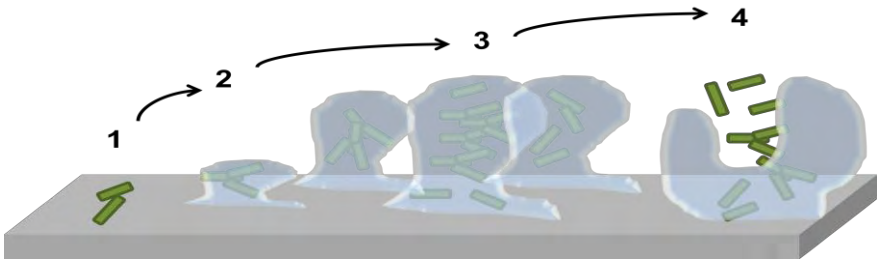

Fig 1.7: Schematic representation of a typical biofilm formation. Planktonic bacteria make contact with a surface and adhere initially through weak, reversible non specific interactions (such as van der Waals forces) (**1**). Specific 'irreversible' adhesion follows, using locking adhesins on the bacterial surface (**2**). Secretion of EPS and subsequent establishment of microcolonies follows, due to clonal growth of the attached cells or by active translocation of cells across the surface, (**3**) which grow in size and coalesce to form macrocolonies. Macrocolonies arise when bacteria are no longer firmly interconnected and attached to the surface, allowing mobility by means of flagella, forming loosely protruding structures, often mushroom like in appearance. Finally, biofilm EPS can rupture, leading to dispersal of microbes (**4**)

Biofilms are composed of slow-growing microcolonies of 10-25% cells encased by 75-90% of slimy secreted extracellular polysaccharides (EPS), also known as "glycocalyx"[52]. In terms of reproductive fitness it seems ecologically unfavourable at first to form biofilms as bacteria in have reduced growth rates relative to planktonic cells. However, biofilms convey a selective

advantage over planktonic cells for a number of reasons, including protection from predation, desiccation, and acquisition of new genetic traits via HGT[53]. Biofilms may contain highly permeable water channels[54], which provide a nutritionally favourable environment and facilitate the efflux of waste. Additionally, microbes in biofilms can tolerate antimicrobial agents up to 10-1000 times the concentration needed to kill genetically similar planktonic organisms[55].

There is therefore a selective advantage for the bacterial ability to adhere to and remain on surfaces. As such, bacteria have evolved a variety of adhesins that enable them to colonise multitude of surfaces, from *in vivo* mucosal surfaces to synthetic polymers and raw materials. Research requiring microbial manipulation on surfaces should therefore take into account the adherence mechanisms of bacteria - both the initial, non-specific forces, and the specific molecular locking mechanisms employed by surface adhesins.

1.2.2 Initial (Primary) Adhesion

Initial deposition of bacteria onto surfaces is governed by forces such as Brownian motion, hydrodynamic forces, and a variety of non-covalent interactions including van der Waals forces (weak, temporary dipoles between molecules), electrostatic interactions (electrostatic overlap of counter ion clouds) , and hydrophobic interactions (displacement of water between two adhering surfaces)[56]. The **rate** and **strength** of the initial adherence of microbes to surfaces depends primarily on the relationship between the (attractive or repulsive) chemical and physical properties of the aqueous phase, bacterial and substratum surfaces[57]. Researchers have devised three main theoretical models to examine bacterial adhesion to surfaces; the thermodynamic model[28, 29], the DLVO model[58] (Derjaguin, Landau, Verwey, Overbeek), and the extended DVLO model[59].

The thermodynamic theory expresses adhesive forces as a measure of free energy. In nature systems strive to be in a state of minimal free energy, and the thermodynamic model calculates the numerical values of free energy of the bacteria, the surrounding solution and the surface to give theoretical adhesion energy values (Gibbs adhesion energy)[60]. Adhesion is said to be more likely to occur if the free energy value is negative. The DVLO model states that initial adherence of bacteria is a balance between attractive van der Waals forces and attractive or repulsive electrostatic interactions (electrostatic tend to favour repulsion as most surfaces and bacteria are negatively charged), and their decay with separation distance[61]. There are some limitations to both models, however. The thermodynamic theory primarily takes into account hydrophobic interactions, van der Waals and somewhat excludes electrostatic interactions. Additionally, the model is based on a closed system, with no additional input or output of energy. Therefore assumptions for bacterial free surfaces energies may be incorrect as they are living, dynamic organisms that can change energy from a system by consumption of local media, for example, and synthesis of extracellular surface features[62]. The DVLO theory does not explain a variety of different attachment behaviours, mainly overcoming an electrostatic barrier. The extended DVLO theory developed by Van Oss *et al.*[59] attempts to overcome these limitations by considering the four fundamental non-covalent interactions van der Waals, electrostatic, Lewis acid-base and Brownian motion.

In summary, there is not as yet a generalised initial adhesion profile valid for each and every bacterial strain and surface, however the research to date has shown that it is a complex process involving many different interactions. In the absence of a potential docking site for bacterial adhesins, however, research has shown that generally bacteria prefer to adhere to hydrophobic surfaces over hydrophilic[63], allowing more hydrophobic interactions, and surfaces that are positively charged[64], as bacteria are negatively charged, therefore increasing the net van der Waals interactions over repulsive forces.

1.2.3 Bacterial Adhesins (Secondary Adhesion)

In order for a bacterium to exhibit irreversible attachment to surfaces following initial adhesion (unable to be removed without excessive force or rinsing), cells have evolved the ability to produce adhesins (receptors) either protruding from or attached to the cell membrane, which bind to specific molecules (ligands) on surfaces, forming a strong but non-covalent bond[56]. The process of recognition usually only involves a portion of the molecules involved and the molecular structure responsible is known as an epitope[65]. The construction of an adhesive surface with the ability to form a robust, specific, irreversible bond with bacterial adhesins is an important factor in cell-cell communications studies, and as such surfaces should be constructed so that they select for one or more of these adhesins.

1.2.4 Major bacterial adhesins

Bacterial adhesins are either directly associated with the cell membrane, or they protrude outwards from the membrane in hair-like appendages[66]. Such appendages are called pili or fimbriae, and they are usually assembled from repeated proteinaceous subunits, with a terminating lectin-like subunit that binds a specific carbohydrate moiety. Initially pili were only identified in Gram negative organisms such as *E. coli* and *Pseudomonas*, but some species of Gram positive bacteria have now been known to produce structurally similar appendages[66]. One of the best-studied examples of pilus assembly is the family of P-pili encoded by the '*pap*' genes, which are expressed in most strains of uropathogenic *E. coli*. They are rigid helicopolymers with a terminating protein subunit called PapG, and bind repeating Gal α (1,4) Gal moieties present on glycolipids coating the surface of erythrocytes and uroepithelial cells[67], allowing the bacteria to colonise the urinary tract and cause infection. Another well-studied example of protruding adhesins is type-1 fimbriae. They are expressed in most strains of enterobacteria, and have similar operons and functionally analogous sequences to P-pili[68], but are structurally different. Type-1 fimbriae are flexible, rod-like fibres that bind specific

mannose moieties with the subunit Fim-H[69] (Type-1 fimbriae and their assembly are explained in more detail in section **1.2.4.1**). A variety of surface-associated (non-polymeric) adhesins can also mediate the attachment of a bacterium to a host cell or surface. Bacterial surface proteins that bind to host extracellular matrix (ECM) proteins such as fibronectin, fibrinogen, vitronectin, and elastin are referred to as MSCRAMMs (microbial surface component recognizing adhesive matrix molecules)[70], and the integration of bacteria with ECM proteins is believed to contribute significantly to the virulence of a number of microorganisms, including staphylococci and streptococci[71].

1.2.4.1 Type-1 fimbriae

Type-1 fimbriae are long, thin, flexible, proteinaceous appendages that protrude outside of the cell body and bind to D-mannose residues[69]. Their thickness ranges from 2-7 nm, and the length can be up to 2 μm[72]. First visualised by Houwink and van Iterson in 1950 using electron microscopy[73], type-1 fimbriae are expressed in abundance (100-1000 per cell) and do not rotate independently of the cell body like flagella (**Fig 1.8 a**). They are protein polymers composed mainly of identical subunits, which are held in the stable threadlike structure via hydrophobic and electrostatic interactions. The individual subunits are coded for by the fim gene cluster, either on a plasmid or on the chromosome (**Fig 1.8 b**). The biosynthesis of *E. coli* fimbrial adhesins has been extensively studied and they have been shown to assemble via a chaperone/usher pathway[74] (**Fig 1.8 c**).

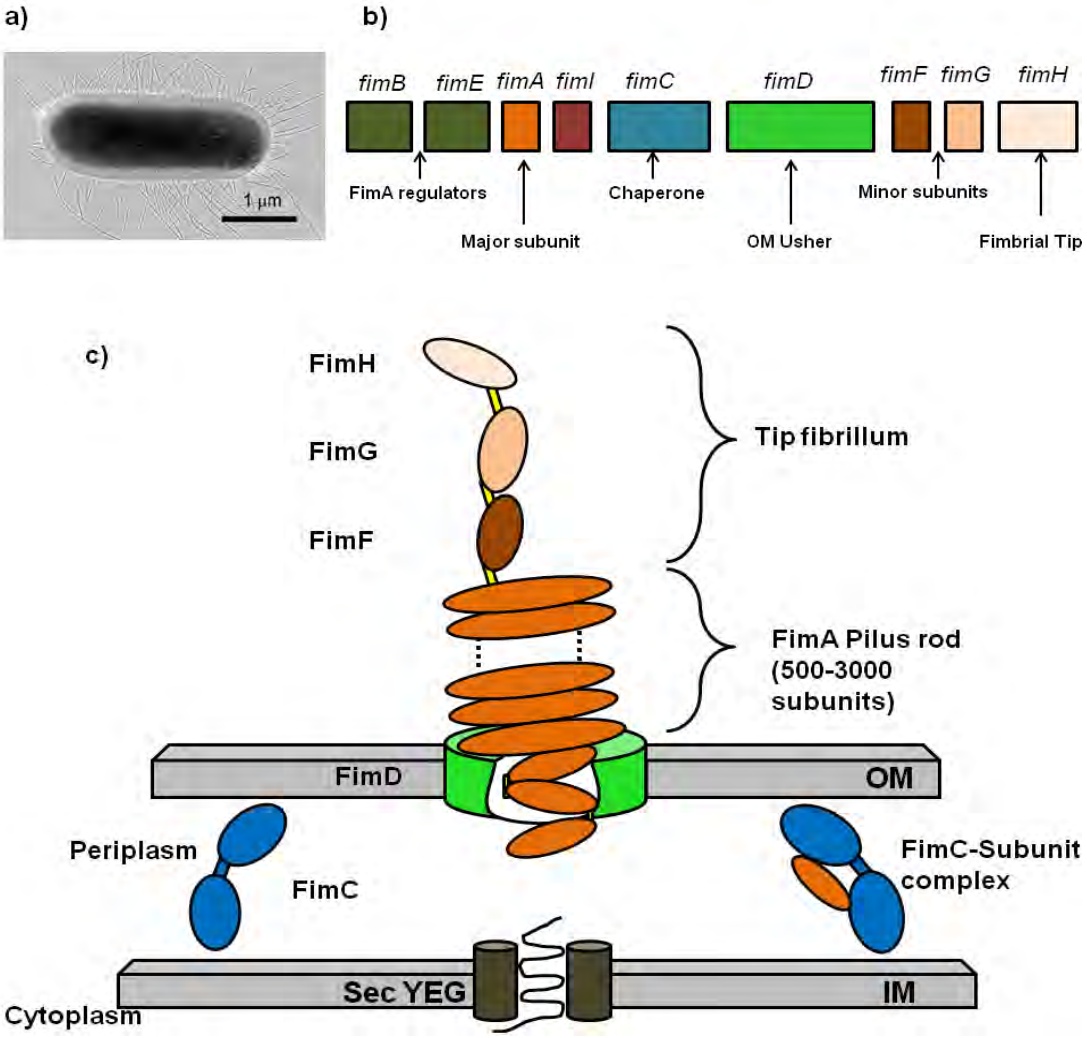

Fig 1.8: Representations of type-1 fimbriae: showing SEM image of fimbriae on *E. coli* K12 (**a**)[75]; the fim gene cluster that encodes for the various protein subunits needed for fimbrial assembly (**b**); and the chaperone usher pathway (**c**). Upon translation, subunits are secreted into the periplasm via the SecYEG translocon. FimC (the 'chaperone') then accelerates protein folding, and delivers the subunits to the pore forming protein FimD ('the usher') in the outer membrane. Here, the subunits are translocated and incorporated into the growing pilus.

In the chaperone-usher pathway, FimC acts as the chaperone – it attaches reversibly to the subunits and prevents premature protein folding, as well as delivering them to the usher, FimD[76]. FimD is a large transmembrane protein that allows translocation of the individual subunits onto the outermembrane. The ushers are polar and lack typical hydrophobic membrane spanning domains, and studies have shown that subunits collect in the periplasm in mutants lacking

ushers[77]. The main length of the pilus is hollow, with an internal diameter of 2 nm and is composed of identical subunits of FimA monomers which are non-covalently associated head-to-tail and organized in a right-helical structure[69]. The helical structure is flexible and has the ability to unfold if pulled, resulting in a considerable length increase of the fimbriae. This is a very useful feature in an environment with strong hydrodynamic shear forces, allowing fimbriated bacteria to colonise many inhospitable environments that are exposed to flow, such as the urinary tract[78].

FimH is the adhesive subunit which binds mannose residues, and the minor components FimF and FimG act as adaptors for integration of the adhesin into the fimbrial structure. Recent studies have shown that FimH is able to interact with the mannosylated surface via a shear-enhanced catch bond mechanism[48-51]. This was surprising, as initially FimH was thought to act like a lectin (a protein that binds non-covalently to mono and oligosaccharides), which are thought to bind via slip bonds that are weakened under shear forces[79]. Structural simulations have shown that the FimH undergoes a conformational change when exerted to force, accompanied by an increase in binding strength. Forero *et a.*, (2006), found that by pulling fimbriae with a mannosylated tip of an atomic force microscope they could withstand intermediate force (between 25 and 60 pN) for prolonged periods of time[80]. Tchesnokova *et al.* (2007), found that the cysteine bond in the mannose-binding domain of FimH contributes to its adhesion strength under shear force, by creating cystein-bond-free mutants[81]. Additionally, Aprikian *et al.* (2007), suggested that the two Fim domains interact with each other (the main pilus and the FimH), and that the main protein has a detrimental effect on FimH binding when the two are in close contact[81]. With shear force, the lectin domain FimH becomes separated from the main protein and allows it to switch from a low affinity to a high affinity state.

This specific shear stress-enhanced adhesion of bacteria to mannosylated surfaces is useful for bacterial adhesion studies as it will allow the micro-patterned bacterial co-cultures to be exposed to shear forces resulting from fluid flow conditions without dislodging the bacteria or causing mixing of the bacterial strains.

1.3 Using Surface Chemistry to Control Bacterial Adhesion

1.3.1 Overview

Molecular surface science has greatly contributed to the advancement of many technologies by providing ideal platforms for engineering arrays and biosensors of cells on a molecular level. There exists, to date, a wide variety of methods employed by researchers to immobilise both mammalian and bacterial cell types to surfaces, each with their own strengths and weaknesses in terms of practical applicability for the controlled study of bacterial cell-cell interactions. Considering the practical set up and longevity needed for the study of HGT in spatially controlled experiments, the supporting adhesive surface must be carefully selected. The following properties are required of an adhesive surface for studying cell-cell interactions:

- **High Bond Strength**. The cells must be able to remain in position on the surface for the longest period of time possible in order to perform time-scale studies. The cells would also be subject to rinsing procedures and fluid flow conditions from addition of supplementary media. The surface features must therefore form strong, robust, bonds with cells; in which case specific cellular adhesins would need to be targeted, rather than relying on whole-cell non-specific interactions. Additionally, the adhesive bonds would need to be stable under shear flow to prevent dislodging of the bacteria and/or cause mixing of the bacterial strains.

- **Flexibility.** In studies of HGT, the cellular adhesin targeted by the surface should be flexible, as extension and retraction of the conjugative-pilus will require slight cell motility, and to create spacing for cell division (*E. coli* replicates on average once every half an hour). Type-1 fimbriae therefore provide ideal targets for cellular adhesion, as opposed to the various MSCRAMM proteins which have little to no protrusion from the cell membrane[82].

- **Compatibility**. The surface selected would need to bind the bacterial cells yet not interfere with normal cellular metabolic processes. Therefore the specific adhesins targeted should not be those that have a metabolic function.

- **Specificity**: The adhesive surface should be selective in that it only binds to specific adhesins on the bacteria cells, and not those present in the media, which may prevent the cells adhering via a stronger bond.

1.3.2 Surface-mediated cellular adhesion approaches

A variety of approaches have been employed by researchers to selectively immobilise bacterial cells onto surfaces. The specificity of antibodies can be harnessed to create arrays of cells on surfaces. For instance, Rozhok *et al.* (2005) made use of goat antibodies attached on predesigned microarrays against the whole cell surface of *E. coli* K-12. However, the antibody-antigen force is relatively weak (~50pN), and does not have a catch bond mechanism such as the one found in bacterial fimbriae; meaning cells are not likely to withstand dislodging in a flow cell environment. In fact, Premkumar *et al*. (2001) performed a similar experiment in a flow cell and only managed to achieve 2% surface coverage of bacteria using antibodies[83].

Poly-L-lysine is also another popular method of cell immobilisation to surfaces; it is a cationic polymer and the negative surface charges of the bacterial cell wall make it an effective way of

attracting cells to surfaces[84]. However, this method of bacterial adhesion is employed by using non-specific forces, rather than via specific bacterial adhesins, meaning that adhesive forces would not be robust enough to sustain immobilisation for prolonged periods of time and through shear forces. Furthermore, some researchers have found that thick layers of poly-l-lysine can actually be anti-microbial, and inhibit growth of cells[85].

One of the most popular methods of bacterial cell immobilisation is through the use of functionalised self-assembled monolayers (SAMs)[93]. SAMs possess important properties of self-organization and adaptability to a number of technologically relevant surface substrates, providing the ideal platforms for the attachment of adhesive molecules.

1.3.3 Self-Assembled Monolayers

1.3.3.1 Self-assembly

Self-assembly occurs ubiquitously in nature[86], and it involves the spontaneous organisation of molecules into large, structurally defined assemblies in 2D arrays or 3-D networks[87]. Examples include cellular processes such as secondary and tertiary protein folding, and lipid bilayer formation, as well as molecular arrays that occur at the liquid/solid interface[88]. Self-assembly is also known as a "bottom-up" approach to supra-molecular architecture[89], as structures are assembled molecule by molecule, as opposed to the molecular "carving" of pre-existing structures in the top-down approach.

Self-assembly occurs in fluid phases or on smooth surfaces, as the individual components are required to be mobile in order to move into position[90]. Non-covalent interactions between individual molecules, including van der Waals forces and hydrogen bonding, create a **stable** structure upon self-assembly. Although individually non-covalent bonds are weaker than covalent bonds[91], multiple non-covalent bond formation favours structurally stable-self

assembly[92].This effectively turns many weak interactions into one collective strong interaction. To create an **ordered** structure, equilibrium between attractive and repulsive forces occurs[93], or molecules shuffle their positions in an aggregated state. The structures formed via self-assembly depend on the intrinsic physical and chemical properties of the individual molecules[94], and many of these structures, including self-assembled monolayers, can be used as building blocks for generating nanostructures for a wide variety of biological and chemical applications.

1.3.3.2 SAM Formation

Self-assembled monolayers (SAMs) are surface structures made from the spontaneous adsorption of surfactant molecules onto a surface[95]. They are used in surface chemistry to provide nanometre thick, highly ordered films that can be used as building blocks for protein[96] and carbohydrate attachment, as well as for biocompatibility, wetting and adhesion studies[97]. Each of the surfactant molecules that constitute the building blocks of the SAM can be divided into three parts, the head group (surface linking group), the backbone and the terminal (active) group (**Fig 1.9**).

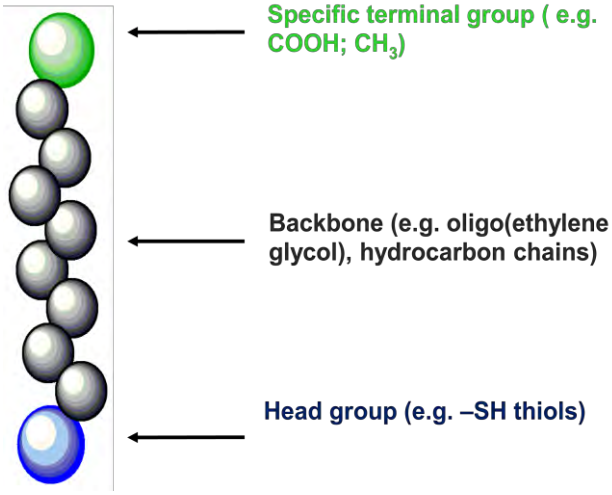

Fig 1.9: Schematic representation of a surfactant molecule

A wide variety of surfactants can be used to form SAMs, including organosilane species on hydroxylated glass[98] and carboxylic acids on metal oxides[99]. However, the most popular form of

SAM construction is that of n-alkanethiols (thiols) on gold[100]. Gold is the metal of choice for a large proportion of SAM studies as it has the lowest surface energy[101], is relatively inert and biocompatible, and does not form oxides with atmospheric gases at room temperature[102]. Additionally, gold substrates are easy to prepare by physical vapour evaporation[103] of the metal onto a glass surface with a chromium or nickel adhesion layer in between (1-5 nm), allowing thin films of gold to be formed (10-200 nm). Thiols are fully saturated and carry the general formula:

$$\mathbf{HS\text{-}(CH_2)_n\text{-}X}$$

They consist of a sulfur head group (**HS-**), which forms a strong, covalent bond with the gold substrate, and a specific terminating group (**-X**), that determines the specific physiochemical properties of the newly formed SAM, as well as providing an anchor point for further surface modification[104]. Separating the head and terminating groups is usually a hydrocarbon chain backbone (**$(CH_2)_n$**), which stabilises the SAM through van der Waals interactions[105]. Thiols can be deposited onto gold substrates either through vapour deposition or from a solution[106], with concentrations of 10-1000 µM. **Fig 1.10** shows the formation of a n-alkanethiol SAM on gold:

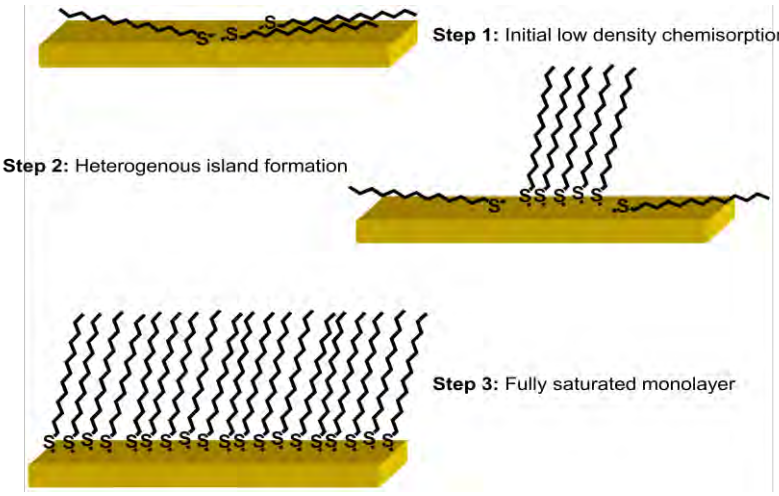

Fig 1.10: Schematic representation of SAM formation

Within minutes of attaching to the substrate surface, the sulfur head group of the thiol molecule forms a strong covalent bond with the gold (chemisorption), ~ 44 kcal/mol^{-1} [107], forming a metal thiolate (**Fig 1.10, step 1**). The widely accepted theory of thiolate formation is that there is an oxidative adsorption of the S-H bond to the gold surface, with a reductive elimination of the hydrogen, forming a S-Au bond[63, 70, 76]. Scanning tunnelling microscope (STM) images have revealed that initially, low density adsorption causes the thiol to align parallel to the gold substrate, and upon a critical surface coverage lateral pressure induces nucleation of heterogeneous island forms[100](**Fig 1.10, step 2**) until full saturation is reached. To minimise the free energy of the organic layer, the thiol molecules adopt *trans* conformations that allow high levels of non-covalent van der Waals bond formation between the methylene groups of the hydrocarbon backbone. The completion of this process can take several hours, depending on the nature of the backbone, and the resulting SAM is that of a densely packed, 2D molecular organisation of thiol molecules. IR and Raman Spectroscopy studies, that measure intensity ratios between CH_3 stretching vibrations, have shown that alkenethiol molecules orient themselves with a tilt angle (α) of 30^{o}[108], as it provides the parameter to maximise the van der Waals chain-chain interactions, leading to effective close packed monolayers (**Fig 1.10, step 3**).

1.3.3.3 SAM functionalisation

When proteins are adsorbed onto heavy metal surfaces such as gold they are often denatured[109] because of the metal's high affinity for sulfur, which disrupts disulfide bridges. Subsequently, SAMs provide a useful way of insulating the protein from the surface without loss of functionality. Additionally, SAMs provide a way of attaching analyte molecules to surfaces via robust covalent bond formation[96], rather than via simple adsorption through weaker non-specific bonds such as hydrophobic and electrostatic interactions. Weak bonds will retain the activity of the protein yet the adsorption is reversible, as molecules can be removed by certain buffers, detergents, or by rinsing[110]. Advancement in SAM technology has developed methods for

covalently immobilising analyte molecules onto surfaces with little to no loss of functionality, through coupling of SAM terminating groups to specific groups on the molecule of interest, either directly or through intermediate linkers[111].

For covalent immobilisation onto SAM surfaces, the main targets on proteins are carboxylic acid (COOH) groups, primary amines (NH_2), thiols (SH) and carbonyls (C=O). A popular method of covalent coupling of proteins to SAMs is by using carbodiimide chemistry[81, 82].

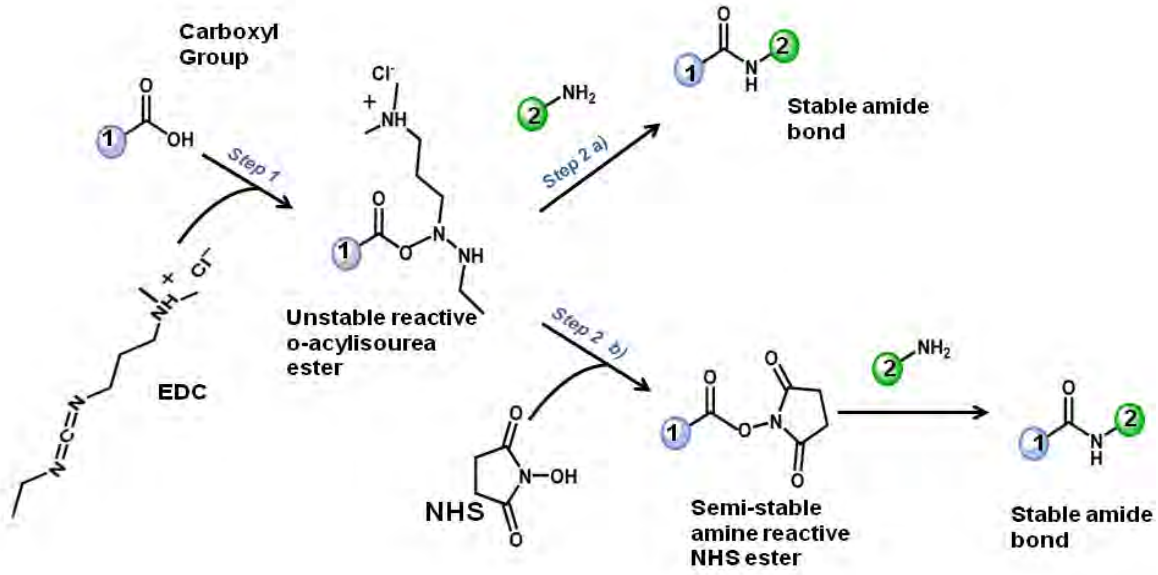

Fig 1.11: Schematic representation of carbodiimide chemistry

Molecules of ethyl (dimethylaminopropyl) carbodiimide (EDC) and N-Hydroxysuccinimide (NHS) are used to bind COOH-terminated SAMs to analyte molecules with NH_2 groups. EDC reacts with the carboxylic acid groups and forms an active O-acylisourea intermediate[112] **(Fig 1.11, step 1)**, which is then displaced by nucleophilic attack from the NH_2 group of protein[113]. The NH_2 group forms an amide bond with the carboxyl group[114] **(Fig 1.11, step 2a)**, and an EDC

by-product is released. However, the O-acylisourea intermediate is unstable in aqueous solutions, so EDC is most often used in conjunction with NHS to form intermediate NHS esters[115](**Fig 1.11, step 2b**), which enhance coupling efficiency when reacted with the primary amines to form stable amide bonds.

The presence of the attached analyte molecule can then be confirmed by using appropriate surface characterisation techniques, such as ellipsometry, X-ray photoelectron spectroscopy, STM, etc, and real time binding of molecules can be determined using optical measurement techniques such as SPR (detailed descriptions in chapter 2).

1.3.4 Applications of SAMs for Cellular Adhesion

SAMs have been used for a variety of research applications, including organic semiconductors for applications in organic electronics, generation of biocompatible surfaces, anchoring proteins to surfaces, deposition of metal organic frameworks on SAM surfaces, and generation of biocompatible surfaces for cellular adhesion studies, which forms the main interest of this project. SAMs have been used in a variety of ways to control both mammalian and bacterial cell adhesion to surfaces, as their properties can be easily changed, for example by coupling biocompatible proteins or sugars to the terminating groups or using thiols with different wettabilities.

1.3.4.1 Anti-adhesive SAMs

There has been considerable interest in the use of SAMs as model systems to study bacterial adhesion for the development of so called "inert surfaces" for biofouling applications[116,117], including developing anti-adhesive coatings for marine vessels, and creating biologically inert materials such as contact lenses and artificial surgical devices such as heart valves and blood vessels[118]. Certain terminating groups of SAM surfaces have been shown to resist the non-specific adsorption of proteins, and subsequently have been able to reduce cellular adhesion and

biofouling. The most widely used and characterized SAMs that resist protein and cellular adsorption are those consisting of oligo (ethylene glycol) (OEG) terminated thiols, with the molecular formula $(EG)_nOH$[80, 89-92]. The simplified theory is that the water in the buffer solution containing the protein sticks to the –OH terminating groups of the SAM, as they are hydrogen bond acceptor groups, forming a stable solid-liquid interphase that causes steric repulsion as the protein cannot replace the bound water[93, 94].

Prime and Whitesides were among the first to demonstrate that ethylene glycol SAMs reduce protein adsorption onto surfaces[119], by using monolayers of varying chain length $(EG)_n$ and characterizing the reduction of protein adsorption by XPS and ellipsometry. They later also found that a helical form of OEG forms a more stable protein adsorption barrier to the *trans* form, as water binds more tightly[120]. Experimentation using OEG SAMs has since extended to many cellular adhesion studies, showing a reduced attachment of bacterial species including *Staphylococcus*[90, 95], and *Helicobacter pylori*[121].

At the other end of the spectrum, a more recent approach to anti-adhesive coatings is the development of superhydrophobic surfaces[97, 98], based on the 'Lotus effect', whereby water drops roll off the Lotus leaf surface under a slight force, taking with it any dissolved biofouling molecules and cells. The idea is that instead of a surface that 'prefers' water to the solute, prevention of biofouling could potentially occur by repelling the water altogether, removing molecules by a slight external force. However, experimentation is still in its infancy, but promises to be a potential alternative to using ethylene glycol moieties.

1.3.4.2 Pro-adhesive surfaces

Although most studies involving bacteria and SAMs have mainly involved developing anti-adhesive surfaces, SAMs also provide platforms for the efficient immobilisation of cells, mainly

thus far with the proviso for biosensor applications. As stated previously, adhesion of bacteria to a given surface can be influenced by several factors such as hydrophobicity, the nature of the material and the immobilization of proteins on the surface. Sousa *et al.* (2008) used SAMs with different terminating groups including NH_2, COOH and CH_3 to determine the appropriate surface wettability for S*taphylococcus* attachment, and found that it lay within the 55^o range[122].

SAMs can be used on their own, or functionalized with proteins or carbohydrates using coupling chemistry to selectively attach bacterial cells to the surfaces. Groups have also tailored SAM surfaces to take advantage of the variety of adhesins available on bacterial cell membranes. For instance, Terratez *et al.* (2002) used a SAM with a terminating enzyme (colicin N) which binds with high affinity to the outer membrane protein OmpF of *E. coli*[123]. SAMs have also been used to exploit the FimH-mannose bond that allows *E. coli* to adhere strongly to mannosylated surfaces. Qian *et al,* 2002 used a mannoside derivative with an amino group to covalently couple to carboxylic-acid terminated SAMs using carbodiimide chemistry, forming mannoside-terminated SAMs which *E. coli* then adhered to via the type-1 fimbrial adhesins embedded in the cell wall[124]. Using a similar method, Liang *et al.* (2000), used mannoside-terminated SAMs to measure the adhesion forces of uropathogenic *E. coli* with optical tweezers[125].

1.4 Cellular Patterning

1.4.1 Overview

The ability to position adhesive-dependent cells on a surface with control over their spatial arrangement is being developed for fundamental biological research[126], as many studies involving interacting microorganisms, either with each other or with the environment, would benefit from simple devices able to deposit cells in precisely defined patterns. The isolation of cells on a surface enables the study of events occurring in each individual cell, instead of relying

on statistical distributions based on populations of cells. Furthermore, patterning in conjunction with adhesive surfaces prevents motile cells from migrating across the surface, and therefore makes it straightforward to observe single cells repeatedly.

The approaches to cellular patterning can be generally grouped in two forms: indirect or active placement patterning[127]. Indirect patterning involves patterning an adhesive biomaterial onto a surface, such that the cells will attach to adhesive regions in the same pattern[128], whereas active placement (a less common technique) involves the direct delivery of cells to an adhesive surface already in a patterned format. The most common patterning procedure that can be used for both patterning types is microcontact printing (μCP)[129], a soft lithographic method that uses relief features created on stamp, to directly deposit or remove biomolecules or cells onto surfaces.

1.5.2 Microcontact Printing

1.5.2.1 The μCP process

The μCP process (**Fig 1.12**) involves the fabrication of polydimethoxysiloxane (PDMS) stamps by depositing a monomeric precursor over a silicon master and subsequently curing it at 60^{o}C (**step a**). The stamp is then peeled from the master and immersed into or with a surfactant solution (**steps b** and **c**). Excess surfactant is then removed from the stamp surface (step **d**), leaving an "ink". The stamp is then brought into conformal contact with the substrate (**step e**), which can include SAM surfaces. The ink is transferred to the substrate where it forms a patterned surface (**step f**).

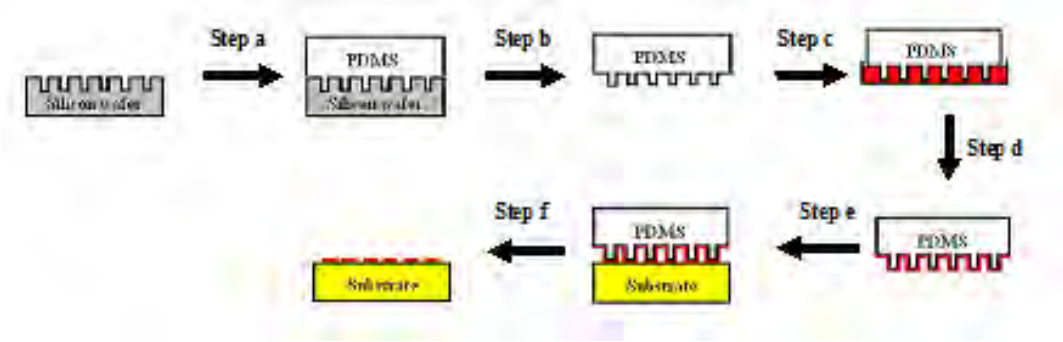

Fig 1.12 The microcontact printing process.

As the stamps can be constructed with almost any pattern, conformal contact can be achieved in many different geometrically controlled ways[130]. PDMS is the material most frequently used as it results in a soft polymer, and therefore conformal contact, although there is recent interest in the use of hydrogel stamps such as agarose for cellular patterning as they are generally more biocompatible. Transfer of surfactant molecules is fast; contact duration of a few seconds is needed and efficiency of transfer can exceed 99%. Patterns of biomolecules obtained in this way have high contrast and resolution because of the mechanical stability of the pattern of the stamp, and because adsorbed proteins show virtually no surface diffusion.

Problems of µCP include swelling of the stamp during inking, resulting in an increase in pattern size. Additionally, PDMS biocompatibility can be an issue as the stamps are very hydrophobic, which can be a problem if used in conjunction with polar inks, and the stamp may deform due to pairing buckling or roof collapse resulting in distorted patterns.

1.4.2.2. Indirect patterning of bacteria with µCP

µCP has been used in a variety of ways for indirect bacterial patterning, usually by directly delivering adhesive or inert biomolecules (including proteins, carbohydrates, thiols and salines) in a patterned format to surfaces for bacterial patterning. For example, Cerf *et al.*, 2008 created

arrays of living bacteria by patterning inert octadecyltrichlorosilanes using PDMS, followed by backfilling with adhesive streptavin-biotin molecules, thereby engineering the surface to selectively attach GFP-*E. coli* cells in patterned 10 µm circles[131] (**Fig 1.13**).

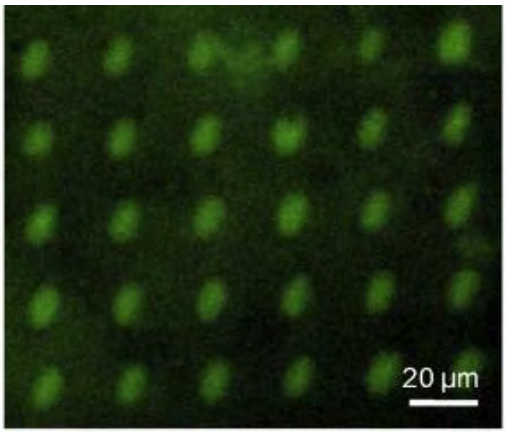

Fig 1.13 Arrays of *E. coli* immobilised onto microcontact printed biotin[131].

Additionally, µCP has been used to directly print thiol molecules. A SAM of an alkanethiol can be patterned onto a gold-coated surface by µCP and functionalised, followed by backfilling the un-patterned regions with an anti-adhesive OEG thiol, thus creating islands of SAMs that absorb proteins and cells, surrounded by SAMs which resist cellular absorption. Rowan *et al.* 2002 used a PDMS stamp to print patterns of hydrophobic and reactive SAMs on gold to produce 'enclosures' that trapped cells of *E. coli*[132].

1.4.2.3 Direct patterning of bacteria with µCP

Instead of printing functional molecules to induce or inhibit cellular adhesion, stamps can be directly 'inked' with bacterial suspensions and printed directly onto a surface. The advantage of this method is that it is relatively rapid, and therefore limits cell exposure time to the environment; bacteria can be transferred directly to surfaces and covered in less than a minute[133]. Recently, Xu *et al*., 2007 employed µCP to directly print bacteria using artificially hydrophilized PDMS stamps onto the surface of a nutrient-containing matrix (*i.e.* agarose), producing high-resolution arrays of living bacteria[134] (**Fig 1.14**)

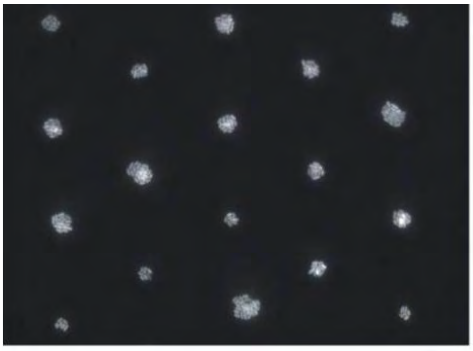

Fig 1.14 Arrays of *E. coli* directly patterned onto agarose substrates[134].

Similarly, Weibel *et al.* (2004) used micropatterned agarose stamps to print patterns of *E. coli* on agar plates (**Fig 1.15**). Agarose is a linear polysaccharide consisting of galactose and 3,6-anhydrogalactose subunits, and can be stamps can be made by casting hot solutions over PDMS masters. The agarose stamps were inked directly with suspensions of bacteria; with stamp features of 200 µm, and they found that the stamp supported many bacterial cell types when culture media was included[135].

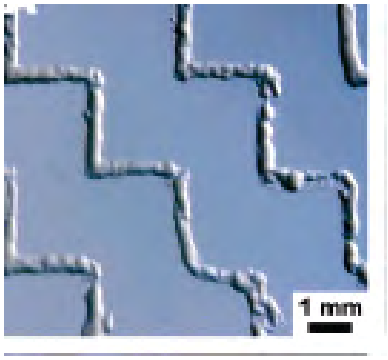

Fig 1.15 Arrays of *E. coli* directly patterned onto agarose substrates using agarose stamps[135]

1.4.3 Other Patterning Techniques

1.4.3.1 Microfluidics

As well as µCP, PDMS has been widely used for creating microfluidic channels and networks which can be used so that they 'capture' or separate cells, and can be used to study cellular

processes such as quorum sensing, and responses to chemical gradients. An interesting adaptaion was employed by Balaban *et al.,* 2004, for producing motile, filamentous cells of *E. coli* with different shapes, by confining and growing the cells agarose microchambers. In the presence of an antibiotic (cephalexin) that inhibits septation, the *E. coli* cells filamented and adopted the shape of the microchambers in which they grew[136]. Microfluidic channels are formed by placing a layer of PDMS with channels created on the surface in contact with glass or a polymer surface that forms the roof of the channel[133]. Laminar fluid flow can then be streamed into networks of branching and recombining microchannels to produce stable gradients of nutrients and cells[137]. An example where microfluidics has been used for cellular patterning includes work undertaken by Takayama *et al.* (2003). They patterned two different cell types by using multiple flow streams in capillary channels. Within these micro-channels, two or more laminar flow streams can flow parallel to each other due to low convective mixing and the width of each cell pattern can easily be controlled by adjusting the flow rate[138].

1.4.3.2 Jet Based Methods

Inkject printers have been used to create large arrays of bacterial cells. There are two main types of inject printer, thermal and piezoelectric. In thermal printers, a resistive heating element causes airbubbles to expand and expel a liquid drop which containing a bacterial suspension[139]. Piezoelectric inkjets use a voltage-induced deformation of a rectangular piezoelectric crystal to squeeze inkjets through the nozzle – these can generally print a wider variety of solvents and are easier to clean[140]. An exciting inkjet patterning experiment employed by Merrin *et al.,* 2007 adapted a simple piezoelectric printer for patterning bacteria onto a substrates, including glass slides, agar plates and nitrocellulose membranes with a printing viability of 98.5%[141]. They were able to form patterned co-cultures as the printhead contained six parallel linear banks of 32 nozzles each, with each bank connected to a different ink source (**Fig 1.16**). Connecting the

inkjet to a motorised stage enabled them to vary the spacing between cultures, and allowed small drop volumes of typically less than 30 pl.

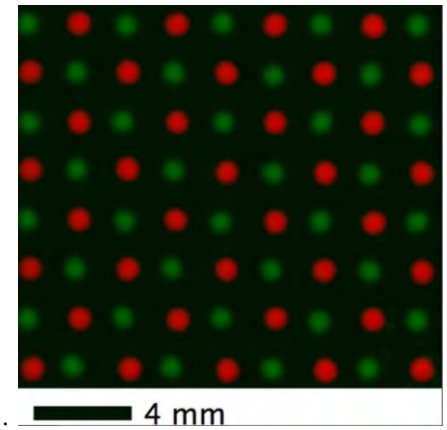

. **Fig 1.16** Arrays of GFP and RFP *E. coli* directly patterned onto agarose substrates using Piezoelectric inkjets[141]

1.4.3.3 Stencils

This approach to patterning is a very simple but effective method, by using PDMS with mico-engineered holes that can be deposited onto an adhesive SAM, followed by immersion of cells into the holes to promote patterned deposition onto the surface. For example, Eun and Weibel, 2009, used freestanding, elastomeric stencils with microfabricated "holes" with different shapes and dimensions to control the spatial adhesion and growth of bacterial cells on polyelectrolyte surfaces, including *Pseudomonas aeruginosa*[142].

1.4.3.4 Robotics

Perhaps one of the most technologically advanced methods of directly patterning bacterial cells is via the use of robotic micromanipulators. Traditionally, printing techniques in laboratories are employed by hand, which can be time consuming and poorly-repeatable. Using micromanipulators with an X-Y-Z controlled stage controlled by computers offers a repeatable and large-scale alternative for constructing massive arrays of bacteria with micrometre resolution[143]. For example, Ingham *et al.*, 2010, used a high throughput contact printing method,

employing a microscope and a stamp with massive arrays of PDMS pins with 20 μm area connected to a motorized stage. They were able to deposit viable bacteria onto porous aluminium oxide followed by effective segregation of microcolonies during out growth[143] (**Fig 1.17**).

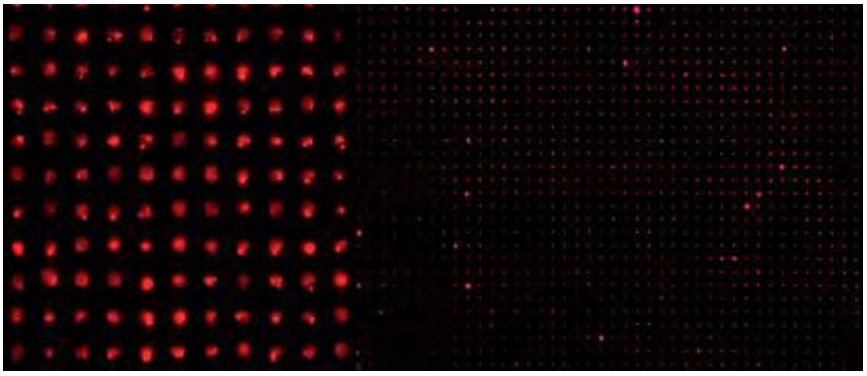

. **Fig 1.17** Arrays of RFP *E. coli* directly patterned onto porous aluminium oxide using PDMS pins controlled with a micromanipulator[143]

1.4.4 Summary of Patterning Techniques

The images of micro-patterned bacteria shown in this section, although constructed through different patterning methods, all look very similar and most have the disadvantage of not being suitable for forming co-cultured patterns. Many are simply too big, creating massive arrays of bacteria and preventing analysis of individual cells. Most, however, have the shortcoming of using anti-adhesive regions to separate the cell colonies. These single-cell systems, although useful for creating large arrays of bacteria, have the disadvantage that the behavior of isolated cells may be very different from when surrounded by other cells, and additionally it makes it difficult for studying cell-cell interactions such as gene transfer. Considering the aim of this project is to study conjugation in *E. coli* using RK2, the existing pattern techniques must be modified for co-culture formation so that the donors and recipients are touching, but clearly defined and ordered so we can follow a "wave" of gene transfer and know where the transfer events are originating from.

1.5 PhD Aim and Objectives

The aim of my PhD degree is to design and fabricate a novel patterning technique for bacterial co-culture immobilisation onto functionalised surfaces, so that conjugation between donor and recipient cells can be observed in real time in spatially defined environments. This project will concentrate on the development of:

1) The construction and characterisation of mannose-terminated SAMs for the efficient immobilisation of *E. coli* via the fimbrial adhesin FimH.

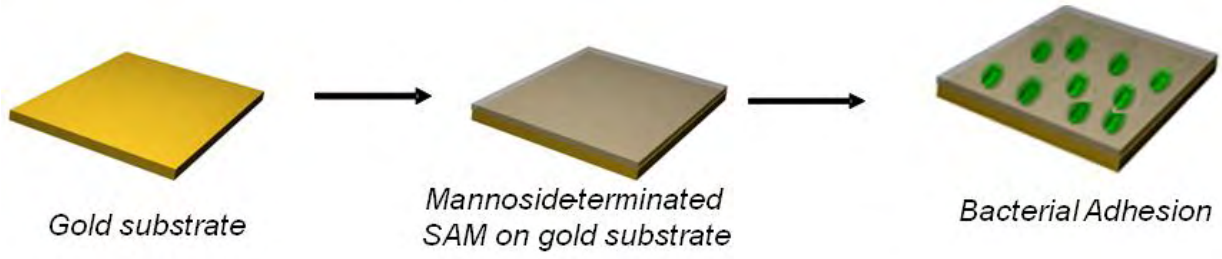

Fig 1.18 Schematic representation showing fabrication of adhesive surface

2) Modification of existing printing techniques to support the robust micro-patterning of co-cultures of *E. coli* onto the SAM surfaces

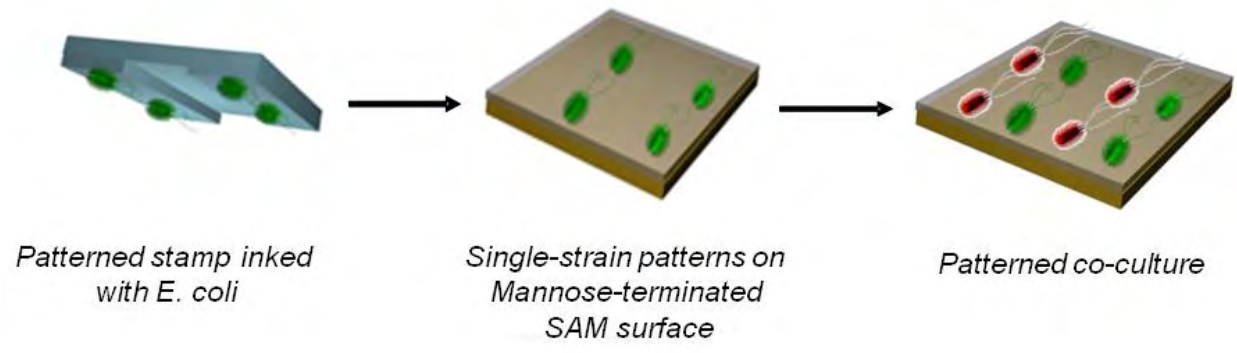

Fig 1.19 Schematic representation showing micro-patterning process

3) Modification of an existing conjugative plasmid (an RK2 derivative) with Lac operator cassettes so that real-time visualization of conjugation can be achieved via the formation of fluorescent foci in the micro-patterned co-cultures.

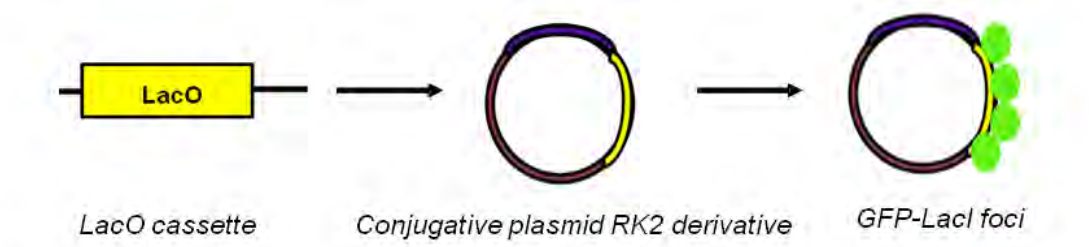

Fig 1.20 Schematic representation of RK2 modification with Lac operator.

Chapter 2: Surface Characterisation and Imaging Techniques

Abstract: *In this chapter, various techniques for surface characterisation are reviewed. Techniques such as X-ray photoelectron spectroscopy (for surface elemental composition, ellipsometry (for surface thickness) and contact angle (for wettability) are employed to characterisethe prepared surfaces. Other techniques are such as fluorescence and confocal microscopy (for cellular visualisation studies) and surface plasmon resonance (for real time binding events on surface) are also utilized to study the cellular adhesion events, patterning processes and gene transfer events in this project.*

2.1 XPS

X-ray Photoelectron Spectroscopy (XPS) is widely used to investigate the chemical composition of surfaces. In surface chemistry the technique can be used to determine the type and quantity of elements present on a substrate, thereby clarifying that the required molecules are present. A solid substrate is irradiated with monochromatic beam X-rays in a vacuum environment, which penetrate up to 100 Å deep and ionize atoms in the surface region[144]. **Fig 2.1** shows the general set up of the XPS machine. Samples are irradiated with X-Ray beams, which cause ionization of electrons that are analysed and detected according to their kinetic energy.

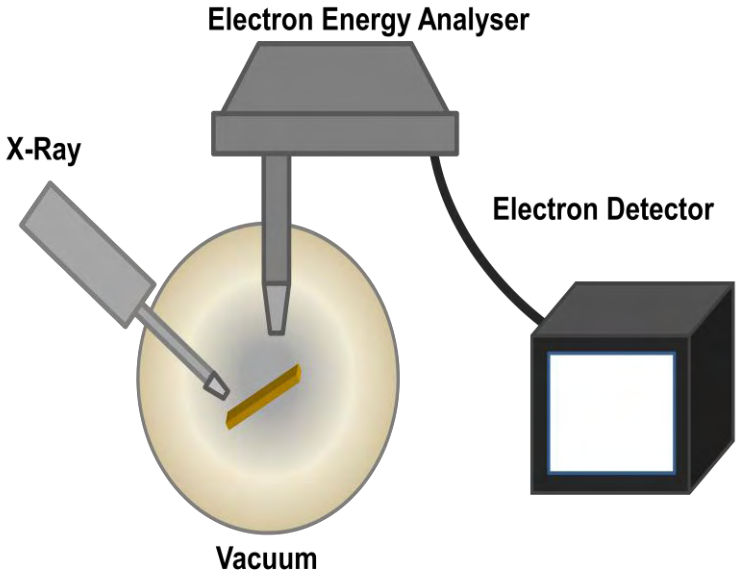

Fig 2.1: Schematic representation of the XPS machine

The purpose of the vacuum is to remove adsorbed gases from the sample, eliminate adsorption of contaminants and increase the mean free path for electrons, ions and photons. Mg Kα and Al Kα X-rays are chosen for their ability to irradiate the surface with high energy photons, which penetrate below the Fermi level in individual atoms to ionize the electrons in *core level* orbitals[145]. Electrons near the Fermi level are at the highest energy state, and are constantly moving due to the reduced binding effect of the nucleus. They are in a similar state in all elements, and they therefore carry little information about a particular element. However, electrons below the Fermi level are close to the nucleus, and will therefore have binding energies characteristic of their element. In XPS the X-ray energy causes these electrons to be excited and overcome the binding energy of their atomic orbitals so they are emitted as photoelectrons, which can be detected with a spectrometer and analysed according to their kinetic energy [103] as shown in **Fig 2.2**, using oxygen as an example:

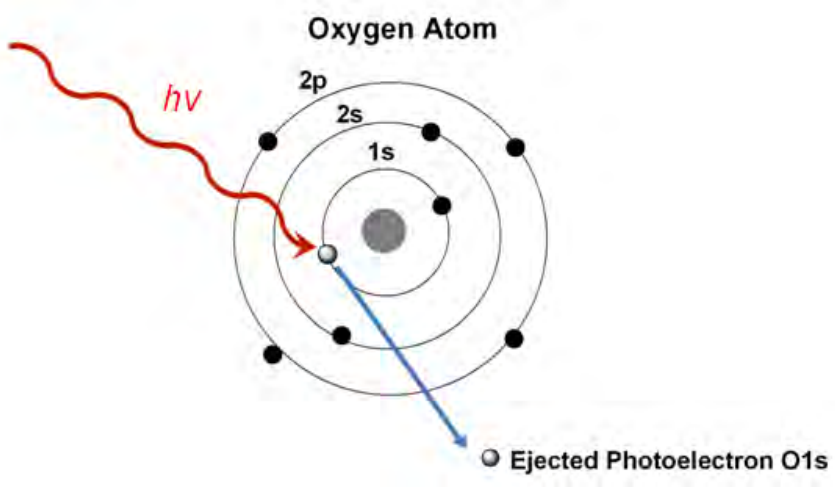

Fig 2.2: Schematic representation of core-electron ionisation in an oxygen atom

The kinetic energy of each photoelectron released can be measured and used to calculate the binding energy of the surface element using **equation 2.1** which shows the relationship between the X-ray (*hv*), binding energy (BE), kinetic energy (KE) and the work function (ø) of the spectrometer[2]. The work function is the difference between the Fermi level and vacuum level.

$$BE = hv - KE - ø \qquad \textbf{(equation 2.1)}$$

The binding energy is essentially given by an energy difference between the initial (ground) state and a final (core–hole) state of an atom[146]. Each element has its own kinetic energy values and subsequently its own unique set of binding energy peaks, which can be used to detect the composition of elements present on surfaces. Electrons are preferentially emitted from the inner shells; in smaller elements such as nitrogen and sulphur the most intense peaks can be found at the 1s and 2p levels respectively, and larger elements such as gold display intense peaks at the 4f orbital level[147]. Ionized electrons produce a spectrum which is plotted as the number of detected electrons against binding energy. Since the number of ejected electrons is proportional to the number of atoms on the surface, a quantitative elemental composition of the surface can be calculated, allowing surface ratios to be derived between different elements[145].

Energy splitting of a photoelectron causes some peaks in XPS to be displayed as spin orbitals, or doublet peaks, which takes into account the total angular momentum of the electron emitted (**j**), which is a combination of the orbital angular (**l**) and the spin (**s**) momenta[148]. Electrons have an **s** of 1/2, and **l** increases with the number of orbitals (s = 0; p = 1; d = 2; f = 3)

There are two possible final states of the total angular momentum shown in equation **2.2**:

$$\mathbf{j_+ = l + s} \textit{ and } \mathbf{j_- = l - s} \qquad \textbf{(equation 2.2)}$$

Fig 2.3 shows an example of the doublet-peaks of gold detected on a surface using XPS. As the electrons are emitted from the 4f orbitals, the doublet peaks will be 4f 5/2 ($\mathbf{j_- = 3 - 1/2}$) and 4f 7/2 ($\mathbf{j_+ = 3 + 1/2}$). Elements such as oxygen and nitrogen have electrons emitted from the s orbitals, so they do not have doublet peaks.

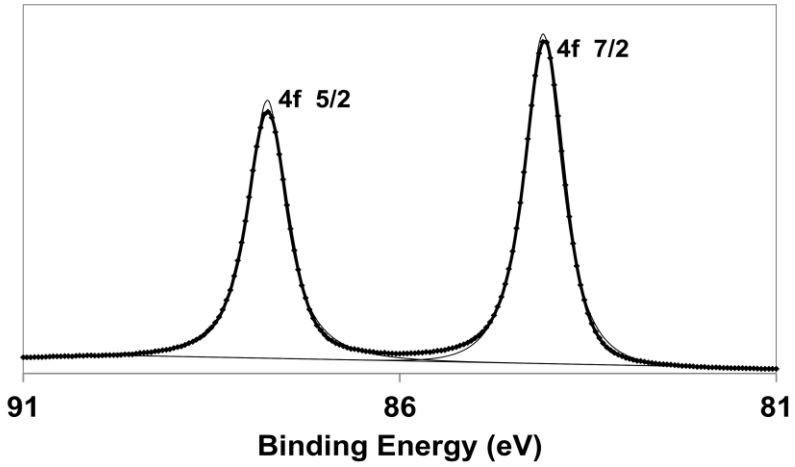

Fig 2.3: XPS spectra of gold detected on a SAM substrate surface

One of the main advantages of using XPS is that it allows the detection of different molecular groups residing on a surface. Chemical bonding between atoms has an effect on both the initial and final energy state of individual atoms, which arise from differences in the chemical potential and polarizability of compound. This changes the binding energy of the electrons, leading to a

chemical shift which displaces the peaks on the spectra, allowing the detection of the chemical state of the surface being analysed[144]. Chemical shifts are tabulated for many elements, meaning the XPS technique can be used to detect, in carbon for example, the difference between a C=O group (289 -291 eV) and a C-O-C group (287-288 eV).

2.2 Ellipsometry

Ellipsometry is a non-contact and non-destructive optical technique used for surface analysis, including the measurement of surface thickness of up to 1000 Å[149]. Ellipsometry measures the change in polarisation of light upon reflection from a surface[150]. In accordance with Maxwell's postulates, light contains two perpendicular vectors; amplitude of electric field (E) and amplitude of magnetic field (B). The variation with time of the orientation of E along the propagation direction at a fixed location is called polarization. Normal light is un-polarized because E oscillates randomly in many different directions; however, it can be polarized using a polarizer, which absorbs and amplifies the light wave whose E is perpendicular to the transmission axis (TA)[151]. The polarized light can be directed at the sample surface at an angle, where it resolves into s-polarized and p-polarized components and is reflected off the surface, as shown in **Fig 2.4**.

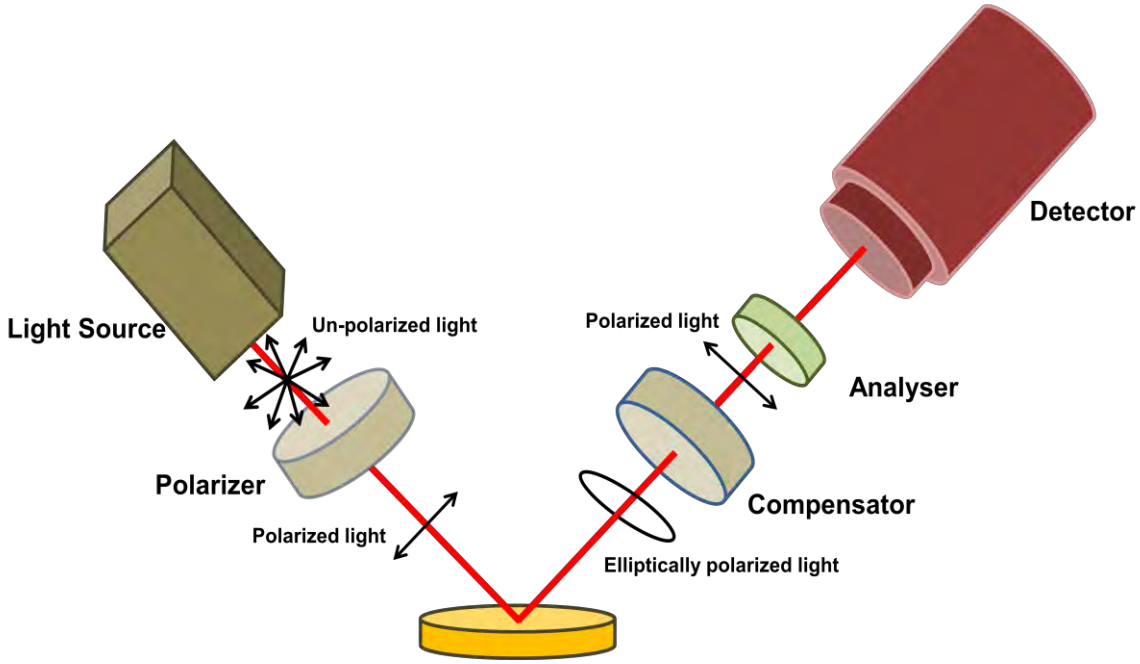

Fig 2.4: Schematic representation of the Ellipsometer

The s-plane is perpendicular to the plane of incidence and the p-plane is parallel to the plane of incidence[152]. These s- and p-polarized components are reflected off the surface differently due to the refraction through the thin film and hence the amplitude and phases of both components are changed. Ellipsometry uses this phenomenon to calculate the thickness of a transition region between the surface and air, by measuring the ratio r between r_p and r_s (the reflection coefficients of the p- and s- polarized light respectively[153]).

Different molecules present on the substrate surface will change the refractive index, and hence the reflection co-efficients of the s and p components. Therefore, a change in reflection equals a change in thickness so differences between samples can be determined[154]. SAM thickness values are based on the model of Air/SAM/Solid in which SAMs are assumed to be defect free (homogenous) and with a refractive index of 1.51[155]. The model is calculated using the Cauchy transparent layer, where the thickness is obtained using multi guess iterations and provides a thickness result with the lowest χ^2(chi-square distribution).

2.3 Contact Angle Goniometry

Contact angle goniometry is a technique that is used to measure the surface wettability of a substrate (i.e. whether it is hydrophobic or hydrophilic) and the surface roughness. The simple set up of contact angle goniometer is shown in **Fig 2.5**:

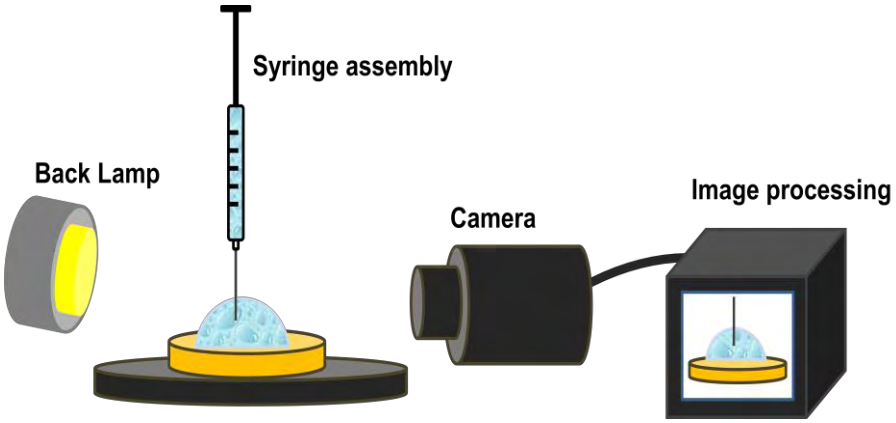

Fig 2.5: Schematic representation of contact angle assembly. Included in the set-up is a syringe filled with the solution of interest (e.g. water), a fibre optic back lamp for illuminating the surface and a CCD camera connected to a computer for analysis.

Contact angle is formed between the solid/liquid interface and the liquid/vapour interface, and can be measured by adding and withdrawing a droplet of water through the needle onto the substrate surface; followed by measuring the profile of the drop and measuring two-dimensionally the angle formed between the solid and the drop profile. The addition of water produces the advancing contact angle ($\boldsymbol{\theta_a}$) and the withdrawal of water produces the receding contact angle ($\boldsymbol{\theta_r}$). The contact angle ($\boldsymbol{\theta}$) is formed at a three phase interface between the liquid-vapour ($\boldsymbol{\gamma_{LV}}$), solid-vapour ($\boldsymbol{\gamma_{SV}}$) and solid-liquid ($\boldsymbol{\gamma_{SL}}$) phases [103, 114] as shown in **Fig 2.6:**

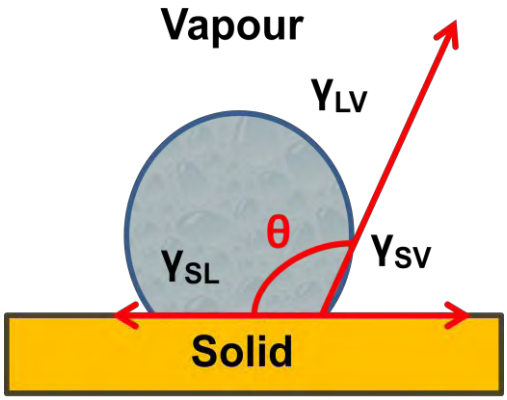

Fig 2.6: A liquid drop on a solid surface forming a contact angle

The static contact angle between a liquid drop and a smooth solid surface is given by the Young's Equation (**equation 2.3**), which is the force balance between the interfacial tensions at the solid-liquid-vapour interface. Young described the relationship between the free energy of a surface as:

$$\gamma_{LV}\cos\theta = \gamma_{SV} - \gamma_{SL} \qquad \textbf{(equation 2.3)}$$

When a droplet is added to a surface, the liquid will cover (wet) the surface until an equilibrium contact angle is reached[156]. The angle formed by the droplet once equilibrium has been reached is determined by the surface energy of the sample[157]; this is the combination of dispersion (non-polar) and polar energy, including forces such as coulomb interactions of polar groups, dipole-dipole interactions and hydrogen bonding. Dispersion energy exists between all molecules but polar energy exists only when polar groups are present; the presence of polar groups on the substrate increases the surface energy, meaning the water droplet will spread out to minimise the free surface energy (**Fig 2.7 a**). Hydrophilic (polar) surfaces therefore have a low advancing contact angle ($<30^{o}$), whereas hydrophobic surfaces tend to have lower free surface energy, leading to reduced spreading of the droplet (**Fig 2.7 b**), thereby eliciting a high advancing contact angle ($>100^{o}$)[158].

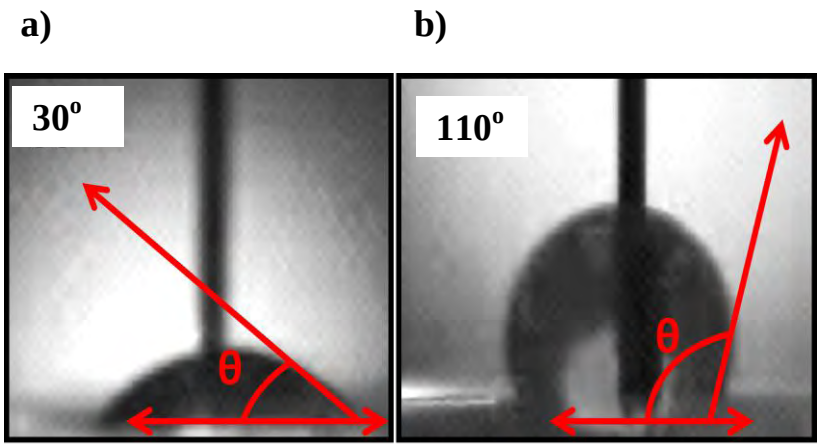

Fig 2.7: A liquid drop on a hydrophilic surface (**a**) and hydrophobic surface (**b**)

Surface roughness can be gauged by measuring the difference between the advancing and receding contact angles, which gives the contact angle hysteresis ($\Delta\theta = \theta_a - \theta_r$). A small hysteresis ($< 5^o$) is an indication of a homogenous, smooth, well ordered surface, whereas a large hysteresis suggests the surface is contaminated, non-homogenous and/or relatively rough[159].

2.4 Surface Plasmon Resonance

Surface plasmon resonance (SPR) measures binding of analyte molecules to surfaces in real time, including binding of proteins and sugars to SAM surfaces[160]. It uses an optical method to measure the refractive index change near a sensor surface inside a flow cell, through which a dielectric aqueous solution passes under continuous flow.

When p-polarised light is directed at metal-coated glass sample at a specific incidence angle (θ_i), light is reflected back off the sample at an angle (θ_r). When this same light is directed through a prism at a sample with a metal/dielectric interface, surface plasmons (SPs) are produced[120, 121]. SPs are charge density electrons that oscillate in resonance with the light wave[161], and that propagate parallel to a metal/dielectric interface[162], as the real part of the dielectric constant Re(ϵ) of the metal and the media are in opposite signs[163]. The electromagnetic field component

of the p-polarized light penetrates the metal layer, and energy is transferred to the free electrons of the metal[164], causing SPs to propagate parallel to the metal-dielectric surface as evanescent waves that have maximum density near the surface, and decay exponentially[165] away from the phase boundary to a penetration depth of approximately 200 nm (**Fig 2.8**).

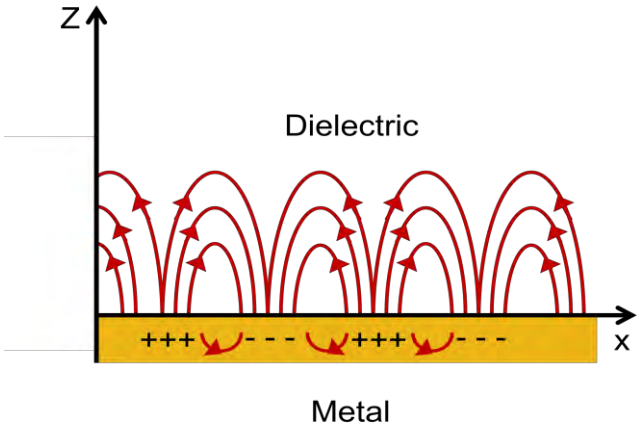

Fig 2.8: Schematic representation of Surface Plasmons. The surface plasmon wave propagates in the x and y directions along the metal- dielectric interface, for up to 100s of microns and decays evanescently in the z-direction with 1/e decay lengths on the order of 200 nm.

The idea of surface plasmon resonance was initially introduced in 1957 by Ritchie[166], who theorized that the loss of energy that fast electrons experience when travelling through thin metal films was the result of surface plasmons. The SPR machine uses this concept to measure the loss of energy after surface plasmon induction; when energy has been transferred to the SPs, there is a decrease in the actual light reflected back off the sample at the angle of incidence, which is detected as reduction in intensity of the reflected light beam by the detector.

However, SPs cannot be excited directly at planar air/metal or water/metal interfaces because the wave vector for the photon and the plasmon need to be equal in both magnitude and direction, and as the field perpendicular to the surface decays exponentially with distance from the surface, the missing momentum must be provided by a coupling prism to enhance the momentum of the incident light[167].

The vast majority of the field of an SP wave is in the dielectric, therefore the propagation constant is very sensitive to changes in refractive index (RI) [164]. The adsorption and desorption of molecules onto the metal surface changes the RI at the metal-dielectric interface, and results in a change in the velocity of the plasmons. This is detected as an angle shift in the intensity minimum of the reflected light (**Fig 2.9 a, b**) therefore SPR is a useful way of detecting real-time binding of analyte molecules to surfaces upon injection into the instrument, which are plotted as response units against time (**Fig 2.9 c**), which in turn translates into the mass of adsorbed materials onto the surface.

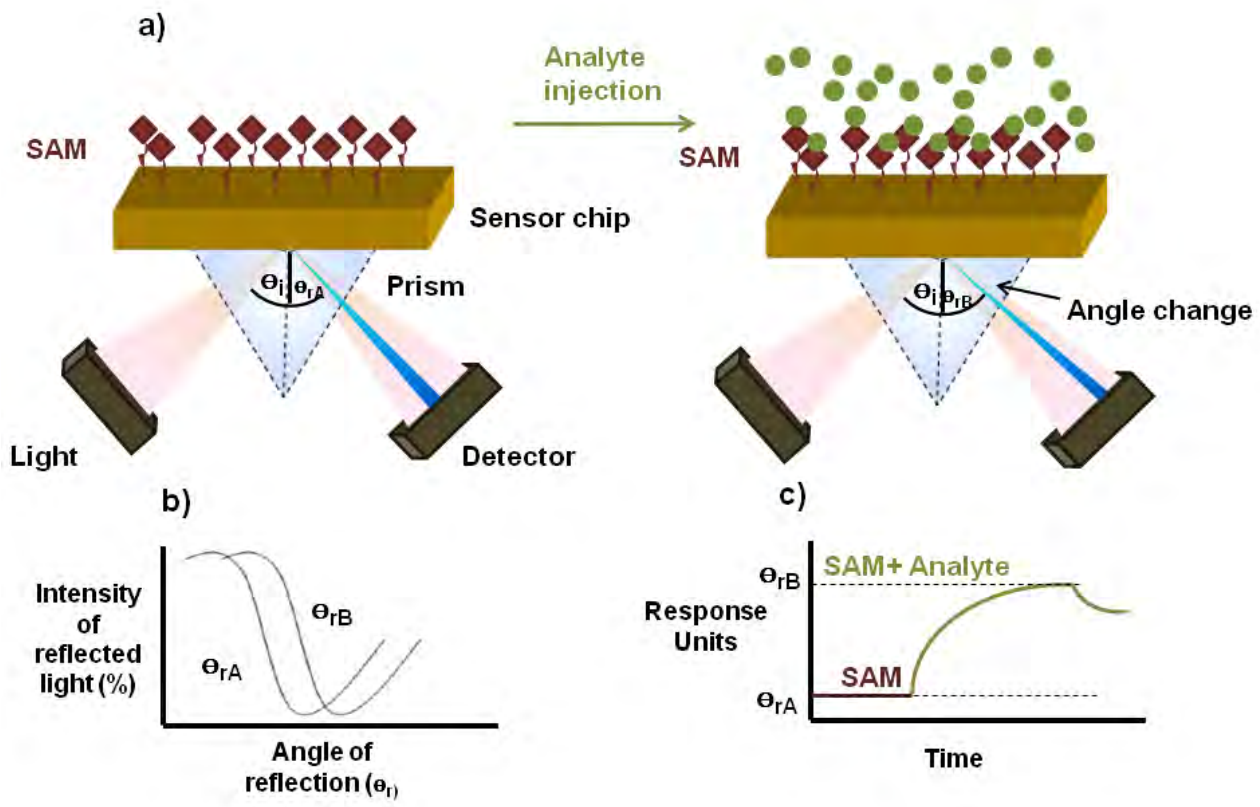

Fig 2.9: Schematic representation of the effect of analyte molecule adsorption onto sensor surface. P-polarized light is directed through the prism, and as a result of the energy transfer, there is a decrease in the reflected light intensity (blue region) at a specific angle of incidence θ_i. After injection **(a)**, biomolecules adsorb to the surface inducing a change in the refractive index and causing a shift of the SPR angle from position $\theta_{rA}$to θ_{rB}**(b)** which is plotted as response units in real time**(c)**

2.5 Imaging Techniques

2.5.1 The Principles of Fluorescence

Fluorescence is a form of luminescence, i.e., the emission of light from a substance due to excitation. Fluorescence occurs when fluorescent molecules absorb electromagnetic radiation of a specific wavelength, and then re-remit the radiation at a different wavelength due to loss of energy. A Jablonksi diagram can further demonstrate the principles of fluorescence to show the different routes by which an excited photon loses its energy. A simplified version is shown in **Fig 2.10**:

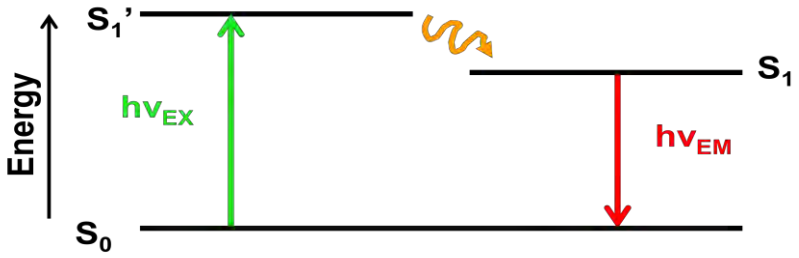

Fig 2.10: Simplified version of the Jablonski diagram, illustrating fluorescence emission by an excited fluorophore

Prior to excitation, the electronic configuration of the molecule is described as being in the ground state **(S_0)**. After absorbing a photon of light ($h\nu_{EX}$), usually of short wavelengths, a fluorophore is excited to higher vibrational level, and the molecule is then said to be in an excited singlet state **(S_1')**[168]. After a finite amount of time, a photon of energy $h\nu_{EM}$ is emitted (S_1), causing fluorescence to be emitted and returning the fluorophore to its original ground state (S_0). This is termed internal conversion and generally occurs within 10^{-12} s or less[169]. Due to energy dissipation during the excited-state lifetime, the energy of this photon is lower, and therefore of longer wavelength. This difference in energy or wavelength represented by ($h\nu_{EX} - h\nu_{EM}$) is called the Stokes' shift, based on the early findings of fluorescence in the 1800's by

George Stokes (**Fig 2.11**). This excited fluorophore is also termed to have "redshifted", i.e., the light emitted from the fluorophore will shift to the right of the spectrum from the excitation light. Therefore, in order to view a fluorophore with red fluorescence, the molecule should be excited with green light.

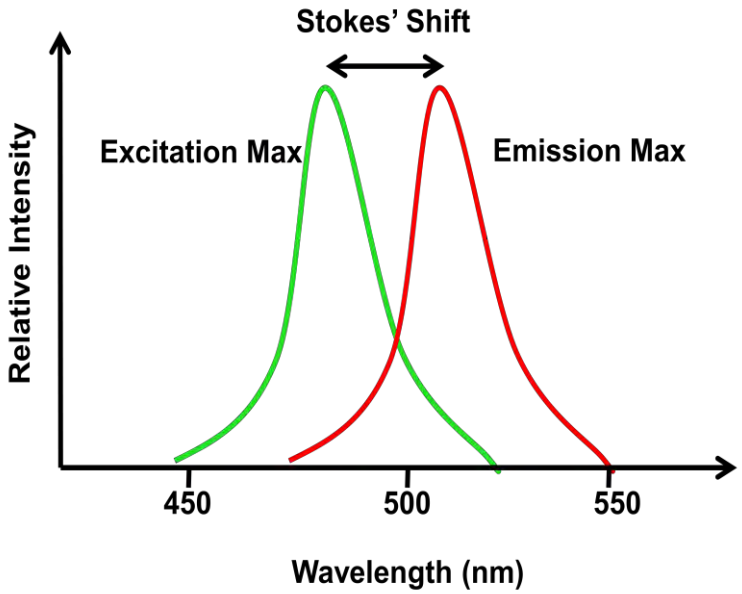

Fig 2.11: Stokes' shift, caused by the difference in wavelength between the excitation max (green) and the emission max (red). A molecule excited with green light would therefore emit red light, and be seen as such through fluorescent microscopy.

2.5.2 Fluorescent Proteins

Any molecule that fluoresces is called a fluorophore, and they are typically aromatic hydrocarbons, and some amino acids including phenylalanine. Direct fluorescence, is when a sample is treated with an engineered fluorescent probe that targets a specific moiety such as a receptor or an enzyme[170]. Examples of fluorescent probes include monoclonal antibodies and antibody fragments[171], peptides, and labelled small molecules[172]. These specific fluorescent probes target specific cellular and sub-cellular organelles and molecules, and non-specific cell dyes target the whole cell, and are generally incorporated into cell membranes.

Indirect fluorescent imaging is when the cell has the ability to produce the fluorescence intrinsically, occasionally with the aid of inducer molecules added to promote expression. The most common method is the introduction of a reporter gene in the cell, which encodes for a fluorescent protein such as GFP[173], which can then be detected with optical imaging methods[174]. Cells can be stably transfected to express FP and report on their position for cell trafficking studies, or the reporter gene can be placed under promoters of interest for studying regulation[175]. In addition, FP genes can be fused to a gene of interest, yielding a chimeric protein that maintains the functionality of the original protein but is tagged with the FP, allowing visualisation of virtually any protein of interest *in vivo*. An example includes the fusion of GFP by Lau *et.al*[176] to tandem repeats of *lac* operators, to permit visualisation of the replication origin and terminus in growing cells of *E. coli.*

A common drawback to the use of both direct and indirect fluorescence imagery is photobleaching. Once a fluorophore has gone through a cycle of excitation and relaxation, it may then be re-excited to continue the fluorescence cycle; however, free radicals generated during the initial excitation process can chemical modify the fluorophore to an extent that it no longer emits light upon excitation, or the fluorophore has undergone covalent modifications with surrounding molecules in its environment[177]. Photobleaching presents many problems for fluorescence microscopy, particularly real-time image generation, as once bleached, images are faded. Different fluorophores will bleach at different rates, as much depends on the chemical structure of the protein and the environment in which it is placed, however experimental modifications including limiting exposure to excitation light can prolong the fluorescent life.

2.5.3 Conventional Fluorescence Microscopy

Fluorescent microscopes detect the energy that is emitted from a sample when illuminated by light at a specific wavelength. The preferred approach in conventional fluorescence microscopy is to irradiate samples with excitation light (I_0), and then spatially detect the emitted light (I_1) which makes up the image[177]. The microscope is fitted with a dichroic beam splitter and an emission filter that selectively removes undesired radiation and allows only the desired wavelength that matches the fluorescing material to pass through to the detector (**Fig 2.12**).

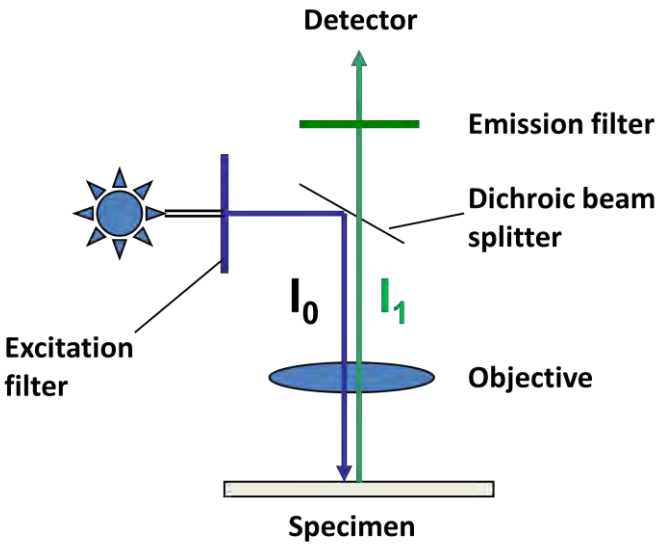

Figure 2.12 Schematic representation of the basic function of the fluorescence microscope.

The radiation collides with the atoms in the specimen and electrons are excited to a higher energy level. The light emitted by fluorescence, which is at a different, longer, wavelength than the illumination, is then detected through a microscope objective. A fundamental difference between ordinary light microscopes and fluorescence microscopes lies in formation of the visible image. Normally, in light microscopes the image is formed by the modification of light passing through the specimen, but fluorescence images are due to light emanating from the specimen after illumination[178]. Therefore in view of the low intensity of most forms of fluorescence and the inevitable light losses of up to 90%, it is essential that the most efficient light source is

employed to illuminate the sample. Traditionally the light source for fluorescence microscopy is therefore via a mercury or xenon burner, rather than an ordinary light bulb.

2.5.4 Scanning Confocal Laser Microscopy (SCLM)

Cells and tissues exist in nature as 3D structures, and one of limitations of conventional fluorescence microscopy is that Z-series images are difficult to produce, partly as the data and images generated are through CDD cameras, rather than computational. Since the development and patent of the confocal and microscope by Marvin Minsky in 1957[179], who built a working microscope in 1955 in order to facilitate improved imaging of neural networks, and its continual modification throughout the years, confocal microscopy has enabled the generation of high resolution images and 3D reconstructions of tissues and cell samples.

Fig 2.13 shows the set up of the confocal microscope. In contrast to conventional microscopes, the illumination in a confocal microscope is achieved by scanning one or more focused laser beams of light through a pinhole across the specimen. The image produced is called an optical section[180]. The pinhole is computationally adjustable and focuses excitation light more directly onto the monochromatic mirror, thereby focusing light more directly to specific regions of the sample, preventing complete illumination of the entire specimen. This minimises photobleaching by directing light to only specific regions of the sample. Emission light passes through a secondary pinhole towards a low noise photomultiplier; this produces a signal that is directly proportional to the brightness of the light[180.] The signal from the photomultiplier is processed with a computer imaging system, and multiple optical sections allow the construction of 3-dimensional data in the form of Z-series. The detected excitation light represents one pixel in the resulting image. As the laser scans over the optical section of interest in an XY direction, a

whole image is obtained pixel by pixel, and line by line, while the brightness of a resulting image pixel corresponds to the relative intensity of detected fluorescent light[181].

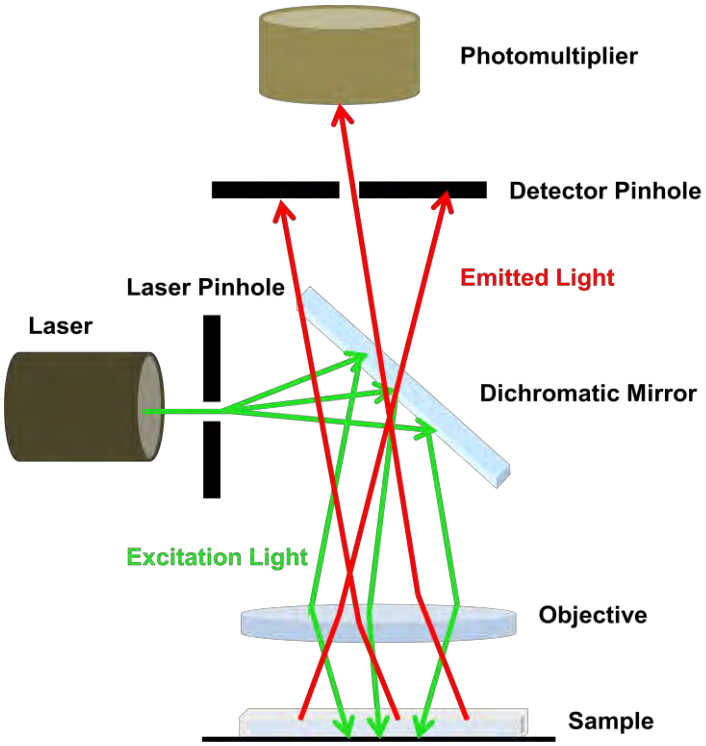

Fig 2.13: Schematic representation of the Confocal Microscope. Incident laser beams of light are directed through a pinhole to the dichromatic mirror, where they are reflected towards the sample. Fluorescent molecules become excited and emit fluorescent light, which is passed through a secondary pinhole towards a photomultiplier, which generates a computational signal allowing image generation and further analysis.

A second pinhole prevents light from above or below the plane of focus from striking the photomultiplier; this improves the resolution of the image, and also limits cross-talk (overlapping of emission spectra) between different fluorophores. Although using conventional fluorescent microscopes is perfectly fine for standard fluorescence imaging, there are problems with photobleaching if used for extended periods as there is no primary pinhole, and illumination of the sample cannot be regulated.

Chapter 3: Construction and Characterisation of Adhesive Surfaces for Bacterial Patterning

Abstract: *The ability to regulate bacterial adhesion on surfaces is of practical impact for the efficient patterning of bacterial co-cultures. This chapter describes the fabrication of mannose-terminated SAMs on gold substrates followed by bacterial adhesion kinetics. This system is based upon the formation of a carboxylic acid-terminated SAM that is subsequently used to bind a mannoside derivative via carbodiimide coupling. It was shown that after two hours on the MT-SAMs bacteria were effectively attached and were resistant to shear flow rates of up to 50 µm/min.*

3.1 Background

The immobilization (and patterning) of bacteria on surfaces provides opportunities for sensing and detecting cell–cell interactions[133] including HGT. Type-1 fimbriae were selected as an adhesive target for bacterial immobilisation for their flexibility[74] and their ability to form tight bonds with mannose residues[182]. They are expressed in most strains of enterobacteria, including *E. coli*, and bind specifically to the mannose functionalised surface via the fimbrial tip-associated subunit FimH. Additionally, it was important to create a functionalized surface that would retain bacterial immobilization under fluid flow conditions, in order to supply the micro-patterned cultures with nutrients. Whereas previous researchers have used biospecific interactions such as antibody-antigen interactions for micro-patterning single bacterial cell types[183], these are unsuitable as they weakened by tensile and shear mechanical force. Recent studies have shown that FimH is able to interact with the mannosylated surface via a shear-enhanced catch bond mechanism[184]. This specific shear stress-enhanced adhesion of bacteria to

mannosylated surfaces will allow the micropatterned bacterial co-cultures to be exposed to shear forces resulting from fluid flow conditions without dislodging the bacteria or causing mixing of the bacterial strains.

SAMs have been used to immobilise cells on surfaces in the study of host–pathogen, and cell-cell interactions. The covalent attachment of biological ligands to the terminal regions of SAMs provides a way of creating a functional surface that can be used to support the adhesion of many cell types, by mimicking the adhesive surfaces of their natural environment[185]. Qian *et al.* (2002) demonstrated that a mannoside-terminated monolayer was able to support the complete adhesion of bacteria on the surface[124], after two hours incubation with *E. coli*. Therefore, for bacterial immobilisation, we used a mannoside-terminated SAM that results in bacterial adhesion mediated by type-1 fimbriae.

3.2 Objective

The first objective of the project was to form an adhesive surface for bacterial attachment, using surface chemistry that would retain bacterial immobilisation under fluid flow conditions. The objective was split into four stages, as depicted in **Fig 3.1**:

a) Carboxylic-acid-terminated SAM (COOH-SAM) formation

b) NHS-ester-terminated SAM formation, allowing coupling of mannoside derivative

c) Covalent coupling of a mannoside derivative to the NHS-ester-terminated SAM, forming a mannoside-terminated SAM (MT-SAM) as an adhesive surface for bacterial attachment

d) Bacterial attachment studies on MT-SAM to confirm the adhesive ability of surface.

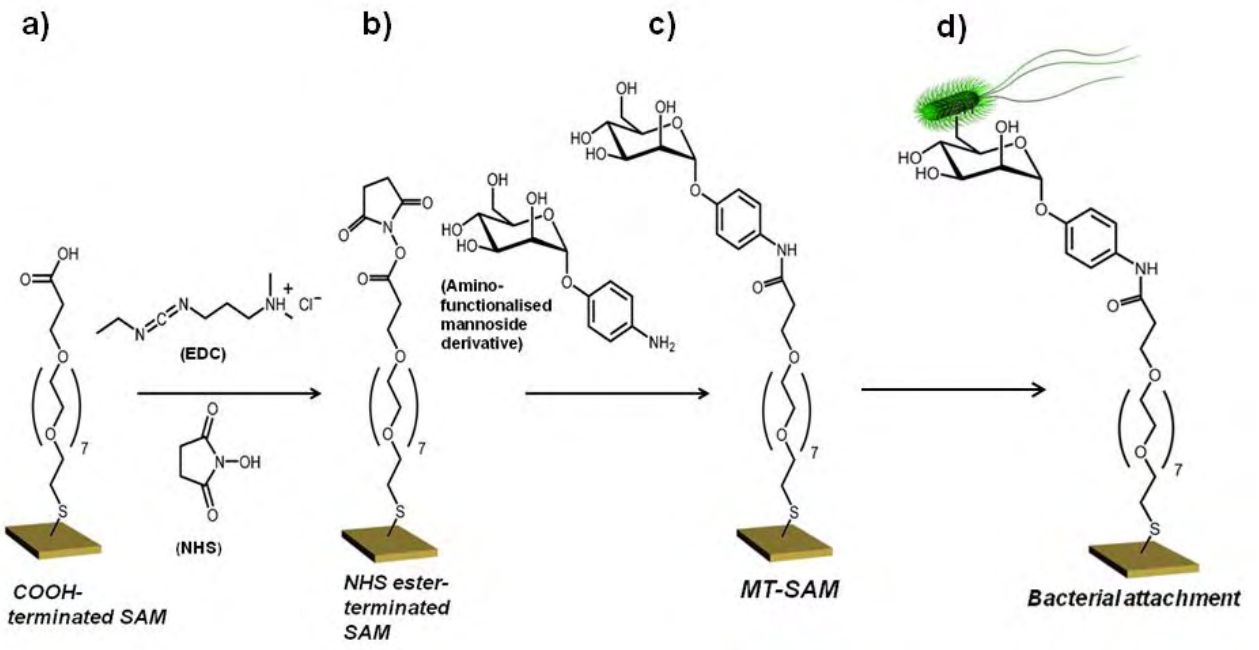

Fig 3.1: Schematic representation of adhesive surface formation, showing COOH-terminated SAMs on gold; addition of NHS in the presence of EDC forming NHS ester-terminated SAMs; covalent coupling of mannoside derivative to form MT- SAMs; bacterial inoculation onto adhesive surface forming a bacterial monolayer

3.2.1 COOH-SAMs

COOH-terminated thiol molecules were selected as the building blocks for mannoside derivative attachment because the carboxylic group can be easily reacted with the terminal amino groups of the mannoside derivative to form an amide bond[124]. Although COOH-terminated SAMs are useful for coupling chemistry, the quality can typically be harder to control than other SAM species such as methyl and hydroxyl, as interplane hydrogen bond formation between the terminal groups of thiolates on gold and free thiols in the bulk solution can cause double layer formation[186], which would block the COOH-groups needed for coupling. Using a small volume of trifluoroacetic acid (TFA) in the thiol solution can disrupt the hydrogen bond between the thiol molecules by forming hydrogen bonds themselves with the thiol molecules. Since these

acids do not have the thiol group when they are rinsed with EtOH containing a base, they are washed away avoiding the formation of a double layer[187].

As well as pure COOH-SAMs, control (anti-adhesive) surfaces were also created using an oligo (ethylene glycol) thiol (EG-SAMs). EG-SAMs are anti-adhesive[94] and can therefore be used as a control SAM surface to confirm the specific attachment of analyte molecules to COOH-terminated SAMs, as well as to confirm that bacterial cells are specifically attaching to the mannoside derivatives, and not via non-specific adsorption.

Before commencing with coupling of mannoside molecules to the COOH-SAMs, they were first characterized by XPS, Ellipsometry and Contact Angle. **Fig 3.2** shows the COOH-terminated thiol molecule and EG-thiol molecule, with the elements and functional groups targeted by surface characterisation techniques.

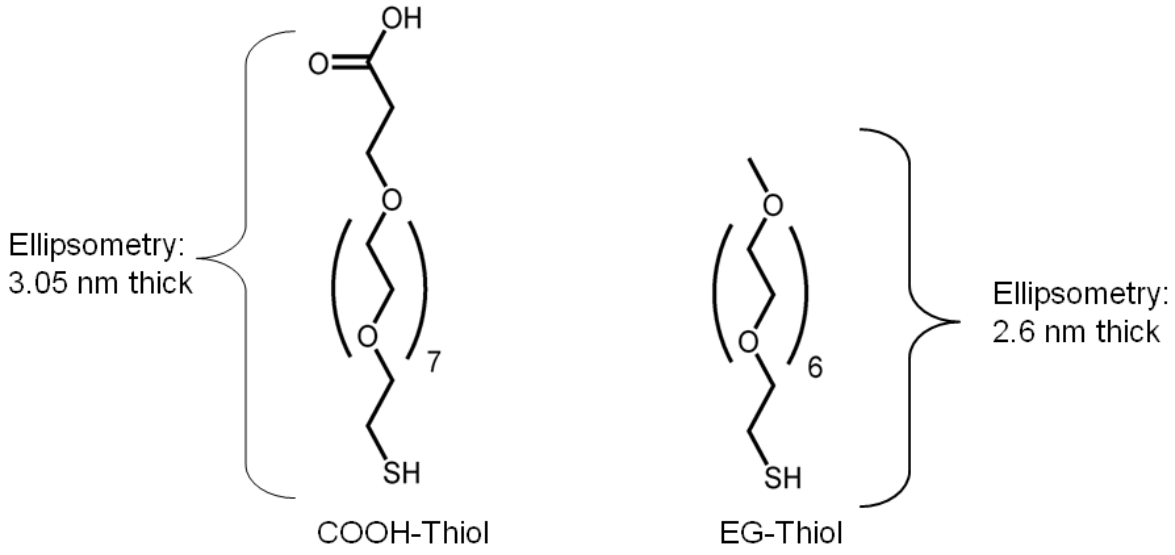

Fig 3.2: Schematic representation of the COOH-thiol molecule

Ellipsometry enables the thickness of the SAM to be determined – the theoretical length as measured by Chem Draw is 3.05 nm. Thicknesses larger than this could indicate double layer formation, meaning that the terminating groups would not be exposed for coupling. Due to the

COOH-terminating group, the advancing Contact Angle of the SAM should be very low, as the surface is very hydrophilic. XPS is a powerful tool that can be used to analyse the specific chemical elements on a surface. Scanning the SAM surface for the presence of sulfur (from the –S-Au bond), oxygen (from the C-O and C=O groups) and carbon (from the C-C, the COOH and the C-O) groups would indicate the presence of the COOH-thiol.

3.2.2 MT-SAMs

A mannoside derivative was selected that was covalently attached to an amino group, in order to enable coupling to the COOH-SAMs using carbodiimide chemistry. EDC in the presence of NHS causes the carboxylic acid groups to be converted into amine-reactive NHS esters; this intermediate can then be used to form a stable amide bond between the amino group of the mannoside molecule and the carboxylic acid on the SAM surface. This reaction is usually completed within 10 minutes, as the intermediate is susceptible to hydrolysis, making it unstable and short-lived in aqueous solution[109].

Before bacterial attachment studies, the mannoside residue was tested for its ability to selectively couple with mannose-binding proteins by attaching a lectin, Concanavalin A (ConA). ConA is a multivalent R-D-mannopyranoside binding lectin. Both Mn^{2+} and Ca^{2+} ions are required for activity, and between pH5.8 and 7.0 the lectin exists as a tetramer and is capable of binding four terminal R-D-mannopyranosyl residues[188]. The binding specificity of ConA to mannose means that its attachment to the MT-SAMs would not only confirm that the mannose residues were coupled to the SAM surface, but would also indicate that they were bioactive, which would allow bacterial immobilisation to commence.

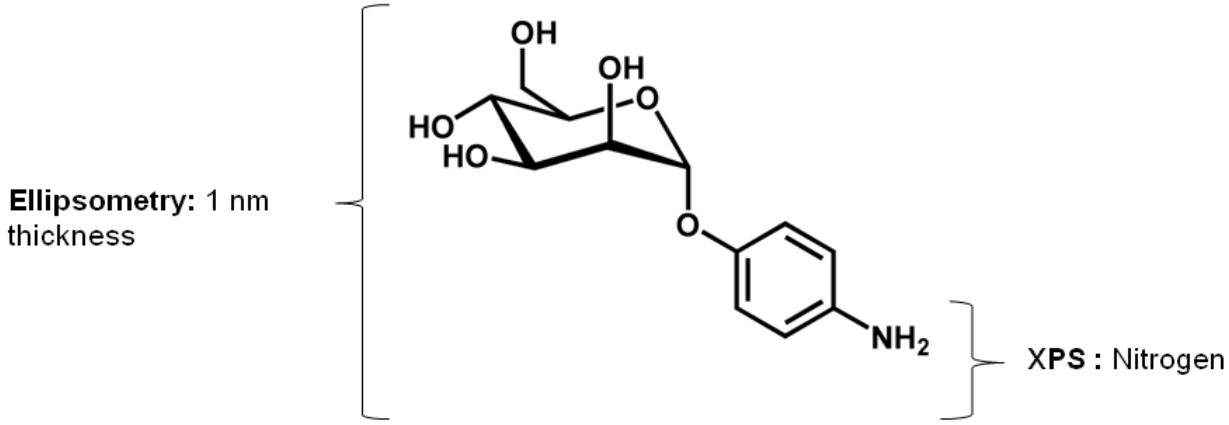

Fig 3.3: Schematic representation of the mannoside derivative

The MT-SAMs formation and ConA attachment was confirmed by XPS, ellipsometry and SPR. **Fig 3.3** shows the mannoside molecule, with the elements and functional groups targeted by surface characterisation techniques. An increase in thickness detected by ellipsometry from the original COOH-terminated SAM would indicate further attachment of the adhesive molecules. Importantly, the mannoside molecule and ConA contain nitrogen, which is not present in the COOH-terminated SAM. XPS can therefore be used to detect the presence of nitrogen on the MT-SAM surface, showing that the mannoside molecule and ConA have been immobilised onto the surface. Additionally, N/Au ratios can be obtained from the XPS data – giving quantitative information of the amount of nitrogen on the surface. ConA is a large protein with many nitrogen containing groups, therefore it is expected that there would be a greater N/Au ratio than the mannoside-residues, allowing the ConA to be detected.

SPR can be used to measure real-time binding of mannoside molecules and ConA to the COOH-terminated SAMs. SPR involves the use of a flow cell that allows aqueous solutions to pass over the Au surfaces at fixed rates. The biomolecule that needs to be attached to the surface (i.e mannose, ConA) is injected into the flow cell, where it passes over the SAMs. As the

biomolecules bind to the surface it causes a change in the refractive index, which is measured in real time, and the result plotted as response or resonance units (RUs)[160]. This technique is very valuable, as it allows the binding of the adhesive molecules to the SAM surface to occur continuously in a contained system, meaning less contamination and experimental error. Additionally, the ability to control the flow means that separate samples can be rinsed at the same rate each time, and all of the excess molecules on the surface can be removed, allowing the distinction between specific and non-specific binding. Additionally, only a small amount of the sample is required for each experiment (typically 500 µl per injection)[189].

3.2.3 Bacterial Adhesion Studies

For initial studies of bacterial adhesion and patterning, a fimbriated *E. coli* strain (verified by yeast cell agglutination) was selected that expresses GFP, to allow detection through fluorescence microscopy. As it can take time for bacteria to attach to surfaces, even with specific bonding mechanisms, a kinetic study was first employed to ascertain the time needed for the cells to fully adhere to the MT-SAMs. Under sterile conditions, MT-SAMs were incubated with *E. coli* and then rinsed with sterile PBS to remove any unattached cells. Fluorescence microscopy was then used to visualise the bacterial monolayers to determine the quantity of cellular attachment.

SPR was also employed to provide complimentary data for fluorescence adhesion studies. As it measures binding of molecules in real time, SPR provides kinetic data for the rate of bacterial adhesion to MT-SAM surfaces.

In order to confirm that bacterial immobilisation was retained under shear force, a flow cell was constructed (**Fig 3.4**) from PEEK (polyetheretherketone), a heavy duty but inert polymer that can withstand heating over to 300^{o}C[190]. The flow cell was designed to take into account the

dimensions of the Au substrate (1 cm by 1 cm), and the maximum working distance of the x63 objective from the Confocal microscope (160 µm). Sterile plastic tubing was connected to both ends of the flow cell, with an internal diameter of 1 cm, with one end attached to a media bottle on a heated stage, and the other siphoning into as a waste reservoir. The media was kept at 37^{o}C, which is the optimum temperature for *E. coli* growth, and it was connected to a peristaltic pump which allowed for control over flow rates. The bacteria coated SAM surface could then be inserted into the flow cell, covered with a glass cover-slip, and placed under the microscope under continuous flow.

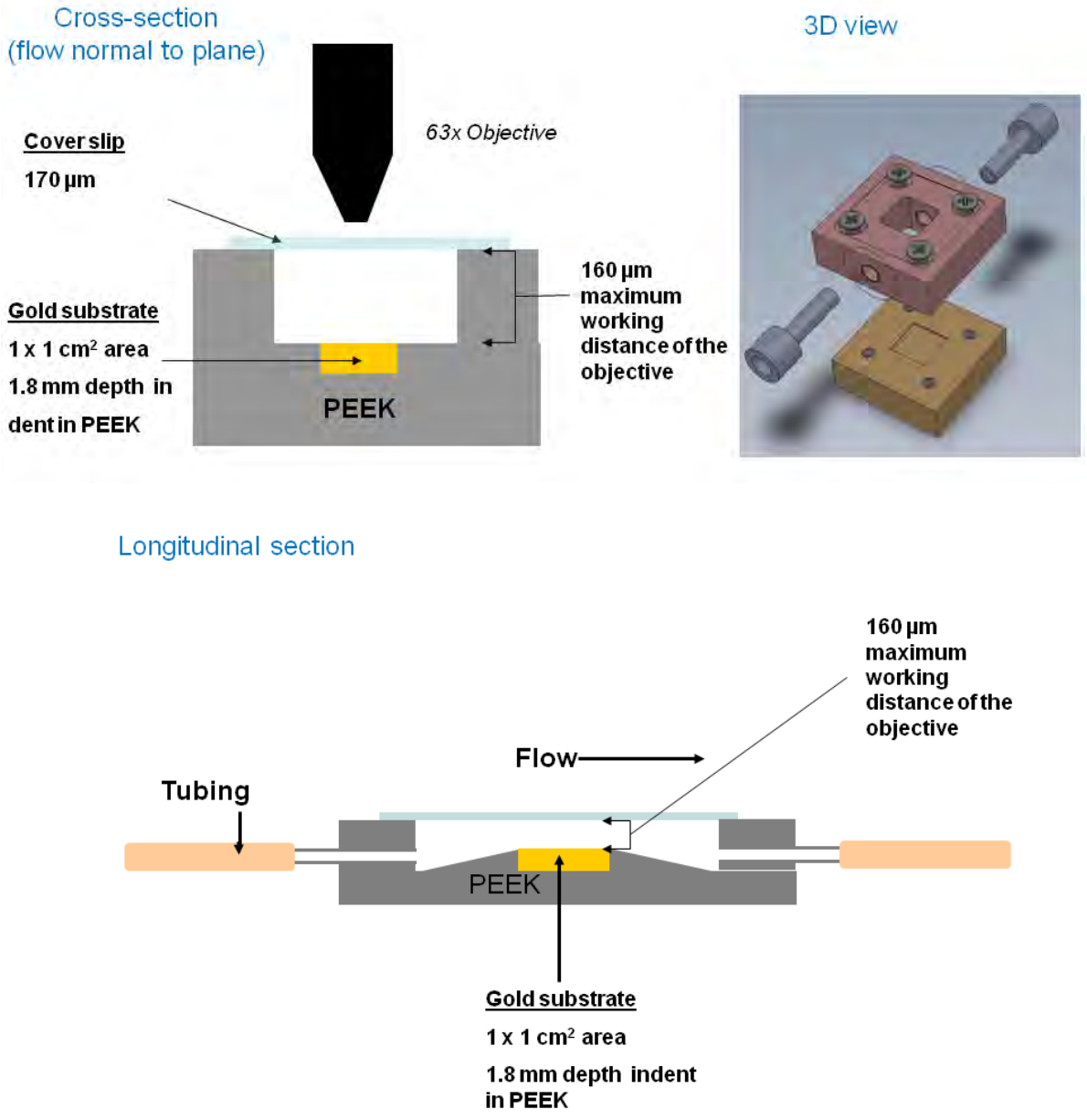

Fig 3.4: Schematic representation of the bacterial flow cell

3.3. SAMs formation

3.3.1 Procedure for the formation of SAMs

Au-coated glass substrates were cleaned with piranha solution in order to remove any organic contamination from the surface (**Fig 3.5 process 1).** The Au substrates were then rinsed with UHQ water and HPLC ethanol, and then immersed in 0.1mM *O*-(2-Carboxyethyl)-O'-(2-mercaptoethyl) heptaethylene glycol in HPLC ethanol (and 3 % TFA) for 24 hours, forming COOH-SAMs (**Fig 3.5 process 2)**.

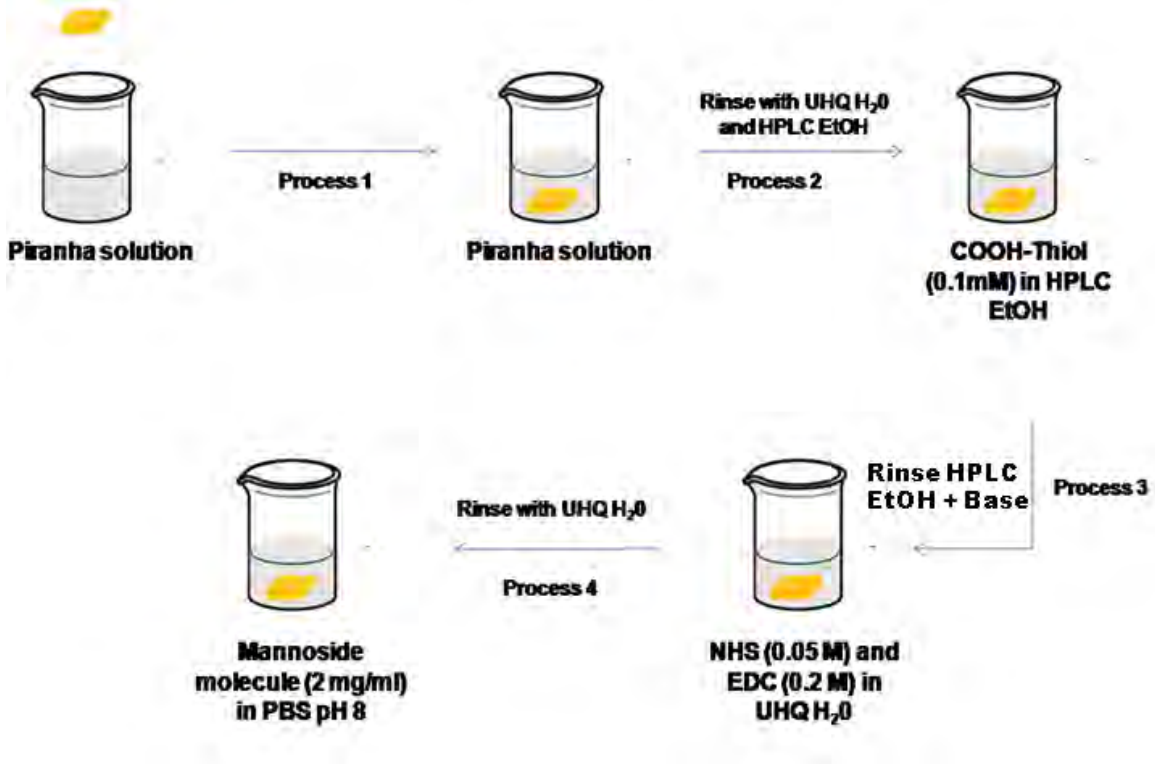

Fig 3.5: Schematic representation of MT-SAM formation

The COOH-SAMs were then rinsed with HPLC ethanol with 10% ammonium hydroxide, then dried with argon and immersed in a solution of (0.05 M) NHS and (0.2M) EDC in UHQ water for 10 minutes **(Fig 3.5, process 3)**, followed by rinsing in UHQ water and subsequent immersion in (2mg/ml) 4-Aminophenyl α-D-mannopyranoside in PBS pH 8 for 1 hour, then rinsing with PBS pH 8 and UHQ water (**Fig 3.5 process 4)**.

For confirmation studies of MT-SAM formation, MT-SAMs were immersed in a solution of (0.01 mM) ConA in Tris-buffered saline (TBS) with Mn^{2+} and Ca^{2+} for 1 hour, and then rinsed with TBS and UHQ water, and dried with argon.

Control studies using an EG thiol were performed following the same procedure depicted in **Fig 3.5**, but the COOH-thiol was replaced with 0.1 mM *O*-(2-Mercaptoethyl)-*O′*-methyl-hexa(ethylene glycol) in HPLC EtOH

3.3.2 SAMs Characterisation

In order to confirm the presence of COOH-SAMs after Au substrate immersion in COOH-terminated thiol molecules, the surfaces were analysed by XPS, ellipsometry and contact angle after Au surface immersion in COOH-thiols for 24 hours.

High resolution XPS spectra confirmed the formation of COOH-SAMs, showing the signals from C1s, O1s and S2p after surface modification. Deconvolution of the S2p core level spectrum gives rise to the characteristic S2p3/2 and S2p1/2 doublets with components at 162.2 and 164eV, respectively (**Fig 3.6 a**); indicative of a thiolate bound to a gold surface[191]. The S2p3/2 and S2p1/2 doublets were fitted with a fixed binding energy difference of 1.18 eV and an intensity ratio of 2:1, which reflected the multiplicity of these energy levels. The binding energy region was also extended to 175 eV to check for the presence of oxidized sulphur species; however, none were observed[192]. However, there was some unbound thiol on our surface - S2p3/2 (164eV) and S2p1/2 (165.2 eV). Peaks at this binding energy indicate –SH species, possibly due to some thiol having not chemisorbed onto the surface properly, but this did not impact on mannoside immobilisation as discussed later.

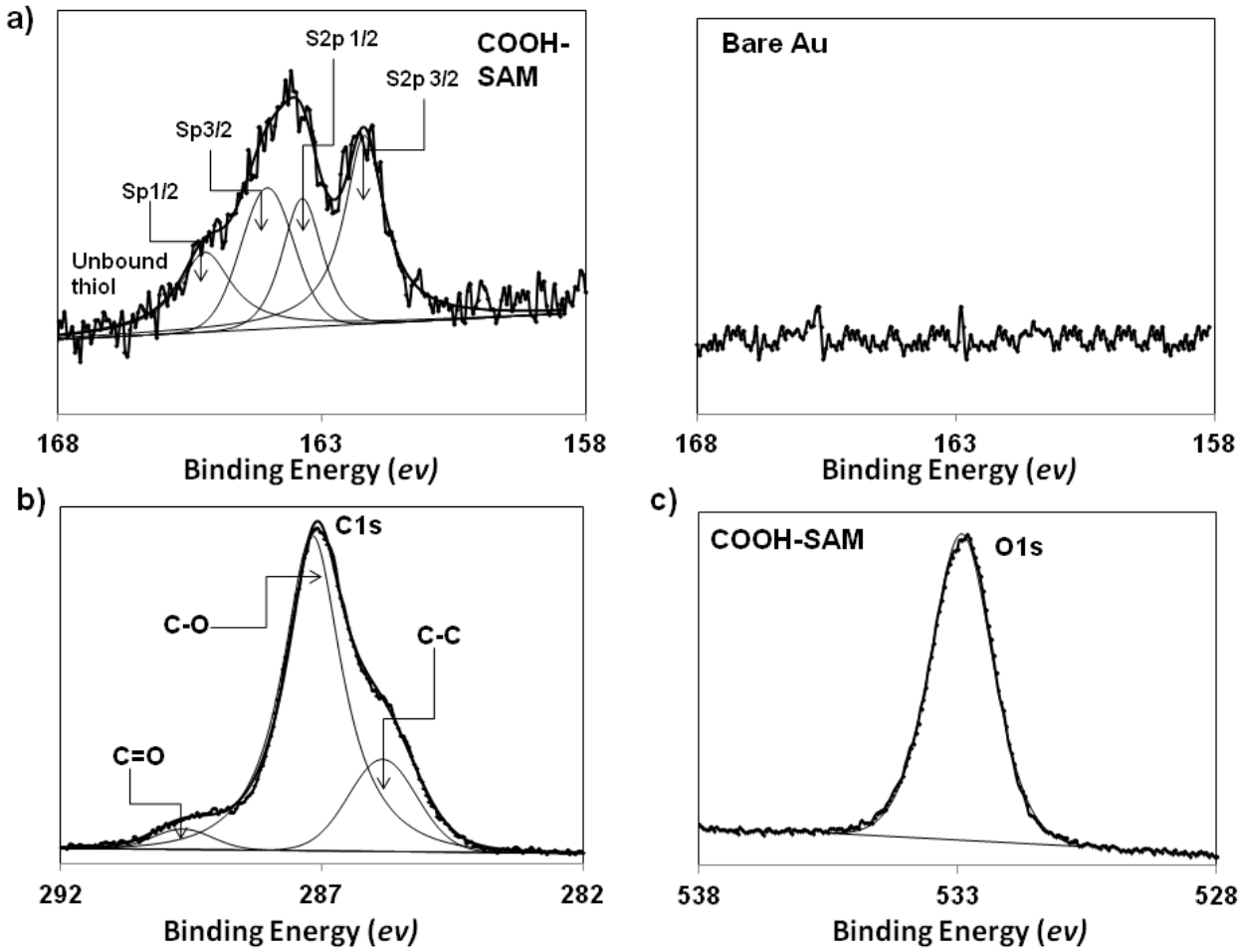

Fig 3.6: High resolution XPS spectra of the S2p regions of COOH-SAMs compared to a SAM-free Au surface (**a**); C1s peaks (**b**) and O1s peak (**c**)

The C(1s) spectrum can be deconvoluted into three peaks, attributed to four different binding environments (**Fig 3.6 b**). The main, predominant peak (287.2 eV) was attributed to C1s of the two binding environments of C-S and C-O-C. The first of the two smaller peaks (286 eV) was attributed to C1s of C-C. The third and final peak (288.9 eV) was attributed to the C 1s photoelectron of the carbonyl moiety, C=O. The O1s spectra (**Fig 3.6 c**) was de-convoluted into two different peaks, corresponding to two different binding environments, arising from the ether moieties, C-O-C (533.5 eV) and the carbonyl oxygen C=O (531.9 eV).

Ellipsometry and contact angle measurements of COOH-SAMs and EG-SAMs after formation for 24 hours are depicted in **Fig 3.7**. The theoretical length of the COOH-thiol molecule was 3.05 nm, and the smaller EG-thiol was 2.6 nm. Ellipsometry showed that the average film thickness for COOH SAMs was 2.8 nm (± 2) and for EG-SAMs it was 2.6 nm (± 1) , in good agreement with the calculated molecular length. The results show that although there is some unbound thiol on the surface, double layers are not forming (which would give results of > 3.05 nm) meaning we have an appropriate monolayer of thiol on the surface.

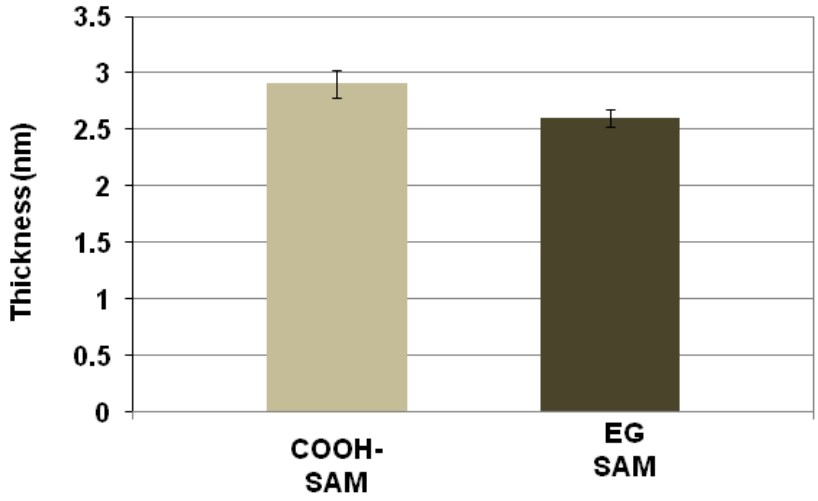

Surface	Advancing (ɵ)	Receding (ɵ)
Clean Au	25° ± 6	13° ± 3
COOH-SAM	10° <	10° <
EG-SAM	32° ± 2	16° ± 4

Fig 3.7: Ellipsometry (top) and Contact Angle (bottom) data for the formation of SAMs on Au surfaces

Ellipsometry results were supported with contact angle measurements. The advancing contact angle of a pure COOH-SAM surface is less than 10^{o}, which is lower than the advancing contact angle of a pure EG surface ($32^{o} \pm 2^{o}$). The decrease in contact angle indicates an increase in wettability, which was expected as COOH-terminating groups readily form more hydrogen bonds with water than EG groups[193], allowing increased spreading of the liquid.

Fig 3.8 shows the N1s XPS spectra of a COOH- SAMs that had been activated with NHS/EDC and coupled to mannoside molecules. These were compared with a (mannose-deficient) COOH-SAM and EG-SAM control, and a MT-SAM that had been coupled with Con A. High-resolution scans of the N1s region show the presence of nitrogen in the MT-SAMs with a 0.08N/Au ratio, whereas no N1s peak was observed in the COOH-SAMs spectra. MT-SAMs have a peak centred at 402.0 eV, attributed to amide (− CONH −) moieties that link the mannoside molecules to the COOH-terminated surface. An increase in N/Au ratio from 0.08 to 0.27 was observed upon attachment of ConA to MT-SAMs, confirming the presence of the lectin and indicating that the MT-SAM is capable of supporting the adhesion of compatible molecules, and that the SAM density was not obstructing adhesion.

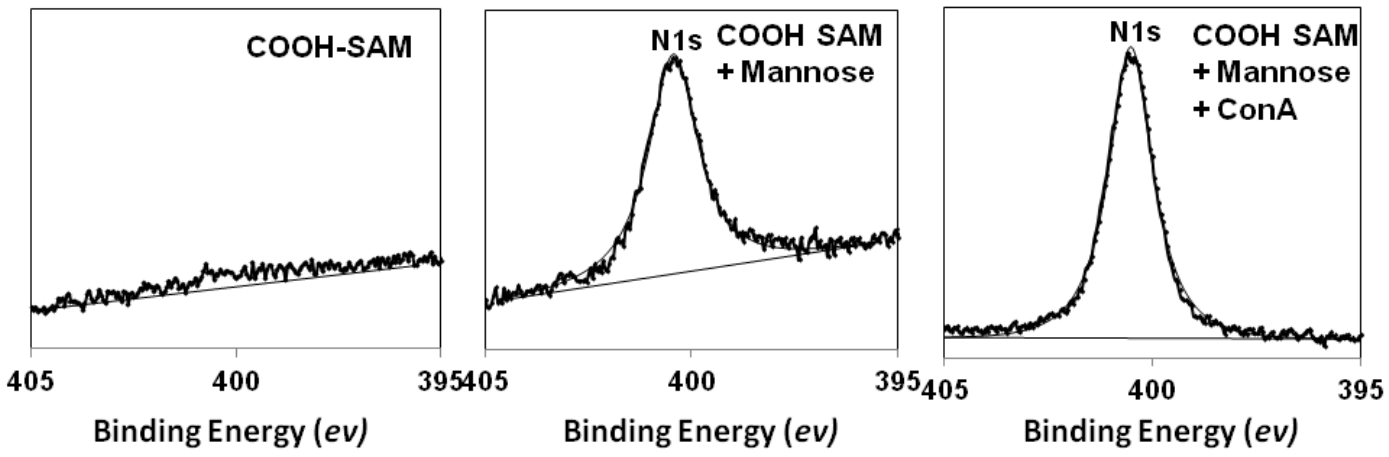

Surface	N/Au Ratio
Pure COOH-SAM	0
COOH-SAM+Mannose	0.08
COOH-SAM+Mannose+ConA	0.27

Fig 3.8: High resolution XPS spectra of the N1s regions of SAM surfaces

Ellipsometry measurements of pure COOH-SAMs coupled with mannoside molecules and ConA are depicted in **Fig 3.9**. The mannose molecule is very small (~ 1 nm) so it is expected that a small increase in thickness would occur upon coupling. In a monolayer of COOH-thiol, there is a 1 nm increase in thickness when a mannoside molecule is attached. ConA is a very large molecule compared to the thiol and mannoside; it is a 24kDa protein, therefore we would expect a large increase in thickness of the MT-SAMs after the lectin has been attached. Attachment of ConA showed a 6 nm increase in thickness in a MT-SAM from a pure COOH-thiol monolayer. This corresponds with the literature, which states that thickness of lectin molecules range from 5-10 nm[194]. These results both confirm the presence of the mannoside molecule and ConA, and correspond with the XPS data N/Au ratios.

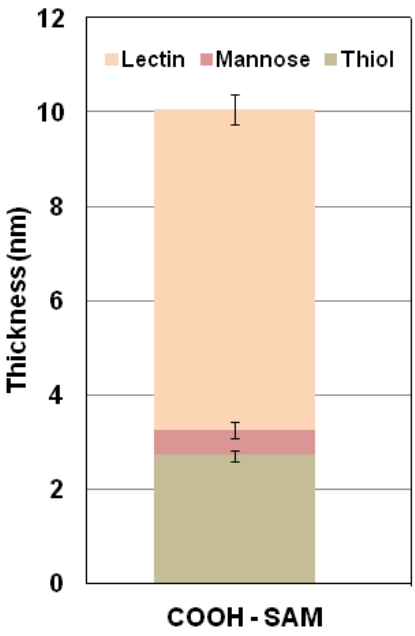

Fig 3.9: Ellipsometry data showing the change in thickness upon attachment of mannoside molecules and ConA to a COOH SAM on Au.

Fig 3.10 shows the results of the real time SPR experiment. From a stable baseline of PBS running over the SAM, mannoside molecules are attached to COOH-SAMs using carbodiimide chemistry, followed by attachment of ConA, using a pure EG-SAM as a non-adhesive control.

Injection of NHS/EDC to activate the surface shows a sharp response of over 4000 RUs, which then drops as the solution is washed away with PBS. The response seen here corresponds well with SPR analysis of carbodiimide coupling in the literature[109]. Injection of mannoside molecules was met with an SPR response of 200 response units showing that the mannoside derivative has been immobilised onto the COOH-SAMs. Injection of Con A was met by further response units of 3000, showing that mannoside molecules were successfully coupled to the COOH-SAMs and then were subsequently able to bind to biospecific proteins. Importantly, the results clearly show that on an EG-SAM there is no increase in RU after EDC/NHS, mannoside or ConA injections and thus the ConA is specifically attached to the COOH-SAM via the mannoside derivative.

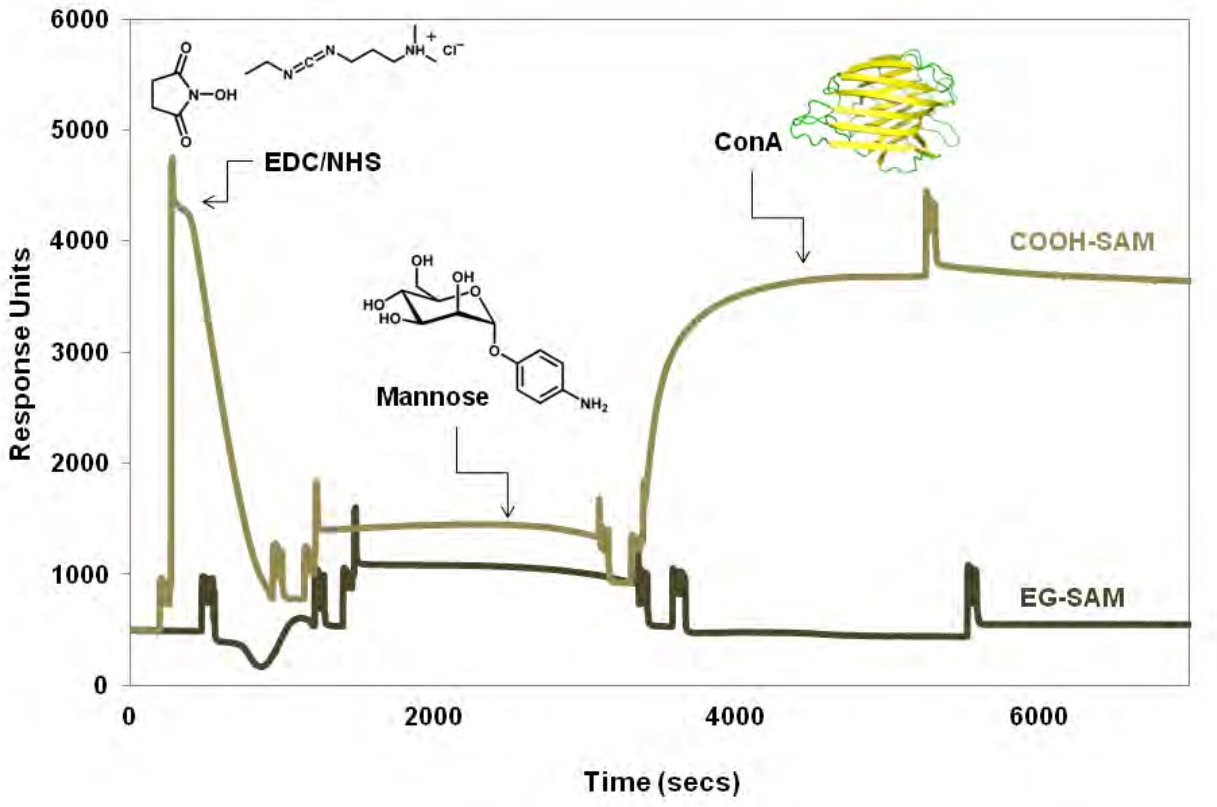

Fig 3.10: SPR sensorgram traces showing the binding of mannoside derivative to COOH-SAMs via EDC/NHS, followed by subsequent binding of ConA to the MT-SAM. No binding was observed for the EG-SAM. After injections for 30 min, the surfaces were washed with PBS for to remove any non-specifically adsorbed molecules

3.4 Bacterial Adhesion Studies

3.4.1 Kinetic Study

GFP-*E. coli* strain DH5α pUA66pacpP ampR (excitation max 485nm, emission max 510) pre-cultures were grown in Luria Broth with shaking at 200 rpm over night at 37°C. The following morning, they were diluted 10 fold into fresh media, and grown to exponential phase with an OD_{600} of 0.6. Bacteria at exponential phase are more metabolically active, and also studies show that production of fimbriae is hindered by phenotypic switching if cells grow to stationary phase[195]. Adhesion was therefore more likely to occur at this OD. Following cell growth, MT-SAMs were then incubated with cells, and kept in an incubator at 37^{o}C to allow attachment. At time intervals, substrates were removed and rinsed thoroughly with PBS to remove unattached cells, and then a cover-slip was placed directly on top of the sample with a thin layer of minimal media to keep the cells viable during microscopy. Initial microscopy images of bacterial adhesion were taken with a fluorescence microscope, at x 100 magnification. Bacterial adhesion to MT-SAMs was also confirmed using SPR, with a mannose-free COOH-SAM as a non-adhesive control.

Fig 3.11 shows that after two hours, there is a full monolayer of bacteria attached to the surface, which corresponds with the literature[124]. When the cells are deposited onto the surface they are they need to settle from the bulk solution onto the surface. Early stages of bacterial adhesion involve non-specific forces such as hydrophobic interactions and van der Waals[56]; however, these are 'reversible', meaning that they are easily overcome by rinsing procedures that allow bacteria to become dislodged. The FimH-mannose bond is the important factor in determining the *E. coli* resistance to rinsing; but this takes time. A single mannose-fimbrial bond is not enough to keep a cell in place but bacteria can produce multiple copies of the fimbriae[74], and with multiple mannoside ligands in place it allows the cells to attach more strongly.

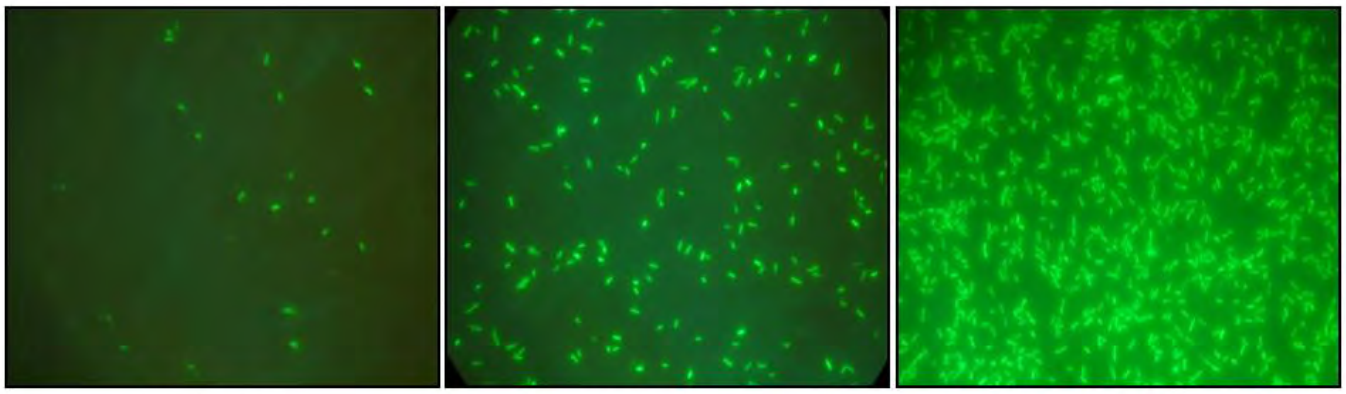

Fig 3.11: Fluorescence microscope images of bacterial adhesion to MT SAMs over time (x 100).

Bacterial adhesion studies were also confirmed using SPR (**Fig 3.12**). A mannoside terminated SAM shows a steady increase in bacterial adhesion from 0 – 2500 seconds, with a response of 2250 RU. Following the experiment, the gold substrate was immediately taken to the microscope and imaged, showing that there are is a full monolayer of cells on the surfaces. In fact, full bacterial coverage occurs much more quickly in the SPR than with cells deposited onto the surface. This supports the catch-bond theory of bacterial adhesion; structural simulations have shows that FimH undergoes a force-induced change that is correlated with stronger binding [194]. Additionally, the SPR data further supports the specificity of the mannose-FimH bond as there was only 250 RU on a mannose-free SAM.

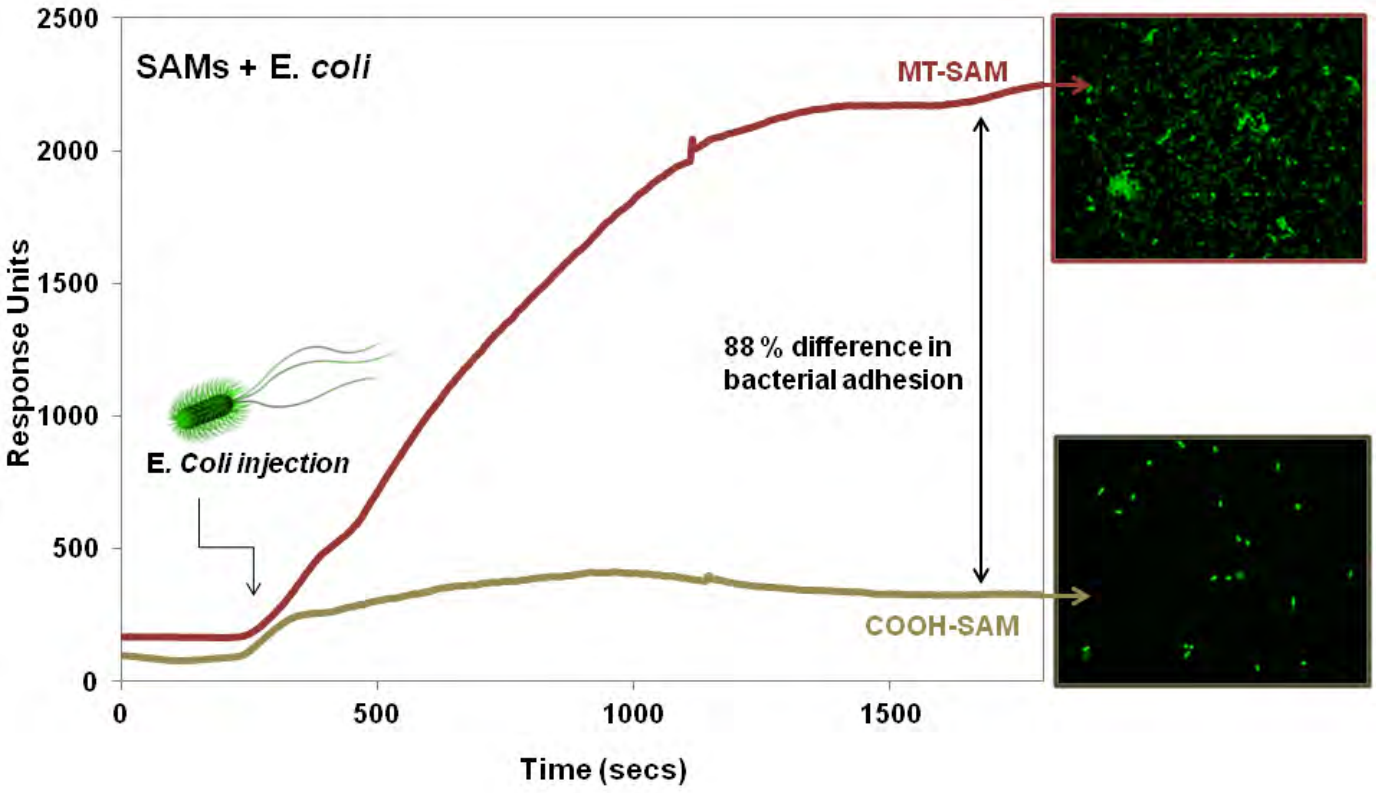

Fig 3.12: SPR sensorgram traces showing the binding of *E. coli* (OD_{600} 0.6) to the MT-SAM, and the reduction in binding when injected over a COOH-terminated SAM. After bacterial binding for 30 min, the surfaces were washed with PBS for 20 min to remove any non-specifically adsorbed cells.

3.4.2 Flow cell Study

A bacterial monolayer on a MT-SAM surface was created for two hours at 37^{o}C, and then placed inside the flow cell under the x 63 objective of the confocal microscope. After adjusting the temperature of the media to 37^{o}C, a low flow rate (10 µl /min) was then started and continued for 1 hour. The flow rate was then increased every hour until the maximum flow rate at which bacteria detached. Additionally, rinsing studies were performed with a flow cell using agarose blocks in place of MT-SAMs (3% agarose powder in M9).

Although it has been shown that the bacterial monolayers form fully after two hours, and initial attachment in a flow cell setting can enhance attachment, it was also important to ascertain whether the cells had long term resistance to rinsing. Focusing on a single patch of cells in the monolayer on one MT-SAM, **Fig 3.13** shows that the cells are resistant to flow rates up to 50 µm/min. The flow rate is calculated by measuring the volume of the flow settings by the cross-sectional area of the 1 by 1 cm Au substrate.

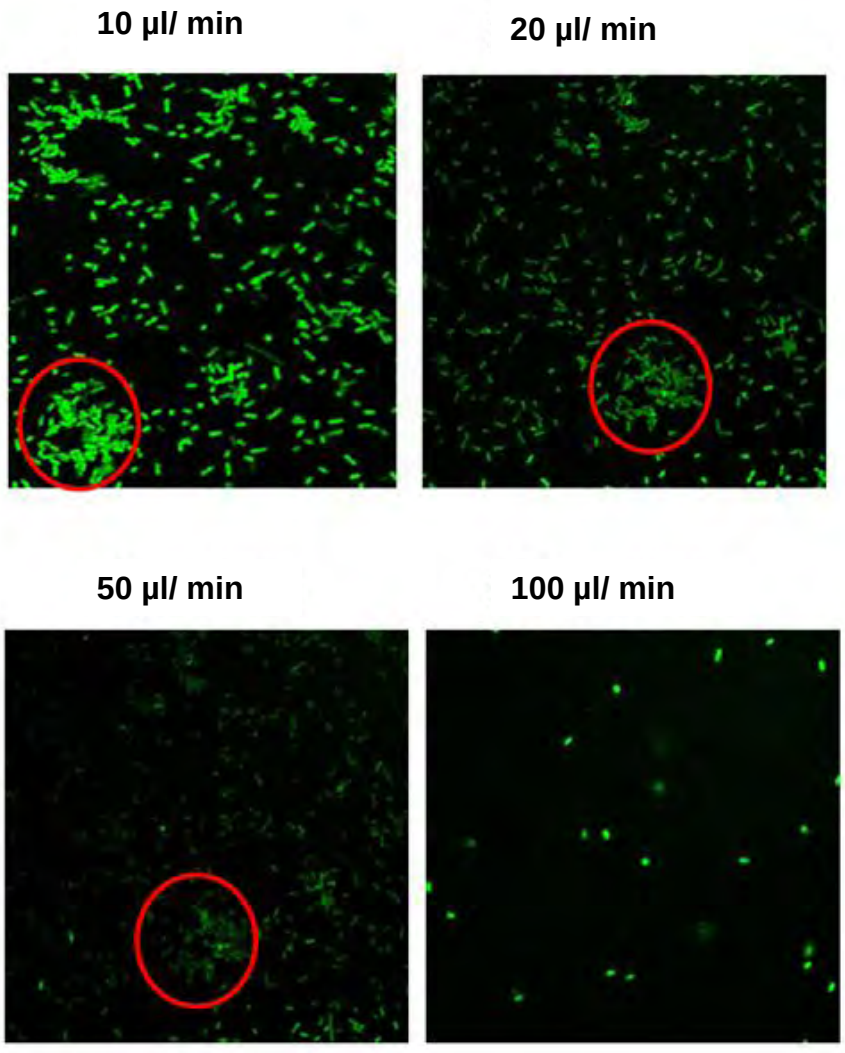

Fig 3.13: Confocal fluorescence microscopy images showing attachment of cells on MT-SAMs under different rates of flow inside the flow cell.

3.4.2.3 Bacterial resistance to rinsing on agarose blocks

As previous researchers have used agarose as a substrate for bacterial patterning[134], we decided to test whether these substrates were suitable for bacterial adhesion by testing bacterial resistance to the same rinsing procedures employed on MT-SAMs. **Fig 3.13** shows the confocal microscope images of GFP-*E. coli* on M9-agarose blocks that had been incubated for 2 hours at 37^{o}C followed by insertion into the flow cell. As the images show, *E. coli* on agarose have poor resistance to rinsing; in fact the flow rate could only be increased to 20 μm/min before all the cells were completely washed away. This highlights the importance of a specific adhesion-mediated bond in the construction of bacterial adhesive surfaces; the galactose residues in agarose will interact with the cell membrane of the bacteria, but there are no binding sites for type-1 fimbriae so there are no catch bonds to mediate resistance to rinsing.

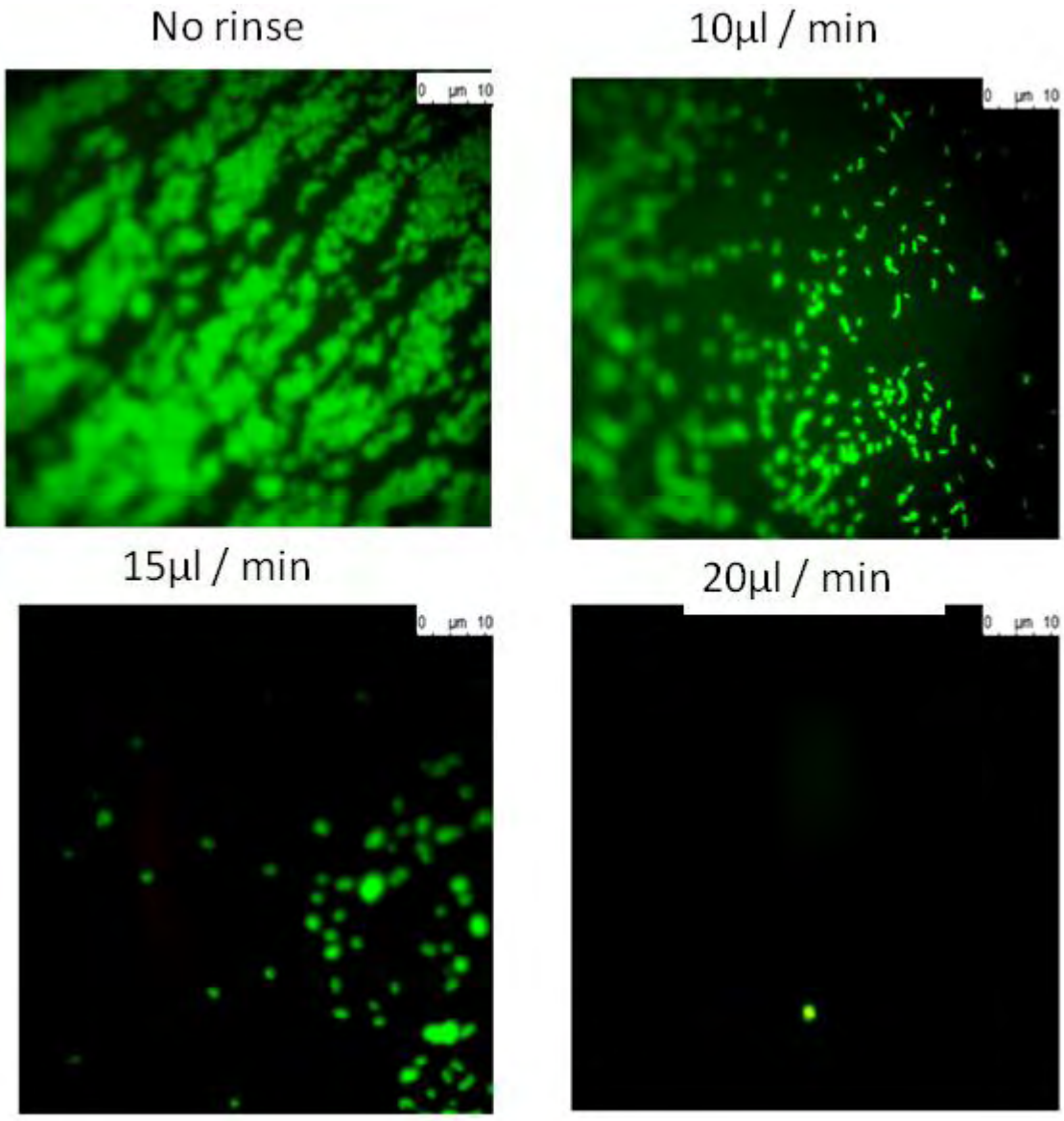

Fig 3.13: Confocal fluorescence microscopy images showing attachment of cells under different rates of flow inside the flow cell on agarose blocks.

3.5 Summary

In conclusion, we have shown that by using surface chemistry we have created a platform ideally suited for bacterial immobilisation. Not only do MT-SAMs provide adhesive support for bacterial monolayer formation after 2 hours, we have also shown that they enable attachment of *E. coli* through a specific FimH-mannose bond, which enables the cells to be resistant to dislodging by rinsing, thereby enabling prolonged periods of adhesion inside a flow cell setting.

Chapter 4: Patterning of Bacteria

Abstract: *The ability to pattern bacterial co-cultures onto adhesive surfaces is of practical import for the spatial studies of cell-cell interactions including conjugation. This chapter describes the fabrication of single-strain patterns of E. coli onto MT- SAMs, followed by the procedures employed to form a micro-patterned co-culture.*

4.1 Background

During the past several years, various methods have been reported for micro patterning *single bacterial cell types* on material surfaces. Generally cells are patterned onto a substrate by printing functional molecules that either support or inhibit immobilisation of bacteria, followed by incubation with bacteria and its attachment on the pre-designed adhesive regions.[183,196-199] For instance, bacterial microarrays have been prepared by attaching *E. coli* K-12 on SAMs patterned by dip-pen lithography or μCP that have been covalently functionalised with poly-L-lysine or anti- *E. coli* antibodies[198]. Unpatterned areas have been passivated with either 11-mercaptoundecyl-penta(ethylene glycol) or 11-mercapto-1-undecanol to resist bacterial cell binding. In another example, bacterial microarrays have been prepared by using self-assembled polyelectrolyte multilayers (adhesive region) and micromolding in the capillaries of poly(ethylene glycol)-poly(D,L-lactide) diblock copolymer (non-adhesive region)[196]. Other methods that have been reported to create adhesive and non-adhesive bacterial regions include capillary lithography,[200] e-beam lithography[201] and photolithography[202]. Bacteria have been delivered directly to a substrate by either ink-jet printing[203] or μCP using micropatterned stamps made from agarose[135] and poly(dimethylsiloxane) (PDMS)[204]. Ink-jet printers have been adapted to generate viable bacterial colony arrays by directly ejecting *E. coli* DH5α cells onto agar-coated substrates[203]. Recently, Xu *et al*[204] employed μCP to directly print bacteria onto the

surface of an agarose block, producing high-resolution arrays of living bacteria. Each of these reported methods has its own strengths and weaknesses with regard to resolution, complexity, immobilisation efficiency and physiological activity of individually immobilised bacteria. In particular, these reported strategies have the common shortcoming of not being suitable for patterning two or more different types of bacterial cells.

Patterning procedures that rely on printing functional adhesive molecules can usually only select for a single cell type, which is suitable for individual cell studies and whole cell arrays; however, for HGT experiments there needs to be a clear separation of donors and recipients, meaning that the substrate has to support two cell types. In this project, the substrate for cell immobilisation (the MT-SAMs) was designed in such a way so that it would not have non-adhesive regions, relying on the patterning to separate the cells.

4.2 Objective

The objective of the second section of the project was to develop a procedure that would allow the formation of micro-patterned bacterial co-cultures on the adhesive MT-SAMs, by expanding and adapting methods used by previous researchers to provide a platform for the spatial study of gene transfer events. The objective was split into two main stages, as depicted in **Fig 4.1**:

1) Formation of a single- strain patterned array of bacterial cells on the MT-SAMs
2) Direct delivery of a second strain of bacteria to the same substrate on the un-patterned regions, forming patterned co-cultures

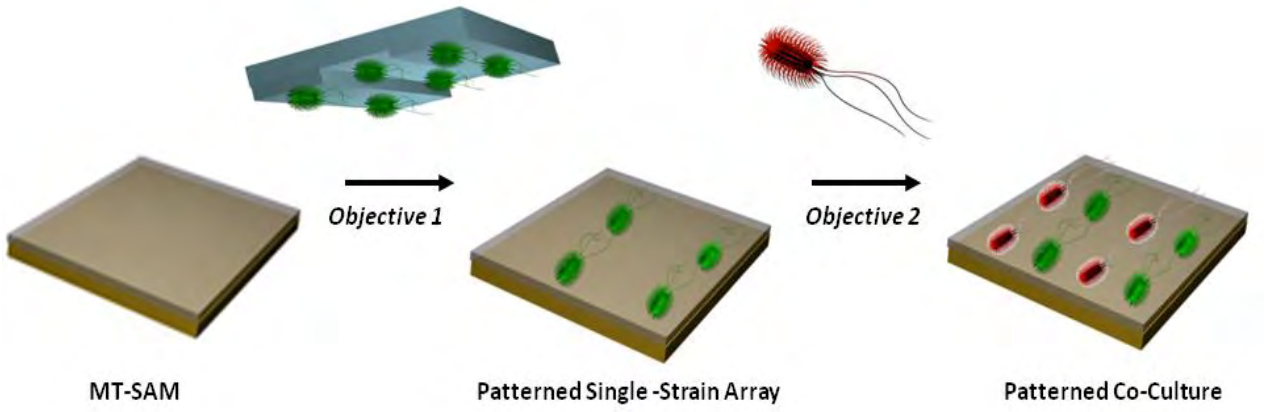

Fig 4.1: Schematic representation of bacterial patterning objectives

4.2.1 Formation of Single Strain Patterns

Before patterned co-cultures were constructed, it was important to establish that single strains of bacteria could be patterned onto the MT-SAMs, in a manner that conferred as little cellular stress as possible, as cells needed to remain viable and metabolically active to perform HGT experiments. In order to achieve this, a variety of patterning procedures and modifications were carried out. Firstly, patterns of *E. coli* were constructed using direct microcontact printing, where patterned stamps made of PDMS or hydrogels such as agarose can be made with features as small as 50 nm[205], and the desired material is traditionally transferred to the substrate by "inking" the surface of a stamp and depositing directly onto the surface. Secondly, patterns were constructed using a subtractive lift-off technique, where instead of directly delivering cells to the MT-SAMs, a monolayer was formed on the surface of the MT-SAM and cells were taken off using patterned stamps.

The stamp type (i.e PDMS, agarose) was also varied to in order to establish which was best for the delivery/removal of cells to/from the MT-SAM, and the stamp surface features were varied by constructing different silicon masters to determine which width and depth yielded the most

robust patterns. Pattern formation was also facilitated by using a micromanipulator to control the amount of pressure placed on top of the substrate, in order to prevent stamp deformation and pattern smudging.

It was already confirmed that cells adhering to MT-SAMs were resistant to dislodging by fluid flow, and subsequently it was also important to determine that the patterned arrays were robust enough to withstand the same rinsing procedures from the flow cell, and from the addition of a second strain of bacteria.

4.2.2 Formation of Patterned Co-cultures

Once a single-strain patterned bacterial array had been formed, a second strain of bacteria was then directly delivered to the substrate by immersion on top of the bacterial patterns. The notion was that the second strain would slot into the gaps left on the MT-SAM in the unpattered regions, leaving alternating rows of cells which would eventually be donors and recipients in HGT experiments.

The second strain cell concentration had to be systematically determined, in order to find the appropriate cell density that would fill the gaps fully, as research has shown that for HGT to occur, donor and recipient cells require cell-cell contact[6]. In addition, the co-cultured arrays had to be subjected to the same rinsing controls as the single-strain array, to ensure that the addition of the second strain was not detrimental to pattern integrity. A blocking protein constructed from the mannose binding lectin, ConA, was also used to see if it assisted in separation of the two bacterial strains.

4.3 Single Strain Patterning

4.3.1 Direct Patterning by Microcontact Printing

4.3.1.1 Overview

Initial patterning experiments were performed using conventional microcontact printing, where a patterned stamp is "inked" with bacterial suspension and then printed onto the MT-SAMs (**Fig 4.2**), forming a patterned bacterial array.

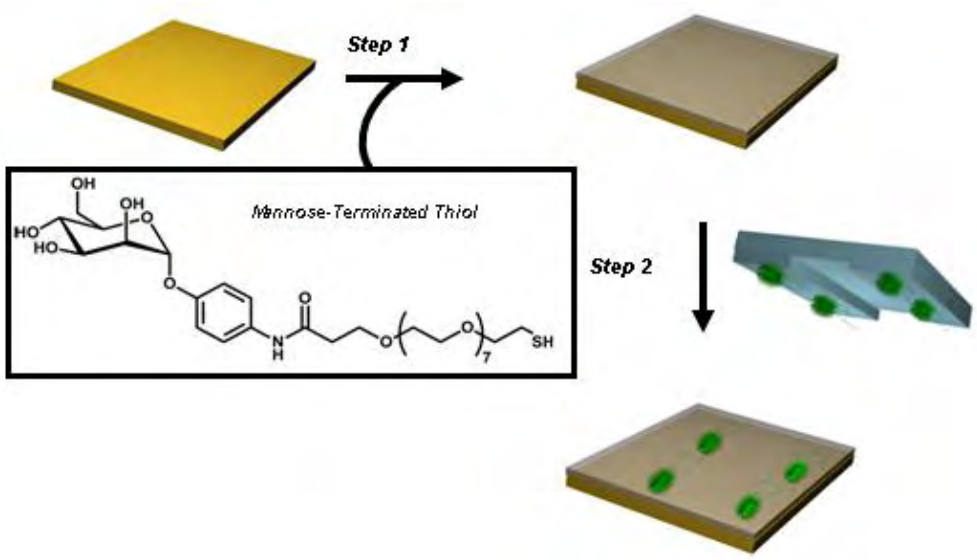

Fig 4.2: Schematic representation of bacterial patterning via microcontact printing

PDMS stamps were fabricated by casting PDMS onto a micropatterned silicon master. After allowing the mixture to degas at ambient conditions for 2 hours, the PDMS was cured for 2 hours at 60°C to promote cross-linking (**Fig 4.3**).

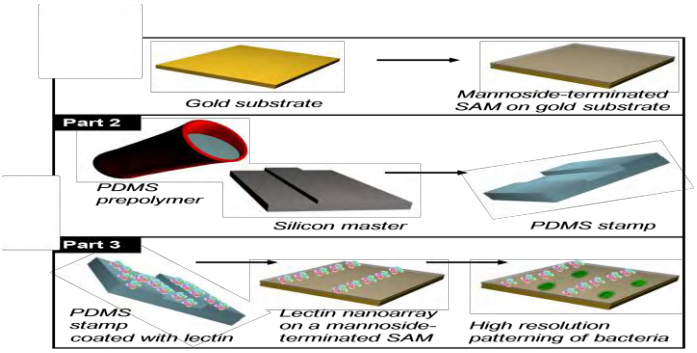

Fig 4.3: Schematic representation of PDMS stamp formation

The solidified PDMS stamps were then carefully peeled from the masters and sonicated in EtOH for 30 minutes for sterilization. For agarose stamps, a replica of the PDMS was made by casting a hot de-gassed solution of agarose over the patterned stamps. The agarose was cooled and solidified at room temperature, then carefully peeled away from the PDMS. The pattern features selected for these initial patterning experiments were lines measuring 5 µm in width, with a 5 µm gap, and a depth of 2 µm (**Fig 4.4**). These features were selected to take into account the width of an individual *E. coli* cell (measuring on average 2 µm in width and 0.5-1 µm in length) to allow the formation of alternating rows of donors and recipients, with one or two cells in each row.

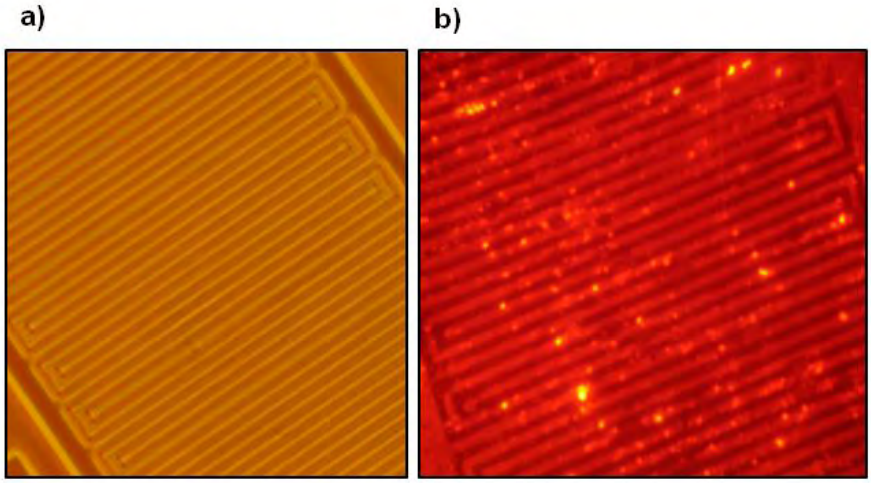

Fig 4.4: Microscopy images of 5 by 5 µm patterns on the PDMS stamp surface (**a**) and fluorescently labelled ConA printed directly onto MT-SAMs (**b**)

4.3.1.2 Direct patterning procedure

Overnight pre-cultures of GFP-*E. coli* in M9 broth (see chapter 7 for M9 supplements) were diluted 10 fold into fresh media with 3 % glycerol, and grown to exponential phase with an OD_{600} of 0.6. The glycerol is used to provide protection from desiccation for the cells during the microcontact printing process[206]. Following cell growth, patterned stamps were incubated with 100 µl cell suspension for 30 minutes at 37^{o}C to allow attachment. Using a sterile absorbent tissue, excess liquid was drained from the surface of the stamp (at the edges to avoid dislodging the cells on the stamp features). The stamps were then carefully placed onto the MT-SAMs feature side down, and then peeled off and discarded, leaving a pattern of cells on the surface of the gold substrate. A cover-slip was placed directly on top of the sample with a thin layer of minimal media to keep the cells viable during microscopy, or the cells were placed directly into the flow cell during rinsing studies.

4.3.1.3 Direct patterning using PDMS onto MT-SAMs

Fig 4.5 shows the fluorescent microscope images of the 5 by 5 µm lines on the PDMS surface after inking with *E. coli*, and the MT-SAM surface after direct printing. Printing onto the MT-SAMs with PDMS stamps gave slight pattern formation (**Fig 4.5b**); however, lines of cells were broken in places, with patches of cells clumped together and big gaps between the lines. It was reasoned that the poor patterning was either due to poor transfer of cells from the PDMS to the MT-SAM, or due to the poor surface coverage on the PDMS surface. Looking at the two images together, they are very similar in that there are broken patches and clumping of cells, suggesting that it was the uneven surface coverage causing the poor pattern formation, rather than the transfer of cells.

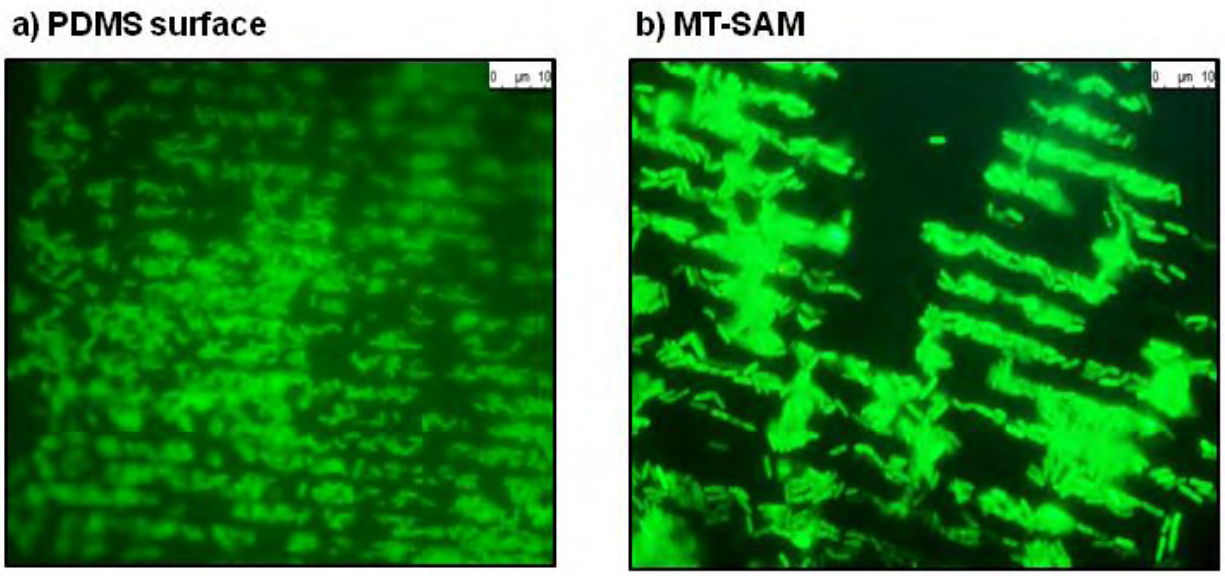

Fig 4.5: Fluorescence microscope image of 5 by 5 μm patterns of GFP- *E. coli* on the surface of a PDMS stamp (**a**) and then printed on MT-SAMs (**b**) (x 100 magnification)

PDMS is very hydrophobic (it has a contact angle of 108^{o}[207]), and it is well known that despite its advantages, poor wettability of PDMS surfaces is a significant drawback in the microcontact printing process, particularly when using polar inks[208]. Researchers performing microfluidic assays with bacteria have found that the hydrophobicity prevents aqueous solutions from entering the microfluidic channels[209], and additionally hydrophobic analytes can readily adsorb onto the PDMS surface, interfering with analysis. The uneven cell distribution on the PDMS surface was therefore attributed to the surface hydrophobicity.

4.3.1.4 Direct patterning using modified PDMS onto MT-SAMs

It was reasoned that converting the hydrophobic stamp to a more hydrophilic surface would allow the bacterial ink to spread out more evenly over the stamp, reducing clumping and perhaps improving final pattern integrity. Stamp surface treatment with oxygen plasma or UV is a well known method for altering the wettability of the PDMS[210,211]. Unmodified PDMS has a chemical structure of repeating $OSi(CH_3)_2O$– units, and when treated with oxygen plasma or UV, a silanol is introduced (Si-OH) which removes methyl (CH_3) groups, converting the surface groups to

hydrophilic $–OSi(OH)_2O$ groups[212]. Compared to oxidizing PDMS with plasma, UV treatment is slower in terms of the time required to achieve the same result[213]; however, the advantage is that it facilitates much deeper modification of the PDMS surface without inducing cracking or mechanical weakening of the PDMS[214].

However, hydrophilized PDMS surfaces from both UV and plasma do not remain hydrophilic for long due to mobile, low-molecular weight PDMS monomers that migrate from the bulk to the air-surface interface[212], which can make the oxidized surface revert back to hydrophobic. Experimentally, using UV alone is therefore not convenient and so additional treatment steps were needed to change the wettability. A solution of Pluronic F-127 was therefore used as an additional treatment for the PDMS. Pluronic F-127 is a series of tri-block co-polymers of hydrophobic propylene oxide (PO) and hydrophilic ethylene oxide (EO). When PDMS is treated with Pluronic F-127, a brush border is formed with the hydrophilic EO exposed[215] (**Fig 4.6**).

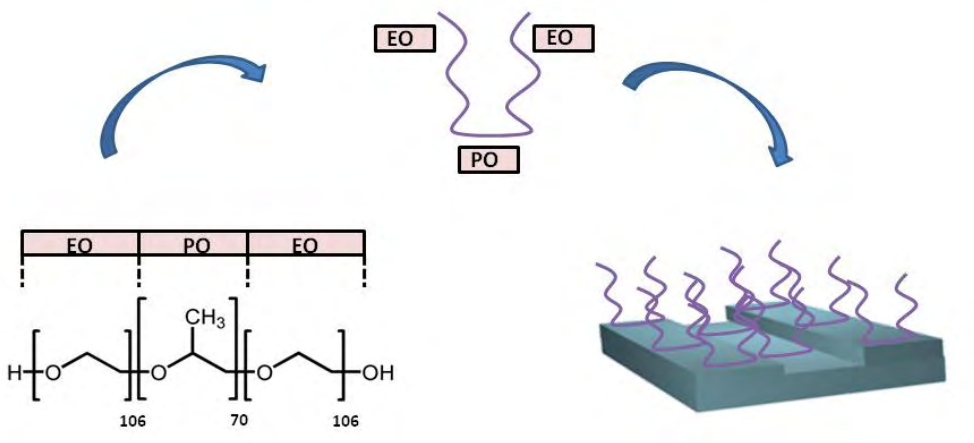

Fig 4.6: Schematic representation of Pluronic F-127 attachment onto PDMS

In order to determine the most appropriate conditions for creating a hydrophilic PDMS stamp, a series of Contact Angle experiments was carried out. PDMS was exposed to UV for time intervals over 120 minutes, before being immersed in Pluronic F-127 for 1 hour and then rinsed

with UHQ water. **Fig 4.7 a** confirms that after two hours with UV treatment, a PDMS stamp is converted from hydrophobic surface with an advancing contact angle of 110^{o}±7 to a more hydrophilic surface with an advancing contact angle of 58^{o}± 3, although after 60 minutes within the error there is an increase in hydrophilicity.

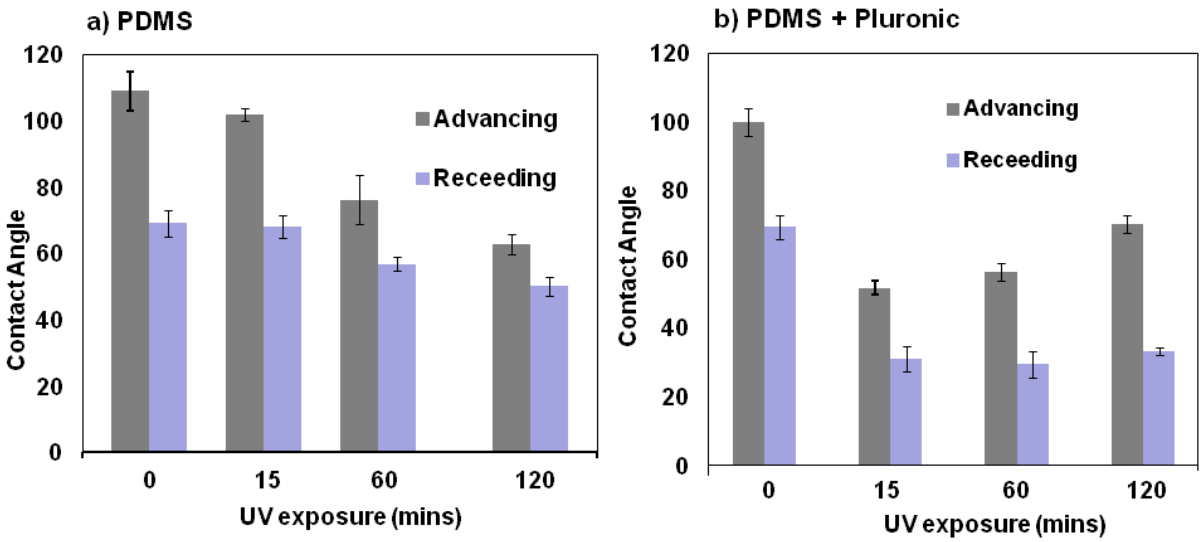

Fig 4.7: Contact Angles of PDMS surface after UV exposure (**a**) and UV exposure plus additional treatment with Pluronic (**b**)

PDMS stamps were then treated with UV over 120 minutes, followed by immersion in Pluronic F-127. **Fig 4.7 b** shows that a 15 minute exposure to UV before Pluronic F-127 immersion provided the most hydrophilic stamp surface, with an advancing contact angle of 55 ^{o} ± 2. A short exposure to UV may produce peroxides and metastable radicals on the surface of PDMS that facilitate the binding of the Pluronic F-127 molecules[216]. Additionally, in a similar experiment, Delamarche *et.al.*, found that stamp hydrophilicity was maintained for nearly a week[216]. UV exposure of 120 minutes before addition of Pluronic F-127 appeared to decrease the overall hydrophilicity of the surface with an advancing contact angle of 71 ^{o} ± 3, presumably as it would be too hydrophilic initially for the hydrophobic PO segments of the molecules to bind.

Once the stamp surface was made hydrophilic, patterning experiments were then repeated, using a UV-Pluronic F-127 stamp instead of unmodified PDMS. **Fig 4.8** shows that pattern integrity improved with the modified PDMS. Although there was still some gaps in the 5 by 5 µm lines, clumping appeared to be dramatically reduced on the PDMS surface (**a**), which then led to better patterning on the MT-SAMs (**b**), with well separated lines. Separation was important in the overall scope of the project, as during co-cultured patterning experiments a second strain of bacteria needed to go in the unpatterned regions.

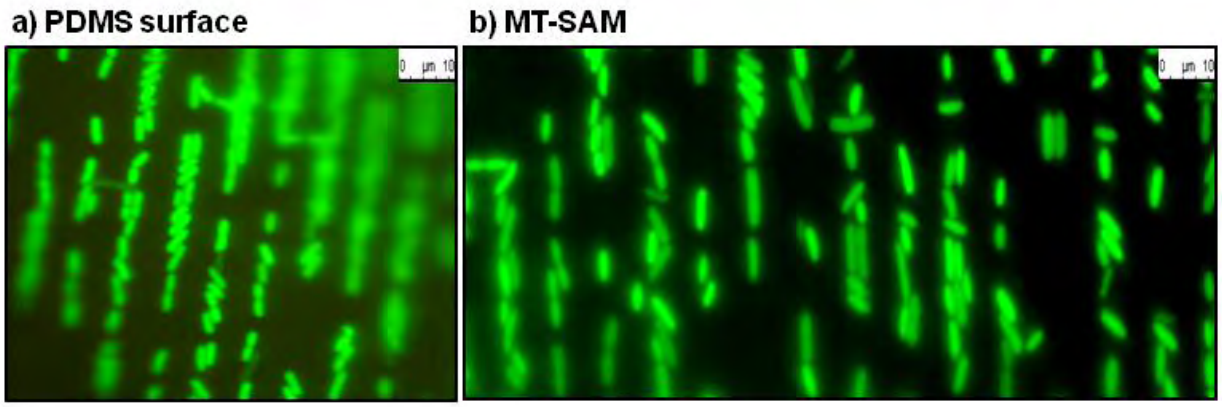

Fig 4.8: Fluorescence microscope image of 5 by 5 µm patterns of GFP- *E. coli* on the surface of a UV-Pluronic F-127 PDMS stamp (**a**) and then printed on MT-SAMs (**b**) (x 100 magnification)

4.3.1.5 Direct patterning using agarose stamps onto MT-SAMs

Previous researchers have used agarose stamps to pattern single cell types, both mammalian and bacterial. For example, Stevens *et.al.,* 2005 used agarose stamps for generating patterns of mammalian cells on porous scaffolds for tissue engineering, with diameters of 200, 700, and 1000 µm[217]. Weibel *et.al.,* 2005 used agarose stamps with features as small as 200 µm to directly pattern *E. coli* onto another block of agarose[135]. Agarose stamps are appealing as they are easy to prepare like PDMS, and they have the added advantage of being able to incorporate culture media into the mix, allowing cells to thrive on the surface. Weibel's group found that this

resulted in a "living stamp" that could regenerate its "ink", and could be used to pattern surfaces repetitively for a month[135].

However, in terms of the scope of this project, one of the drawbacks of agarose gels is that they are softer than PDMS, and do not have the “rubbery” flexiblilty that allows PDMS to make conformal contact with surfaces, meaning that potentially surface structures could collapse upon impact with the surface. In particular, most groups have only used surface features for patterning cells that were 200 µm or above – larger and more easily patterned than the 5 by 5 µm lines. **Fig 4.9** shows the results of patterning attempts with agarose stamps supplemented with 10 % minimal media. The concentration of agarose powder was varied, in order to determine whether a “harder” stamp would generate more robust patterns.

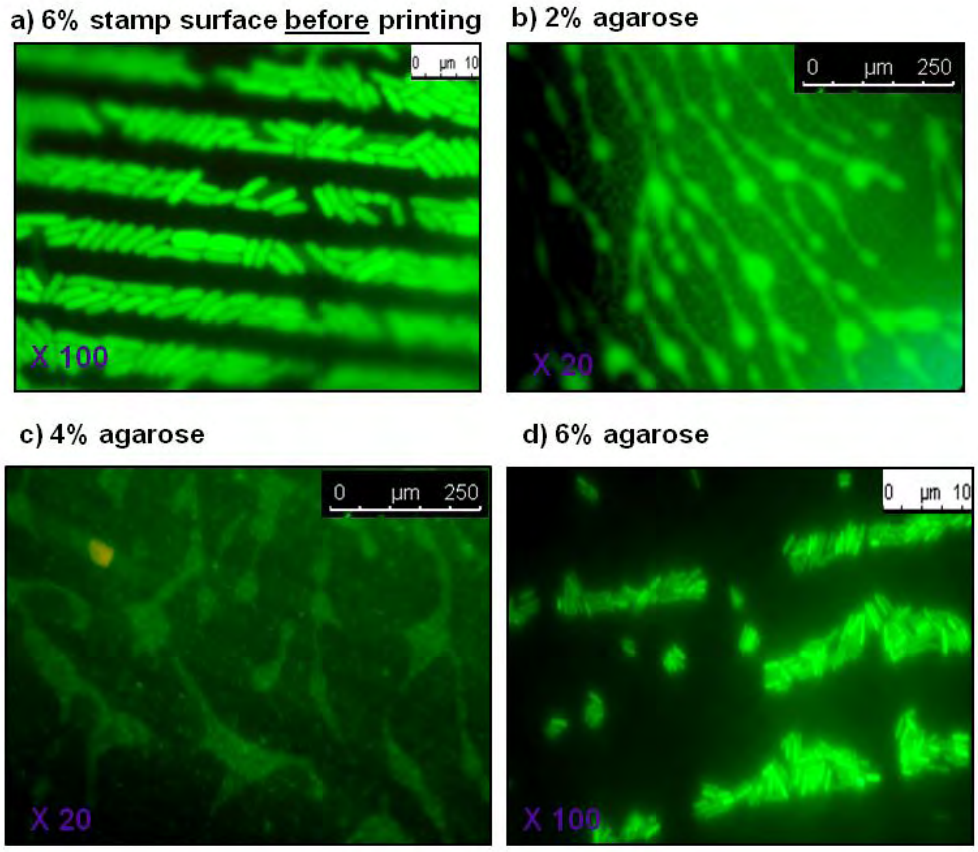

Fig 4.9: Fluorescence microscope images of 5 by 5 µm patterns of GFP- *E. coli* on an agarose stamp surface (**a**); images of the gold substrates following printing with different concentrations of agarose stamp (**b-d**)

Firstly, images were taken of the stamp surfaces before printing, to ensure that the stamp features had retained their integrity following PDMS molding. **Fig 4.9 a** shows the 6 % agarose stamp surface, with perfect 5 by 5 µm lines inked with *E. coli*. Stamp surfaces for 2 % and 4 % agarose had similarly good surface features. The 2 % and 4 % stamps did not manage to produce robust patterns. As **Figs 4.9 b** and **c** show, the *E. coli* are smudged, with large pockets of cells agglomerating due to structure collapse upon impact to the Au surface. Pictures taken at x 20 are shown here to show that this effect was widespread across the sample. The 6 % agarose stamp proved to be much adept at producing patterns; however there is still some slight smudging and gap formation. Additionally, it is worth noting that the 6 % stamp patterns were not very repeatable, some attempts produced decent patterns and some produced very poor patterns, suggesting that the pressure applied to the stamp plays an important role. As shown in later sections of the thesis, attempts were made to control the pressure applied to the sample by using a micromanipulator.

4.3.1.6 Pattern susceptibility to rinsing

Although patterns produced with a Pluronic F-127-modified PDMS stamp were of a good standard, it was important to determine whether the patterns were susceptible to shear flow. For patterned bacterial co-cultures, the single cell arrays would need to be incubated with a second strain of bacteria to fill in the gaps left by the patterns; the patterns would therefore need to withstand the force applied by the liquid and the cells of the second strain. Additionally, as stated previously, in order to perform long-term experiments the patterns would need to remain robust inside the flow cell.

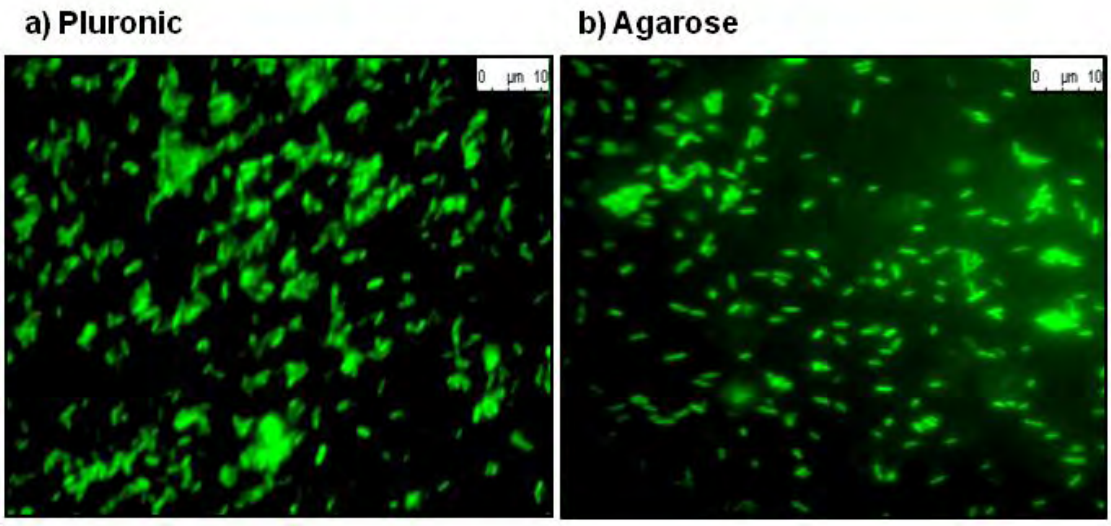

Fig 4.10 shows the images of *E. coli* that had been rinsed with 500 µl of sterile PBS after patterning with Pluronic F-127 treated PDMS (**a**) and agarose (**b**) stamps

The images clearly show that both patterning techniques display poor susceptibility to rinsing procedures. For the modified PDMS surfaces there is just about the remnants of a pattern, but certainly not robust enough to take to co-culture stage.

These poor results revealed some major flaws in the patterning procedures. Firstly, the cells were clearly not adhering to the MT-SAMs in the same manner shown in chapter 4; the initial adhesion results depicted show that it takes up to two hours for the bacteria to form a complete monolayer on the surface of the MT-SAMs, and that agarose substrates have very poor adhesive ability even after two hours. However, leaving bacteria for two hours on the MT-SAMs after printing would cause over-exposure to the elements, cell desiccation and loss of viability. Secondly, the stamps were dried before patterning, and were printed onto a dry MT-SAM meaning that there was no liquid to facilitate the binding of fimbriae to the mannoside residues. Preliminary studies showed that patterning with a wet stamp produced very poor, smudged samples.

It was therefore reasoned that the way to overcome this was to either incubate the sample with a thin layer of liquid (approximately 50 µl minimal media) immediately after printing for up to two hours, or to create a "humidity chamber" that would allow a thin layer of moisture to develop on top of the MT-SAM surface before printing, to facilitate fimbrial binding to MT-SAMs. **Fig 4.11** shows the results of bacterial pattern incubation with media directly after printing over a two hour period

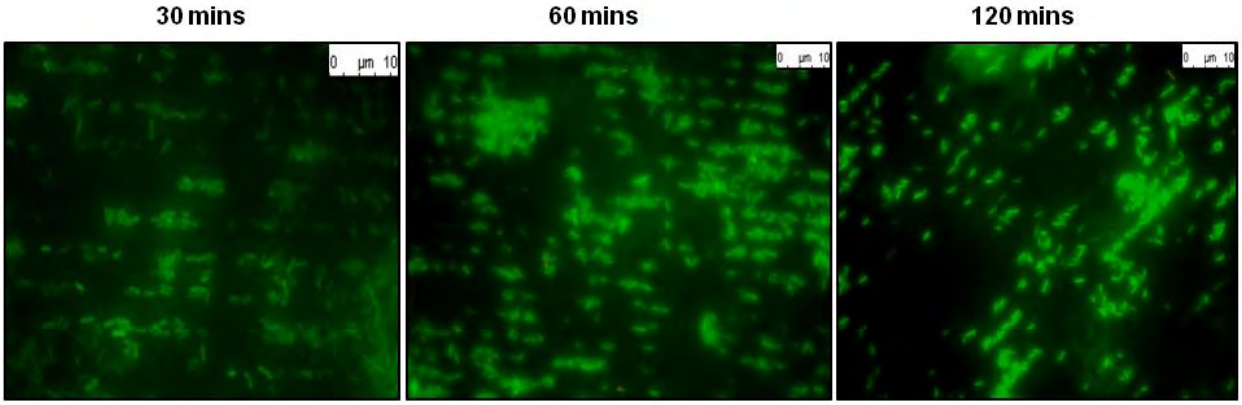

Fig 4.11: Fluorescence microscope images of 5 by 5 µm patterns of GFP- *E. coli* remaining after being immersed in 50 µl minimal media after printing with a Pluronic F-127-modified PDMS stamp

It was concluded that this procedural alteration did not improve pattern integrity after rinsing, and in fact it proved difficult to maintain experimentally as the layer of media evaporated within 1 hour, and had to be replaced. Using a humidity chamber additionally did not work, as no patterns were formed even before rinsing, due to smudging of the surface.

4.3.1.7 Summary

In terms of direct printing of bacteria, using Pluronic F-127 to modify the PDMS stamps proved to be a useful way of controlling bacterial spreading on stamp surfaces, and yielded the best patterning results overall. For creating single cell arrays, this is a promising development for

bacterial micromanipulation; however, in order to use the patterned cell arrays for HGT experiments it was clear that the cells were not interacting with the MT-SAMs as required. The inability to maintain pattern integrity under fluid flow conditions becomes problematic when considering the construction of patterned co-cultures, and the fact that cells need to be kept viable using liquid media.

4.3.2 Lift-off patterning

4.3.2.1 Overview

As mentioned previously, the main problem with the initial attempts to pattern a single strain of *E. coli* was that the cells were easily removed with rinsing. Therefore, it was decided to make a simple adjustment to the patterning procedure by performing everything in reverse, focusing on adhesion first and foremost by allowing the cells to attach for the two hours required to form a monolayer, and then removing cells with a patterned stamp instead of printing them. We termed this "lift-off patterning"; although in the literature it is also known as subtractive printing[130].

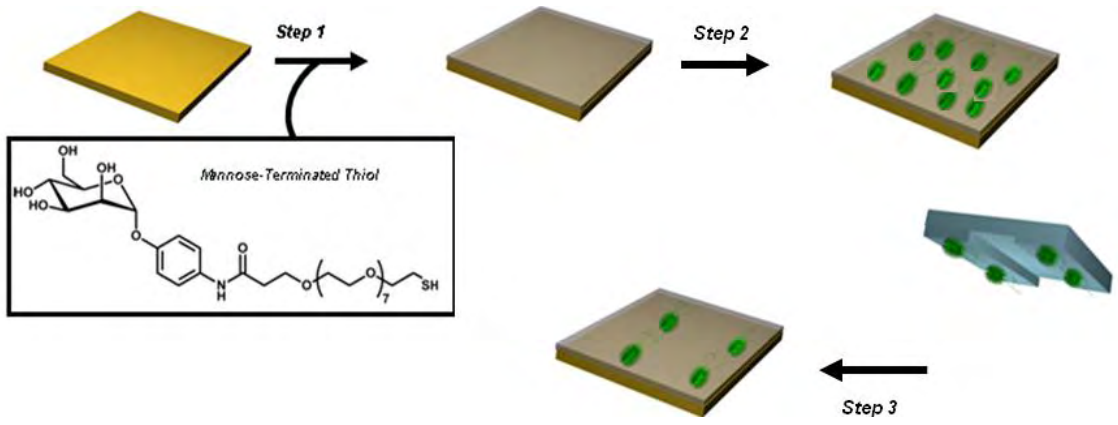

Fig 4.12: Schematic representation of bacterial patterning via microcontact printing. A MT-SAM is formed as normal, but before patterning the substrates are incubated with *E. coli* for 2 hours at 37^{o}C. Once a monolayer had formed, cells were then removed with stamp features, and the cells remained formed a pattern.

Fig 4.12 shows the procedure used for lift-off patterning. Giving the cells appropriate adhesion time would theoretically enable them to be less susceptible to rinsing dislodgment once in the patterns, and be able to withstand the addition of a second strain of bacteria to fill in the gaps.

4.3.2.2 Lift-off patterning procedure

GFP- *E. coli* cultures were grown to OD of 0.6 after dilutions from overnight cultures. MT-SAMs were incubated with 100 µl of the cell suspension at 37^{o}C to allow attachment. After two hours, unattached cells were removed by rinsing with sterile PBS. The micro-patterned stamps were then carefully placed onto the bacterial monolayer feature side down, and then peeled off to remove selected cells on the surface, leaving a pattern of cells remaining on the MT-SAMs. A cover-slip was placed directly on top of the sample with a thin layer of minimal media to keep the cells viable during microscopy, or the cells were placed directly into the flow cell during rinsing studies.

Additionally, after re-evaluating the original procedure further it was decided that a new silicon master should be produced, with features that had a greater depth than 2 µm. The length of an average *E. coli* cell is between 0.5 and 1 µm, meaning that there is only 1 µm difference between the stamp surface and MT-SAM once the stamp is placed on top, leaving very little margin for error. This could have potentially made lift-off patterning problematic, as cells that are not in contact with the stamp features may also be lifted off, even if there is only slight feature deformation or collapse. New silicon masters were therefore fabricated, with a feature depth of 9 µm (**Fig 4.13**). However, as the depth had increased, the width of the lines had to be increased to 10 µm in order to avoid feature instability. Therefore, subsequent bacterial arrays were patterned with 10 by 10 µm lines.

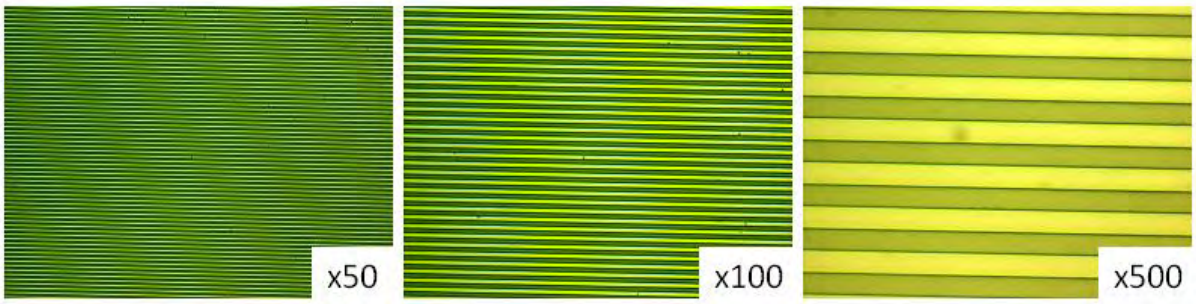

Fig 4.13: Schematic representation of SU8 master; pattern features are 10 by 10 μm lines with a final depth of 9 μm

Even with the new silicon masters, a stamp with a feature depth of 9 μm was still susceptible to deformation and structure collapse if the pressure placed on top was too great. Although patterning by hand can be enhanced with experience, it is unreliable as pressures will not be the same each time, and it can be difficult to perform using tweezers. Previous patterning attempts required that multiple MT-SAMs be fabricated in order to get one or two good images – we therefore needed a more reliable and repeatable method of patterning that could be controlled computationally. Towards this aim, a triple-axis (x, y, z) motorized micromanipulator was used for lift-off patterning procedures (**Fig 4.14**). Briefly, a specially designed stamp holder was mounted to the bottom of the z-axis stage of the micromanipulator, which could then be moved into position computationally. The stage could be moved step-wise in increments as small as 1 nm, and for gauging the pressure applied from the stamp to the MT-SAMs, a 'load cell' was designed that would measure the pressure signals in terms of voltage, which can be converted into Pascals using appropriate equations.

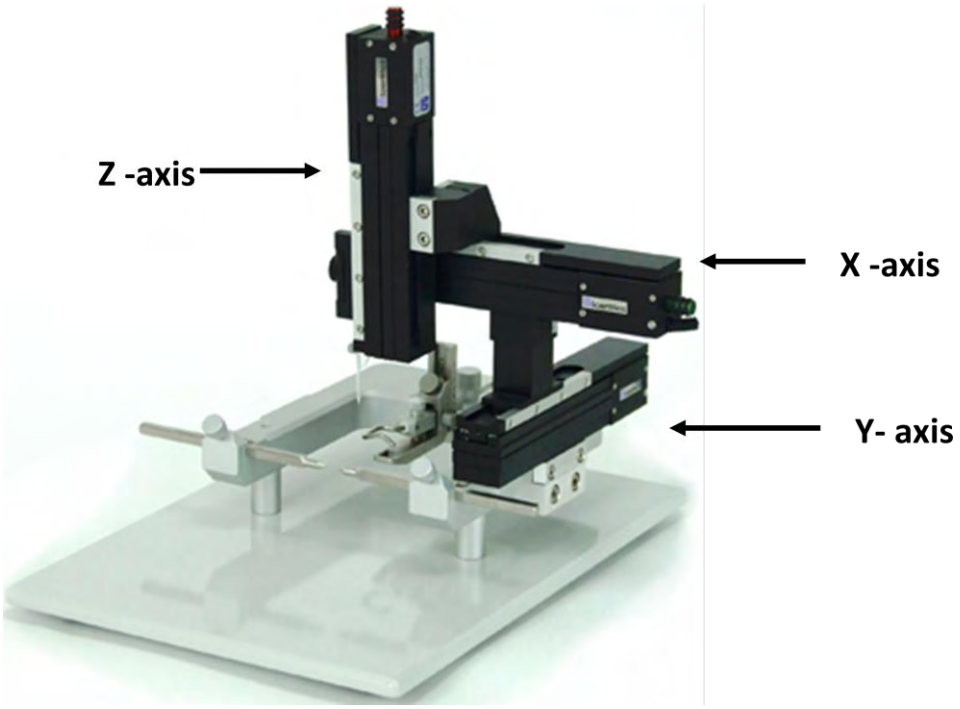

Fig 4.14: The triple axis, motorized micromanipulator

4.3.2.3 Effect of stamp type

As with the direct microcontact printing method, it was important to determine the appropriate stamp type for lift-off patterning. A Pluronic F-127-modified PDMS stamp and an agarose stamp (6 %), both with 10 by 10 µm features, were placed feature side-down on MT-SAMs coated with a bacterial monolayer and then lifted off to reveal the pattern. **Fig 4.15** shows that the best patterning results were obtained using an agarose stamp. The features are better defined, and although there are some break-away cells in the gaps, a lower magnification (x 20) shows that the pattern was made uniformly across the surface. Previously, **Fig 4.9 a** showed that the agarose stamp surface had almost perfect rows of cells, however, once printed the features were deformed and the pattern destroyed. The modified printing method along with the increased feature depth appears to have rectified this.

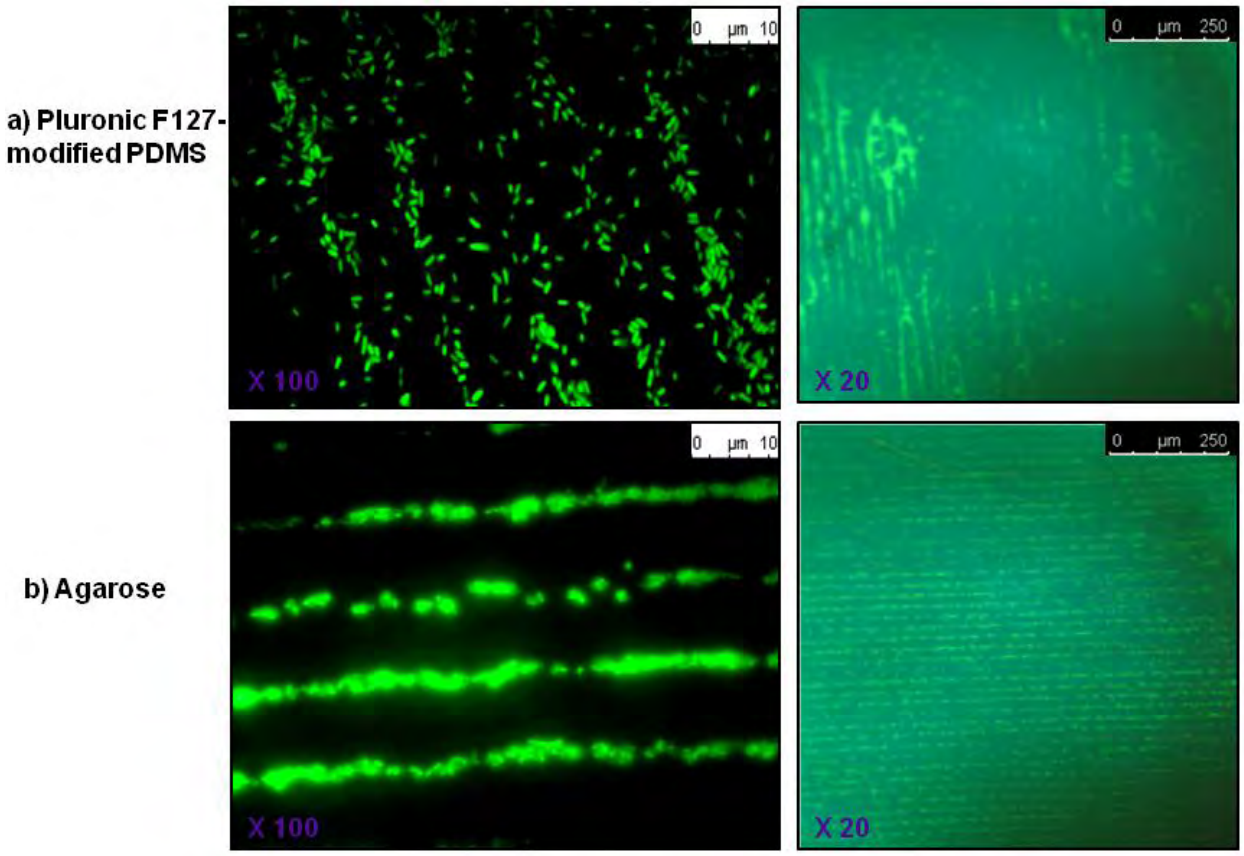

Fig 4.15: Fluorescence microscope images of 10 by 10 µm patterns of GFP- *E. coli* formed by lift-off patterning with a Pluronic modified stamp (**a**) and a (6 %) agarose stamp (**b**)

With direct printing, the PDMS does not need to be particularly adhesive; the important factor was that the contact angle changed and the cells spread uniformly across the surface. In fact, it is better for the PDMS to not be adhesive so that cells can be transferred easily. Therefore Pluronic-F127 stamps were the best choice. However, with lift-off patterning the cells are already attached to the MT-SAMs, and therefore we need a stamp that can remove them. Both Pluronic-PDMS and agarose are hydrophilic, so wettability is not a major factor in the patterning difference in this regard. Agarose works better than PDMS in potentially because of the texture; it does not form specific bonds with the bacteria but may act like putty, as it is soft and the cells can easily become embedded in the patterned features.

One of the potential problems of lift-off patterning was that it may have removed the MT-SAMs along with the bacteria; therefore it was an important control to ensure that the MT-SAM was still in place by removing the cells and then re-establishing a monolayer (**Fig 4.16**). Cells were removed using an un-patterned block of agarose (approximately 5 mm by 5 mm) and then the surface was re-inoculated with fresh *E. coli*, and cells were able to adhere again onto the same surface for 2 hours, suggesting that the MT-SAMs remained intact.

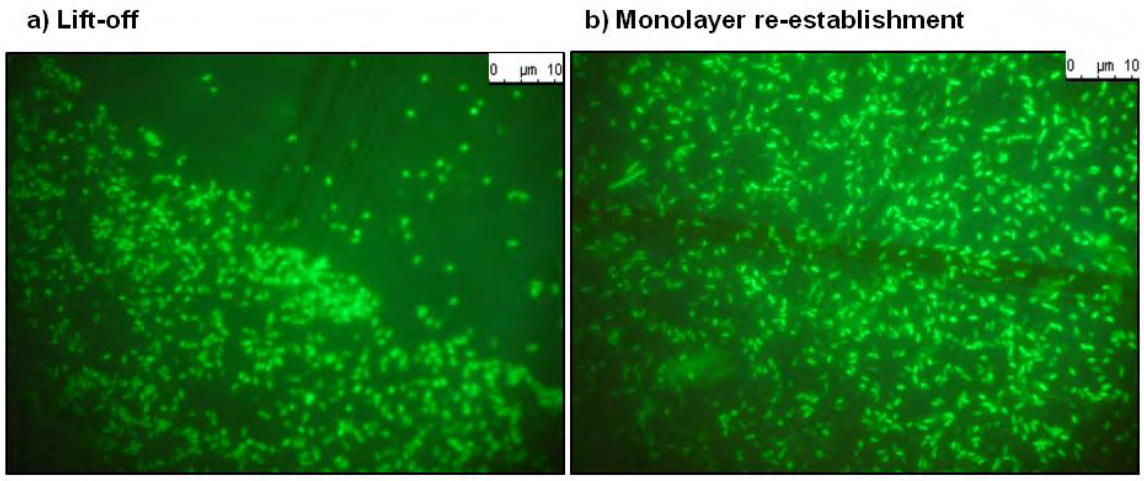

Fig 4.16: Fluorescence microscope images of a control lift-off experiment of GFP- *E. coli* on MT-SAMs (**a**) followed by re-immersion and re-establishment of the monolayer in the gap left by the agarose stamp (**b**).

4.3.2.4 Lift-off patterning with micromanipulation

After determining that agarose stamps were best suited for lift-off patterning, the micromanipulator was then employed in order to have greater control over the pressures applied to the bacterial monolayer. Once bacterial adhesion had occurred, the gold substrate was placed on top of the load cell, and the agarose stamp secured onto the stamp holder on the Z-stage. The Z-stage was then carefully lowered using a remote control onto the bacterial monolayer. As soon as the stamp holder made contact with the gold substrate, a voltage signal was detected; this was proportional to the pressure/weight on top of the load cell. Before experimentation, a calibration curve for voltage/weight was established using pre-measured weights (**Fig 4.17**). Voltage

readings could then be converted to weight (g/cm^2), and then to pressure (Pa), as 1 g/cm^2 is the equivalent of 98 Pa.

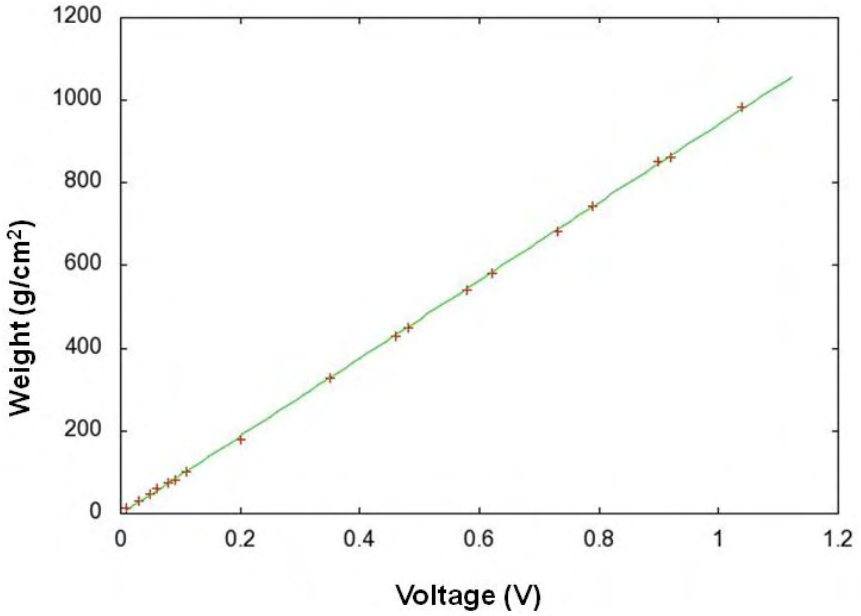

Fig 4.17: Calibration curve for the load cell, showing voltage readings at increasing weights.

Fig 4.18 shows the lift-off patterning results using agarose stamps at different pressures. The patterns produced at 13.9 kPa were the best, with almost perfect removal of cells from the surface, little gap formation and clear separation between the lines. As a control, at the extremes there was either too little cell removal at very low pressures (0.96 kPa), or too much cell removal caused by stamp deformation at very high pressures (36.3 kPa). This was an important development in the cell patterning procedures, as the optimum pressure for pattern formation was now known, and could be programmed and reproduced a lot more reliably than patterning by hand.

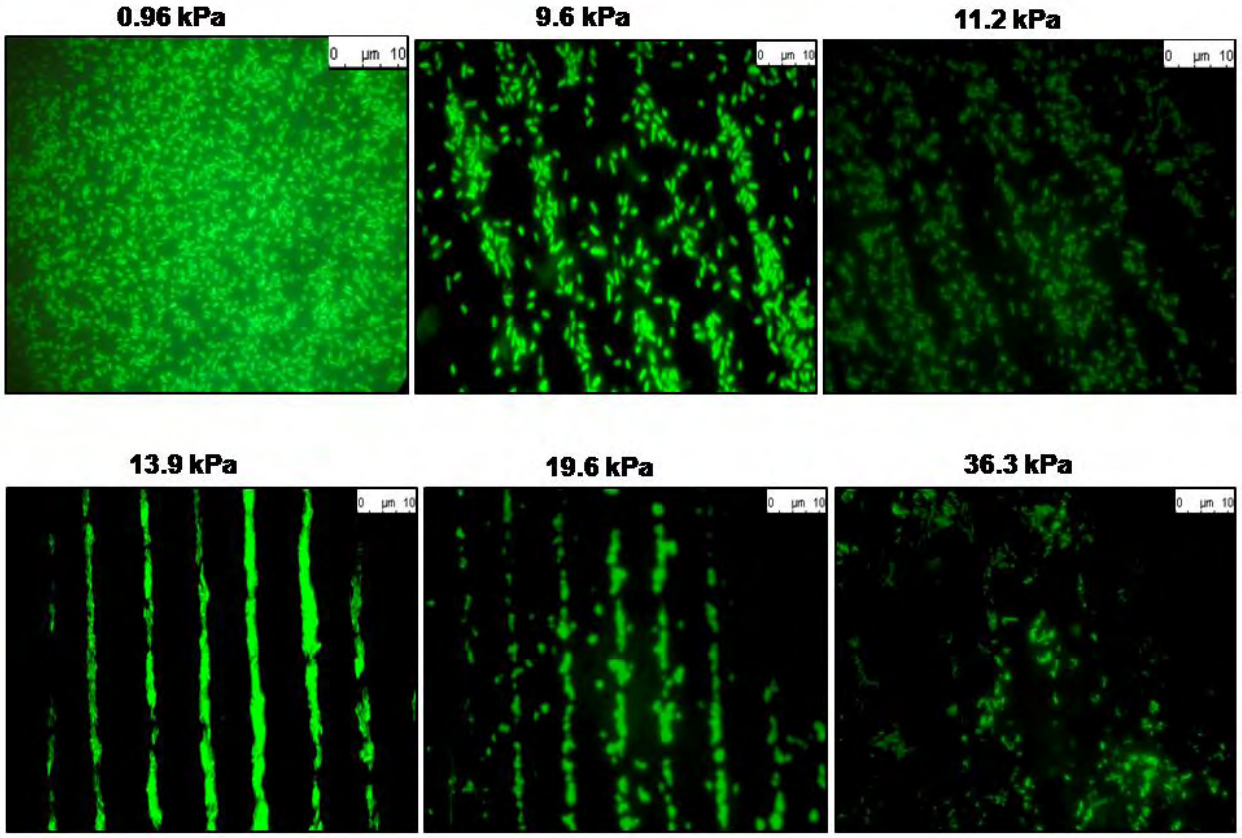

Fig 4.18: Confocal microscope images (x 63) of 10 by 10 µm lines of GFP- *E. coli* on MT-SAMs using agarose stamps at different pressures

4.3.2.5 Pattern Longevity

Another important control was to ensure that cells were growing on the gold surfaces once in the patterns. The rate of growth of a cell culture is a measure of metabolic activity, and HGT is a metabolic process[15]. Although conjugative plasmids are self transmissible, they still require energy for pilus formation, replication and recombination, and therefore logically we would expect to see more transfer events in a growing culture compared to a static culture. **Fig 4.19** shows the results of 10 by 10 µm patterns of *E. coli* that had been left growing at 37^{o}C with minimal media. The images show that over the 8 hour period, the thickness of the lines increased, the gaps were filled in and the cells began to branch out from the patterns.

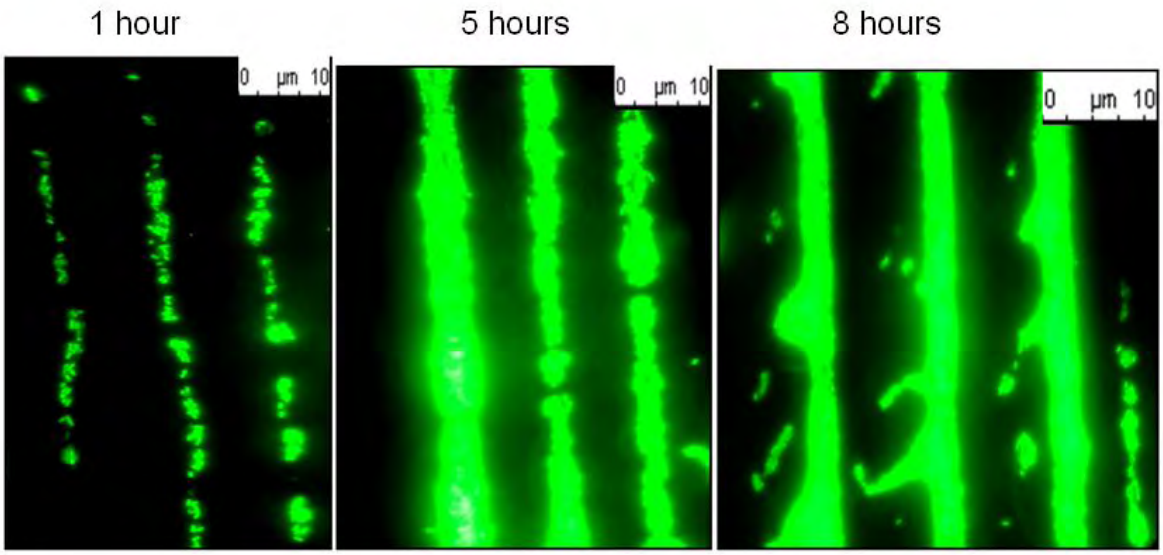

Fig 4.19: Confocal microscope images (x 63) showing growth of 10 by 10 µm lines of GFP- *E. coli* on MT-SAMs

MT-SAMs growth rates were compared with cells growing on M9 agarose. Even though we cannot sustain patterns on agarose, the growth rate of cells is substantially higher than that on gold; we see a complete surface coverage within 5 hours from a low inoculation (10^5 cells/ml) (**Fig 4.20**).

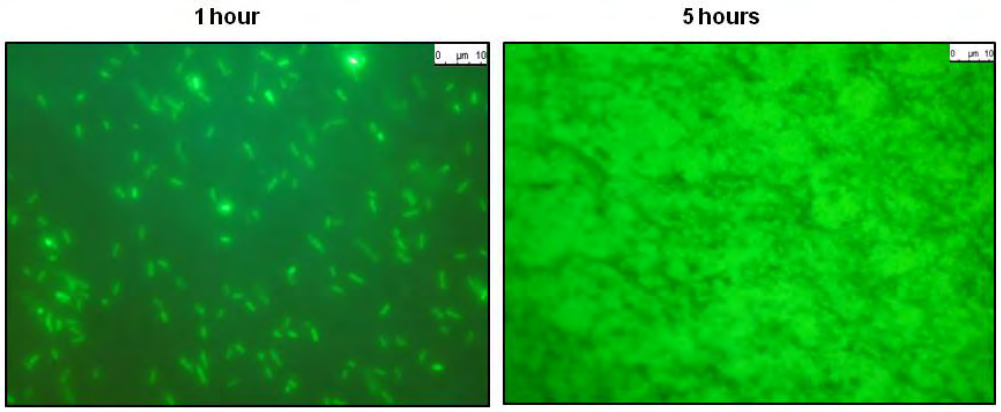

Fig 4.20: Fluorescence microscope images (x 100) showing growth on M9 agarose

To confirm the images, plating experiments were performed by inoculating M9 agarose and MT-SAMs with exponential phase *E. coli* over a 6 hour time period. Cells were incubated for 2 hours at 37^{o}C, and then rinsed with 100 µl minimal media to remove free-floating bacteria. The

substrates were then incubated with a thin layer of media for up to 6 hours, and the cells were removed by sonication and recovered by plated onto LB agar. **Fig 4.21** shows that although there was bacterial recovery on both substrate types, there is less recovery from cells incubated on MT-SAMs than on an agarose substrate; this could be attributed to a longer lag phase on the MT-SAMs than on the agarose, causing a delay in cellular replication. . Even though they are kept in the same media throughout experimentation, the cells appear to take to adjust to the new conditions on the MT-SAMs. From this data, therefore, in terms of the HGT experiments it would likely take longer for transfer events to occur on gold substrates than agarose.

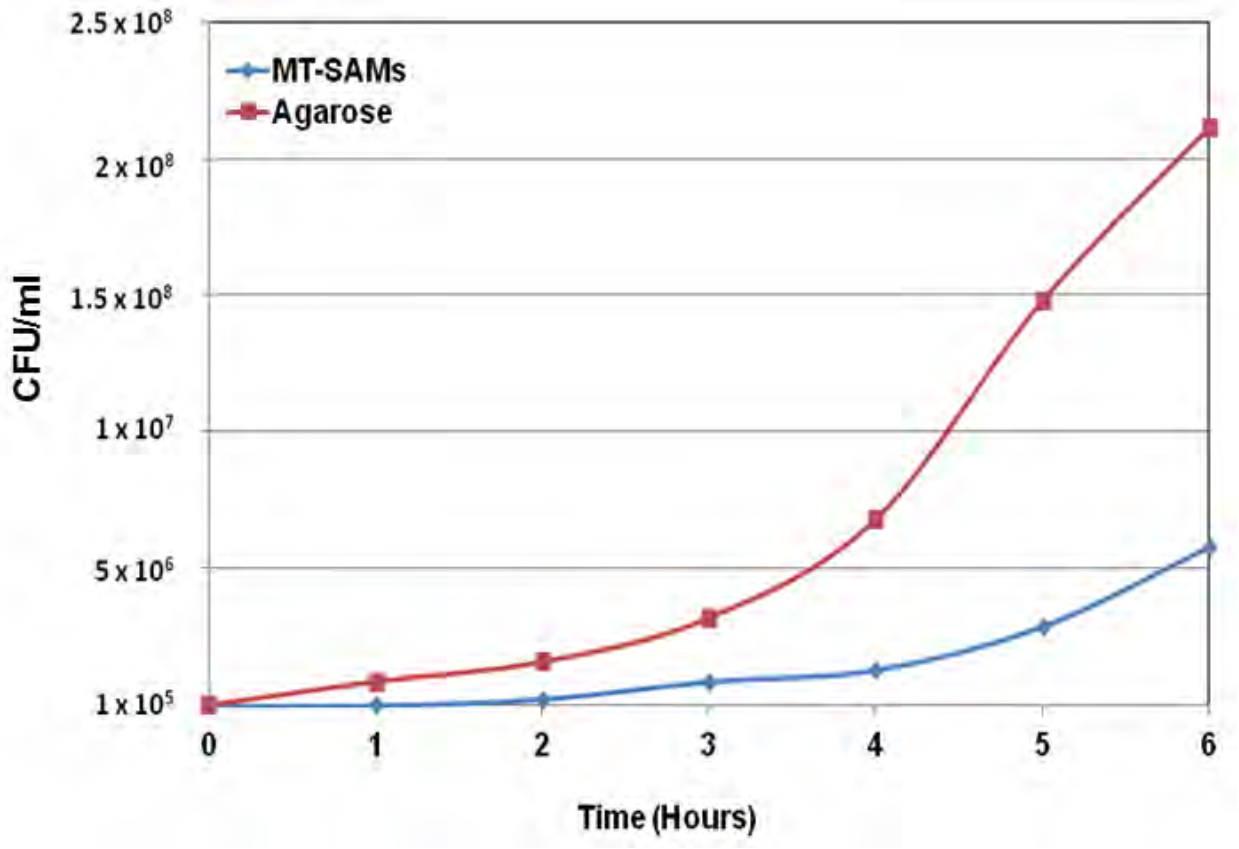

Fig 4.21: Bacterial recovery after growth on MT-SAMs and agarose substrates

4.3.2.6 Pattern susceptibility to rinsing

As with previous patterning procedures, it was important to check the patterned cells' durability to rinsing. Unlike the direct printing method, the new patterns remained after rinsing with 500 µl sterile medium, so the samples were transferred to the flow cell to test their resistance to long-term flow. **Fig 4.22** shows that at 20 µl/ minute, patterns remained for at least 2 hours, with some dislodgement of cells after three hours.

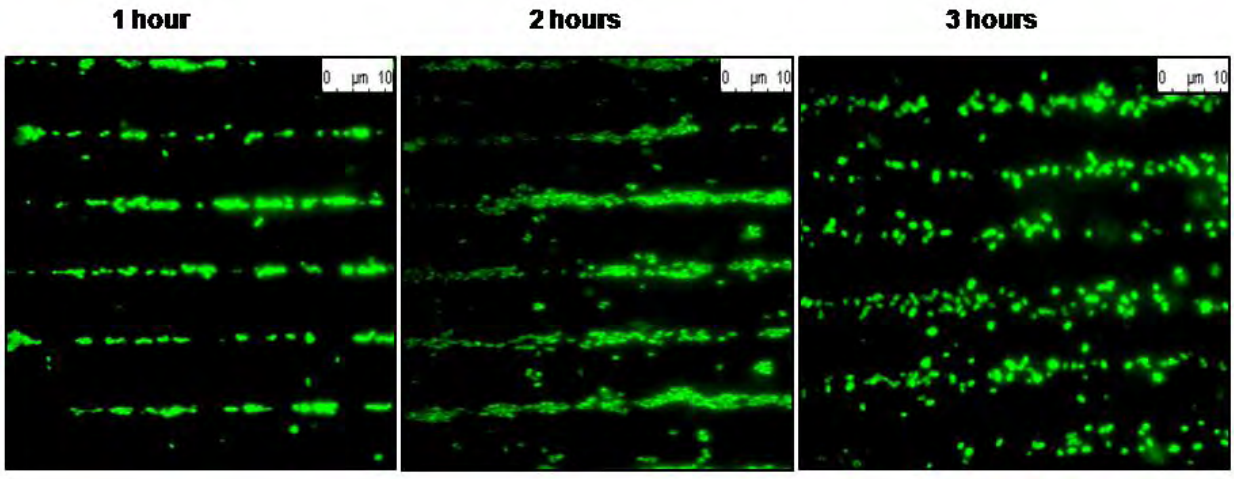

Fig 4.22: Confocal microscope images (x 63) showing growth of 10 by 10 µm lines of GFP- *E. coli* on MT-SAMs in the flow cell over a three hour period

4.4 Patterned Co-Cultures

4.4.1 Co-culture Formation

For co-culture formation, single-strain patterns were prepared using the lift-off procedure. Then, patterns were incubated with 100 µl RFP-cell suspension (strain DH5 α mCherry, cloned in the standard multicopy cloning vector, pJet1.2, ampR; excitation max 587 nm, emission max 610 nm) for 1 hour at 37^{o}C to allow attachment to the unpatterned regions of the MT-SAMs. Second strain concentrations were verified by a systematic study. Subsequently, a cover-slip was placed directly on top of the sample with a thin layer of minimal media to keep the cells viable during microscopy, or the patterned co-cultures were placed directly into the flow cell during rinsing

studies. For studies with a blocking protein, concentrations of (0.01 mM) ConA in Tris-buffer with Mn^{2+} and Ca^{2+} or (0.01 mM) ConA mixed with (0.03 mM) D-mannose were immersed onto the MT-SAMs after bacterial monolayer formation before single-strain patterning, and then rinsed with sterile PBS before immersion of the second *E. coli* strain.

4.4.2 Second Strain Concentrations

The first stage in patterned co-culture formation was to ascertain the optimum cell concentration necessary to fill in the un-patterned regions of the MT-SAM. Single-strain patterned arrays were formed via lift-off patterning from a RFP- E. *coli* monolayer, with an agarose stamp using the micromanipulator with a pressure of 13.9 Pa. The substrates were then immediately immersed in GFP- *E. coli* in minimal media and incubated for 1 hour at 37^{o}C. Although for initial monolayer formation the cells were incubated for 2 hours to allow attachment; during experimentation HGT may start to occur within a short time frame, so ideally the second strain should be deposited onto the surface as quickly as possible.

Fig 4.23 shows the confocal microscope images taken of the patterned co-cultures with varied GFP- *E. coli* concentrations, with the images separated out to show RFP patterns, the GFP-*E. coli* that had attached to the unpatterned regions. After immersion with GFP-*E. coli* at an OD of 0.2, the patterns remained relatively intact, however the cell concentration was not high enough to fully fill the unpatterned regions. As stated previously, HGT with an RK2 plasmid requires cell-cell contact, so it was imperative that the both strains were touching. Increasing the cell concentration rectified this problem, however it also had a detrimental effect on the original pattern. As the images at 0.4 and 0.6 OD show, increasing the second-strain cell concentration and then immersing for one hour on the substrate caused RFP-*E. coli* to break away from the

pattern and become mixed with the GFP- *E. coli*. In addition, it was also observed that if there were small gaps present in the pattern, then the GFP- *E. coli* would also fill these gaps.

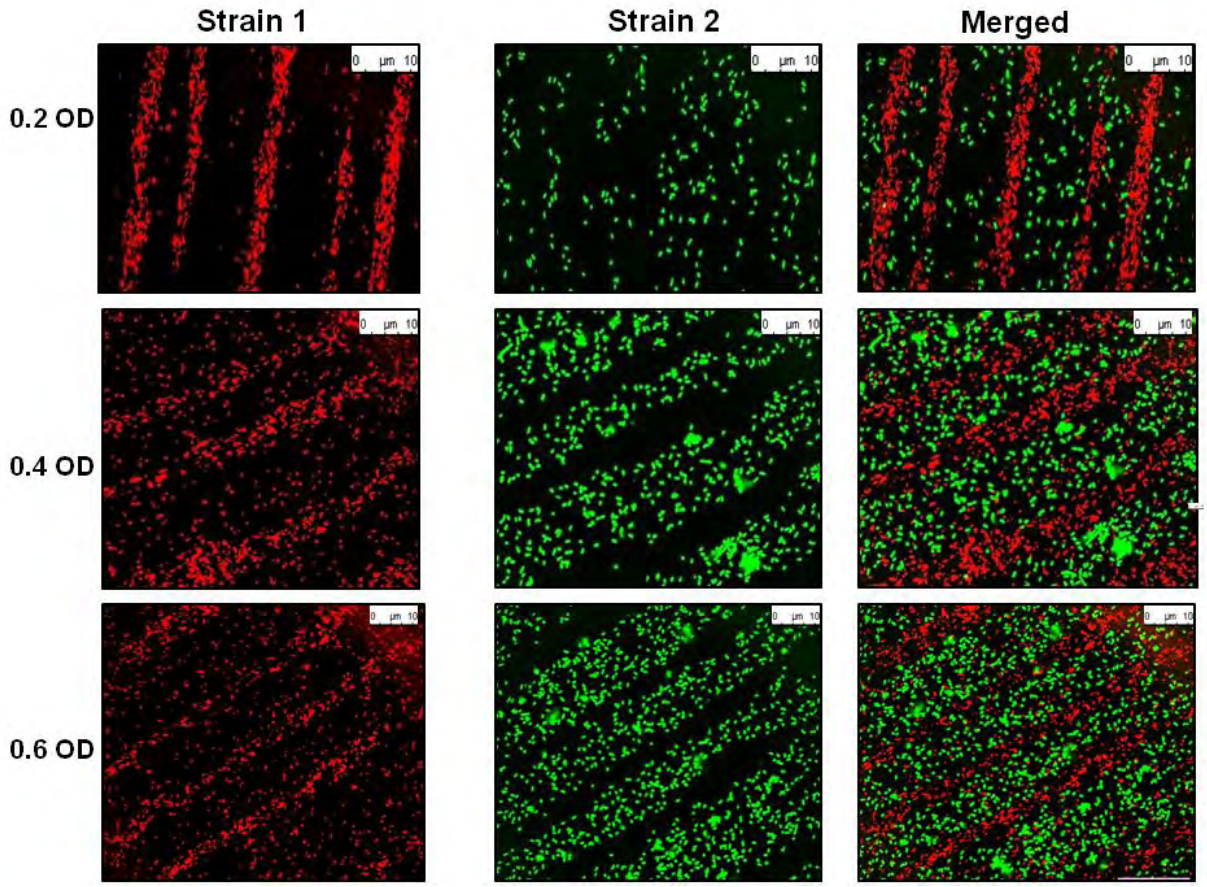

Fig 4.23: Confocal microscope images (x 63) RFP-*E. coli* patterns (strain 1) alongside GFP-*E. coli* in the unpatterned regions incubated on the patterns for one hour (strain 2), forming patterned bacterial co-cultures (merged image)

Therefore the initial co-culturing experiments yielded two major problems to rectify: pattern dislodgement and unwanted gap filling, both of which caused mixing of bacterial strains. During HGT experiments although the donors and recipients need to be touching, ideally we wanted to have a clear distinction between the two (alternating strips, rather than an undefined mixture), so that we could follow a "wave" of plasmid transfer from one strip to the other – the point of the patterning being that we have control over the positioning of the donor cells where we want them, so that at each transfer event we know where the plasmid has come from.

4.4.3 Effect of a Blocking Protein on Strain Mixing

4.4.3.1 Overview

In order to try and prevent mixing of bacterial strains in small gaps in the patterns, a "blocking protein" was constructed using ConA. As depicted in **Fig 4.24**, the idea was to form the initial monolayer of *E. coli* with a low concentration of blocking protein, which would fill in any small gaps on the MT-SAM. During lift-off patterning, the ConA would theoretically be lifted-off in addition to the *E. coli*, and remain in the patterned regions, so that upon immersion of the second strain the ConA would prevent the binding of cells in the patterned regions.

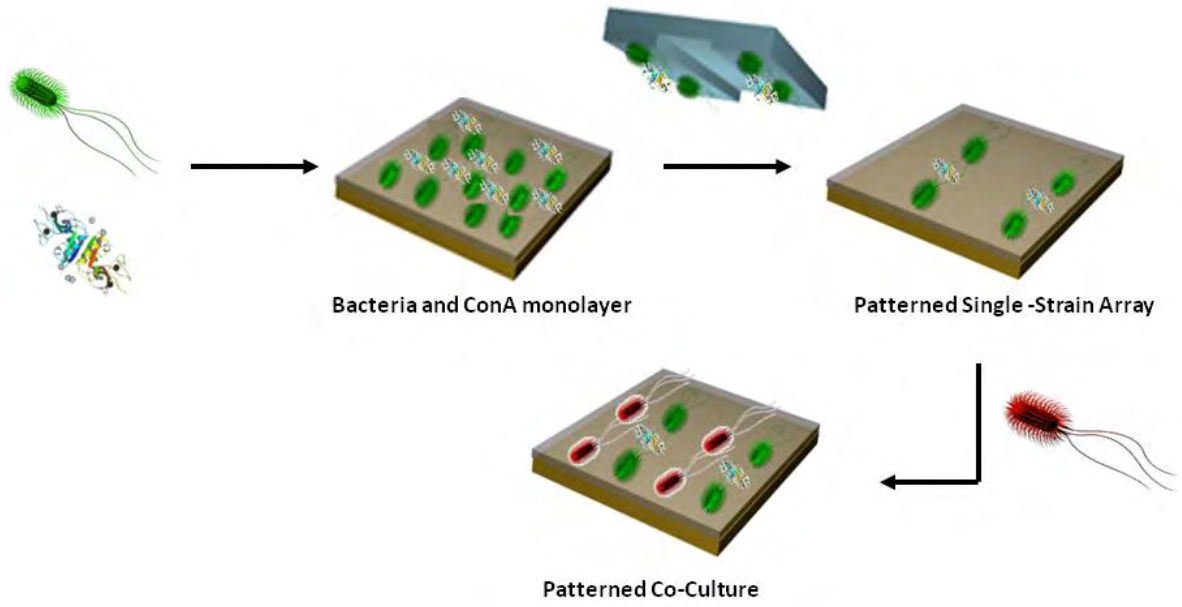

Fig 4.24: Schematic representation of blocking protein procedure

ConA is a tetramer, with four binding sides for mannose residues. As bacterial cell walls can contain mannose-rich glycans[218], the cells may attach to the ConA proteins as there would still be three binding sites available after immobilization to the MT-SAMs. Therefore, before immobilisation, the ConA was mixed in a 3:1 molar ratio with D-mannose, to fill up the additional binding sites, and hopefully prevent the cells from attaching.

4.4.3.2 Effect of blocking protein on cell attachment to MT-SAMs

Before the blocking protein was tested with the pattern co-cultures, we needed to ensure that it prevented bacterial adhesion. **Fig 4.25** shows the results of an SPR experiment, in which an *E. coli* suspension was injected over monolayers of ConA (with no mannose) and the 3:1 mannose-ConA molecules, against controls of a MT-SAM and a COOH-SAM. Confocal images of the SPR chip were taken directly after experimentation. There was a reduction in binding from the MT-SAM to the 3:1 blocking protein of 1500 RU, suggesting that the blocking protein was successfully inhibiting bacterial adhesion. However, there was only a 100 RU difference between a mannose-free ConA monolayer and the 3:1 blocking protein, suggesting that even though three ConA sites were available for mannose-binding, the binding sites were not readily accessible for the bacteria.

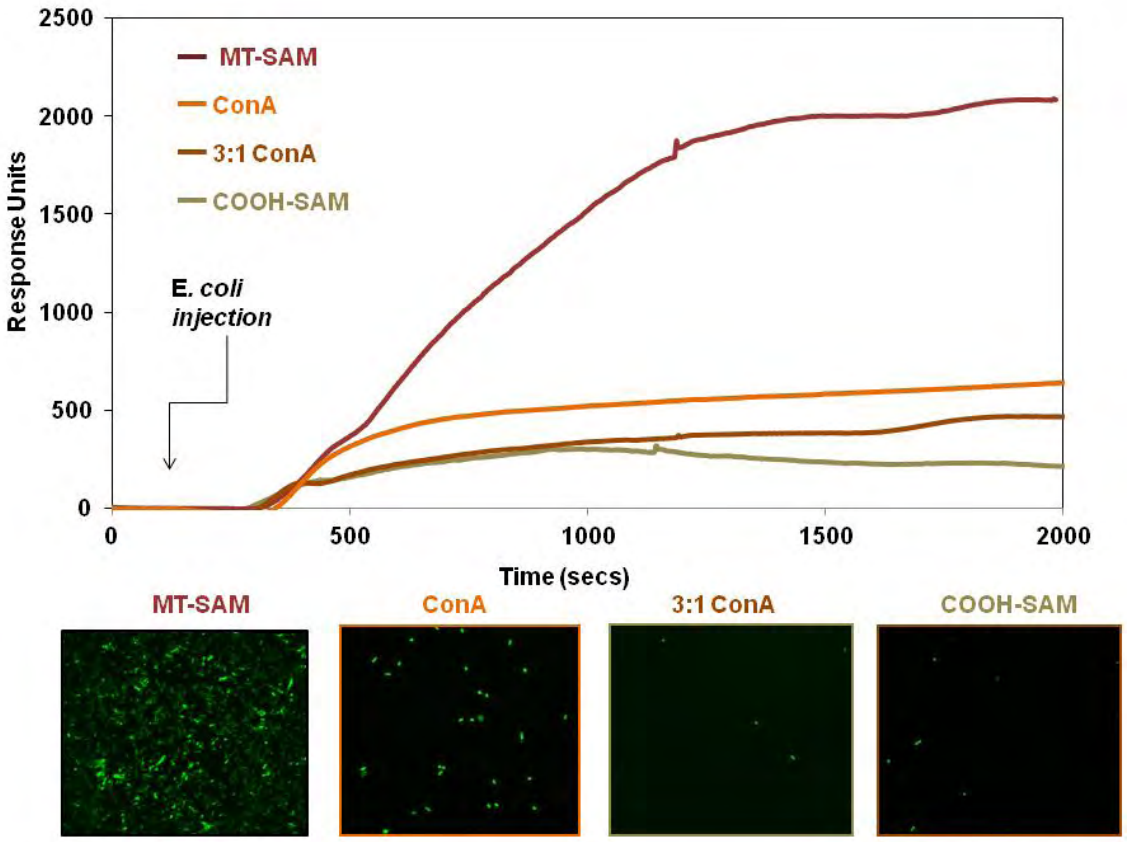

Fig 4.25 SPR sensorgram traces showing the binding of *E. coli* (OD_{600} 0.6) to the MT-SAM, and the reduction in binding when injected over a ConA-terminated SAM, a 3:1 ConA-terminated SAM, and a COOH-SAM. After bacterial binding for 30 min, the surfaces were washed with PBS for 20 min to remove any non-specifically adsorbed cells

Before patterning experiments, another control was devised to ensure that the blocking protein would still inhibit a second strain when mixed with the first strain of bacteria. A solution of the 3:1 blocking protein was incubated over an RFP- *E. coli* monolayer following bacterial attachment for 2 hours at 37^{o}C as usual. Excess blocking protein was then rinsed, and the substrate immediately incubated with GFP- *E. coli* at 0.4 OD_{600}, mimicking the original co-culture experiments but without patterning. **Fig 4.26** shows that with low concentration of ConA added the RFP- *E. coli* monolayer remains intact. When no blocking lectin was used, the GFP-*E. coli* could still attach to the surface as not all of the binding sites on the MT-SAMs were filled (**b**); however, with a 30 minute blocking protein incubation there was a slight reduction in binding and with 60 minute incubation there was an even greater reduction. Therefore, the blocking protein appeared to be binding to free mannose sites on the MT-SAM not occupied by the bacteria, and it was capable of inhibiting the adhesion of a second strain of *E. coli*.

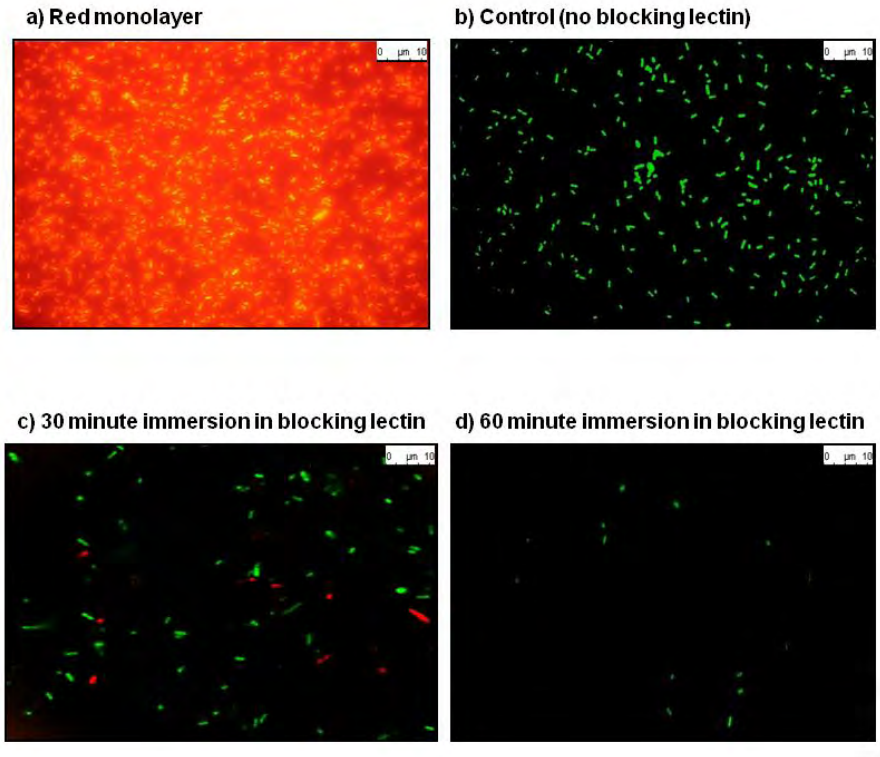

Fig 4.26: Confocal microscope images (x 63) of an RFP-*E. coli* monolayer with a 1 hour incubation of blocking protein (**a**); GFP-*E. coli* attachment to an RFP-*E. coli* monolayer in the absence of blocking protein (**b**); GFP-*E. coli* attachment to an RFP-*E. coli* monolayer after 30 minutes (**c**) and 60 minutes (**d**) immersion in blocking protein.

4.4.3.4 Effect of blocking protein on strain mixing in patterned co-cultures

Once it had been established that the blocking protein was capable of inhibiting a second strain of *E. coli*, the experiments were repeated with the patterning procedures. A GFP- *E. coli* monolayer on MT-SAMs was incubated with blocking ConA protein for 60 minutes, and then lift-off patterning was employed to create 10 by 10 µm patterns on the surface. The patterned substrate was then incubated with RFP- *E. coli* (concentration 0.4 OD_{600}) for 1 hour at 37°C. As **Fig 4.27** shows, the presence of blocking protein still allowed patterns to be formed (**a**); however it also prevented RFP- adhesion on the un-patterned regions as well as in the gaps in the pattern (**b**). Compared to the second strain immersion images in **Fig 4.23**, we are seeing a large reduction in adhesion in the un-patterned regions at the same cell concentration, suggesting that the blocking protein was not being removed from the surface during the lift-off patterning. The ConA is a protein, and much smaller than the bacteria, so therefore it is possible that the stamp features did not make contact with it.

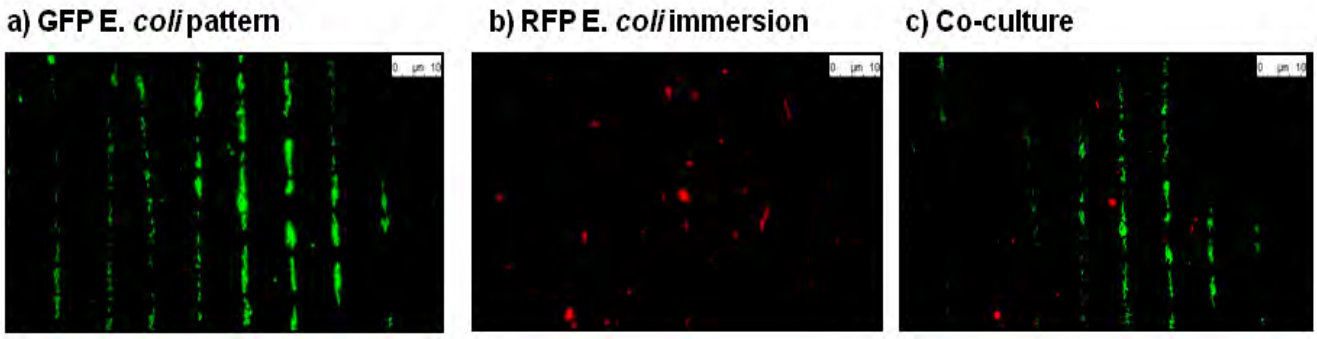

Fig 4.27: Confocal microscope images (x 63) of GFP- *E. coli* 10 by 10 µm patterns formed after a 1 hour incubation of blocking protein (**a**); RFP-*E. coli* attachment to the patterned array (**b**); and the final co-culture image (**c**)

Due to time restraints, we decided to not to pursue the blocking protein theory and concentrate on improving pattern integrity upon second-strain immersion. However, it is still an interesting result and could be built upon in the future.

4.4.4 Improving pattern integrity in co-cultures

Even though unfortunately the problem with mixing in gaps in the patterns could not be rectified, attempts were made to prevent the cells in the patterns from becoming dislodged. Even if we could not control the positioning of the second strain (the recipients) as such, being able to control the first strain (the donors) would be an improvement.

Looking back to the original rinsing experiments performed with a bacterial monolayer on MT-SAMs, the cells had great resistance to dislodgment via fluid flow after 2 hours attachment time, due to the catch-bond mechanism of the FimH-mannose bond that provides binding strength at shear forces[184]. After the single-strain lift-off procedures, the patterns were still maintained for 2 hours under shear flow, however the resistance to rinsing was not as effective as the monolayer of cells without patterning, as there was some dislodging of cells once patterned. Similarly, after adding a second strain of bacteria, the cells in the patterns become even more dislodged and mix in with the second strain. The likely cause of this therefore is the patterning; pressure from the stamp could break some of the mannose-FimH contacts on the bacteria at the edges of the surface features, meaning that the some cells left on the surface would not be adhering as strongly to the surface as others. We had already experimented with stamp pressures previously, so the next logical step was to give the cells some time to form more contacts with the MT-SAMs before immersion in the second strain.

Following lift-off patterning, the patterned cells were incubated at 37^{o}C with a thin layer of minimal media gently applied to the surface before second stain immersion. **Fig 4.28 a** shows that the 30 minute incubation before attachment of the second strain meant that the RFP- *E. coli* patterns were more robust after following the addition of the GFP- *E. coli* (0.4 OD), and even though some of the GFP 'recipient' cells had attached to the gaps in the pattern, we still had control over the positioning of the RFP 'donors'. Additionally, this improvement meant that the

patterned co-cultures were now more resistant to rinsing procedures (**Fig 4.28 b** and **c**); after a 4 hour rinse at 20 µl/ min the patterns remained intact.

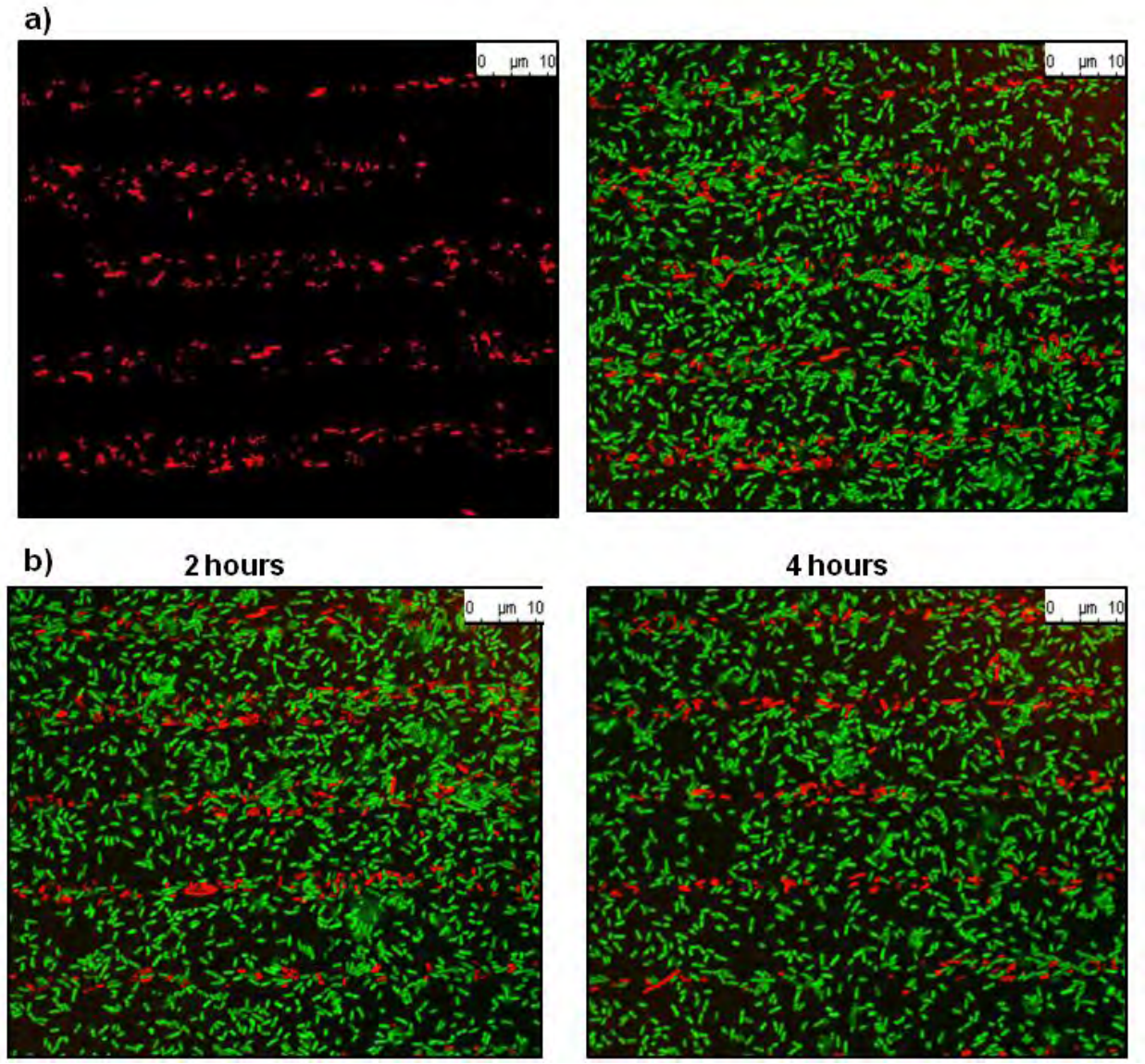

Fig 4.28: Confocal microscope images (x 63) of RFP- *E. coli* 10 by 10 µm with GFP- *E. coli* attachment in the unpatterned regions (**a**); flow cell images of the patterned co-cultures at 2 hours and 4 hours at a flow rate of 20 µl/ min (**b**)

4.5 Summary

Overall attempts to pattern *E. coli* onto MT-SAMs have yielded some interesting results. The direct printing method is useful for a quick and easy pattern formation, however we have shown

that on SAM and agarose surfaces the bacteria do not remain immobilized when exposed to fluid flow. Cells could still be kept viable in these patterns by using an inverted microscope and sealing with a thin layer of agarose, but that would leave no control over the growth rates. Furthermore, bacterial co-cultures could not be formed using the direct printing methods as cells need to be in liquid form in order to attach to surfaces.

We found that by first ensuring cells were properly attached to MT-SAM surfaces, robust patterns could be formed using lift-off patterning with an agarose stamp that were resistant to rinsing procedures. We have shown that using this method bacteria can be patterned with features as small as 10 μm, ideal for the study of cell-cell interactions that require close contact (most groups thus far pattern cells in much larger arrays). We also found that by using a micromanipulator, pattern integrity could be more readily and repeatably controlled, and is a lot more reliable that patterning by hand.

Finally, we have developed and refined a protocol for the construction of micro-patterned co-cultures at the single-cell level - a procedure that has thus far been fundamentally lacking in the field of microbial manipulation. These micro-patterned co-cultures are robust, have longevity and resistance to rinsing procedures, enabling a wide variety of applications including the study of conjugation between donors and recipient bacteria.

Chapter 5: Horizontal Gene Transfer

Abstract: *The ability to study gene-transfer events in real-time in spatially controlled environments will provide important insights into the logistics and kinetics of plasmid transfer. This chapter describes the modification of an existing conjugative plasmid with lacO cassettes so that real-time visualisation of the plasmids can be employed in the form of fluorescent foci*

5.1 Background

In recent years, studies of gene transfer have progressed from determining the population dynamics of transfer events in bacterial communities by cultivation techniques[13] to more advanced methods allow real-time visualisation of transfer events as they happen, particularly by monitoring fluorescent colour changes or through biolumisence[42]. The ability to form hybrid reporter molecules by fusion of fluorescent probes to proteins that bind genes of interest, such as the GFP-LacI repressor protein has enabled direct visualisation of plasmids as they enter recipient cells, by forming fluorescent foci [43, 45]. However, most experiments employing these procedures use random deposition of cells onto surfaces – they lack the spatial control that patterned co-cultures can give.

Although the structures of the conjugative plasmid RK2 and its derivatives have been extensively studied, including the location and function of the transfer machinery, there has been a distinct lack of studies collecting real time data and visualisation of plasmid movements from donor to recipient cells. For example, we know that the conjugative pilus of RK2 is short and rigid, requiring that cells be in close contact with each other, but we do not know whether cells need to be orientated end to end, or side by side for conjugation to occur. Controlling the spatial arrangement of donor cells on a surface could also eventually lead to systematic studies related to the differences between different types of conjugative plasmids.

5.2 Objective

The final objective of the project was to use the micro-patterned co-cultures to look at the dynamics of plasmid transfer between alternating strips of donors and recipients. The GFP-LacI repressor system was used to detect plasmid transfer events, as it enables real-time visualisation of fluorescent foci when a conjugative plasmid containing lac operators enters a recipient cell containing GFP-LacI.

The objective was split into two main stages:

1) Modification of an existing conjugative plasmid (RK2 derivative pUB307) with lac-operators, so that fluorescent foci can be formed upon transfer to a recipient cell containing GFP-LacI (**Fig 5.1 a**)
2) Transformation of donor cells of *E. coli* with the pUB307-*lacO* plasmid, followed by single-strain patterning of the donor cells and immersion in GFP-LacI recipient *E. coli*, allowing real-time detection of plasmid events in the micro-patterned co-cultures (**Fig 5.1 b**)

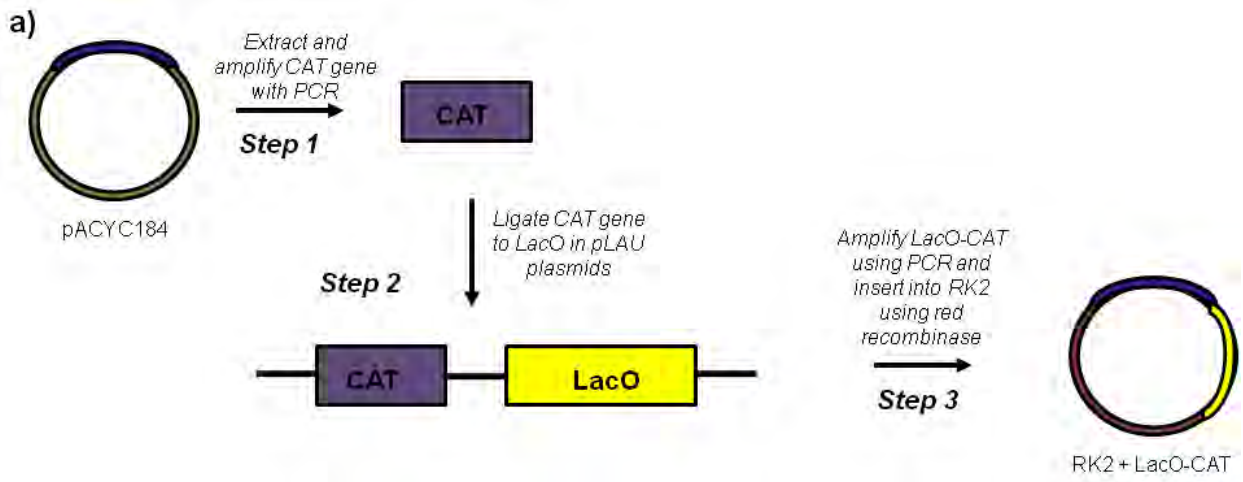

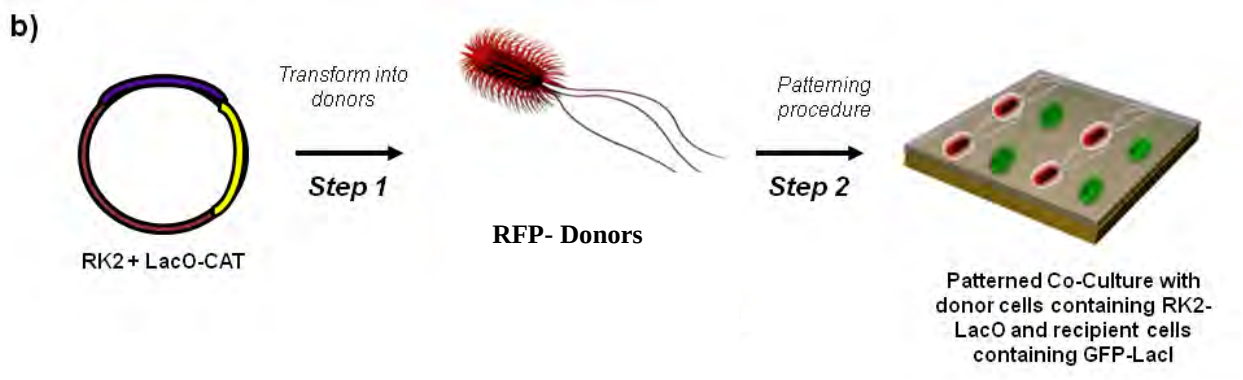

Fig 5.1 Schematic representation of the HGT detection procedure in micro-patterned co-cultures, beginning with the modification of pUB307 with *lac* operators (**a**) and the subsequent transformation of fluorescent donor cells of *E. coli* with pUB307-*LacO* before forming micropatterned co-cultures with recipient (GFP-LacI) cells (**b**)

5.3 Construction of pUB307-*lacO*

The first part of the HGT section of the project was to modify a conjugative plasmid (pUB307) with *lac* operators, in order to create binding sites for the repressor protein LacI that had been fused with GFP. At its simplest, this involved extracting the *lacO* cassette from a non-conjugative plasmid (a pUC18 derivative) and then inserting them into the pUB307. However, the process involved a number of sequential steps to ensure that we could separate and select for cells containing pUB307-*lacO* from the bacteria carrying the unmodified pUB307.

5.3.1 Step 1: Creating an antibiotic resistance marker for *lacO*

5.3.1.1: Overview

First, we needed a way of selectively growing bacteria with conjugative plasmids containing the *lacO* cassette. The first step in modifying pUB307 was therefore to select an antibiotic resistance gene marker (reporter gene) that could be inserted upstream of the promoter for *lacO*, so that bacteria containing plasmids with *lacO* could then be selected for with antibiotic supplemented media. As pUB307 already contained ampicillin and kanamycin resistance, chloramphenicol was

the antibiotic of choice. Chloramphenicol is a bacteriostatic antibiotic which prevents cell growth by binding to ribosomes and preventing protein synthesis[219]. The presence of the chloramphenicol resistance gene (*cat* gene) in a cell confers antibiotic resistance through the production of chloramphenicol acetyl transferase, which covalently links to the hydroxyl groups on the chloramphenicol molecule, preventing it from binding to the ribosome[220]. Cells containing the *cat* gene are therefore able to withstand concentrations of up to 35µg/ml chloramphenicol in the culture media.

5.3.1.2: Amplification of *cat* gene using PCR

The small 4.2 kb plasmid pACYC184 is a standard cloning vector containing both chloramphenicol and tetracycline resistance genes. The *cat* gene was amplified from the non-conjugative plasmid pACYC184 (**Fig 5.2**) by polymerase chain reaction (PCR).

.

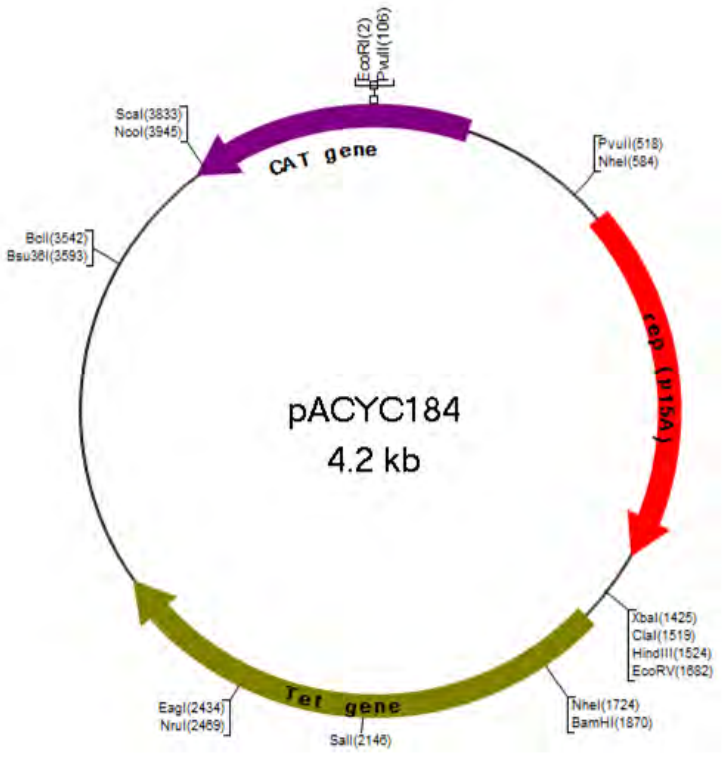

Fig 5.2 Map of pACYC184, showing location of the 1kb *cat* gene (purple); replication origin (red) and tet (green).

PCR is a process based on the annealing and extension of two oligonucleotide primers that flank either side of the target gene(s) in DNA. Following denaturation of the duplex DNA (breaking hydrogen bonds) each primer hybridises to a separated strand and extension from each 3' hydroxyl end is directed toward the other using a DNA polymerase[221]. Many cycles of PCR allow amplification of the target gene, so that at the end of a PCR run, many copies of the gene are present in the PCR mix.

A culture of DH5α *E. coli* containing plasmid pACYC184 was grown at 37^{o}C with shaking at 200 rpm for 12 hours in LB broth supplemented with chloramphenicol (30 µl/ml). Cells were then pelleted by centrifugation at 8000 rpm for 1 minute, and the supernatant disposed off. Plasmids were then extracted two ways, using a boil-preparation[222] or with an Accuprep® plasmid extraction kit. Primers were designed to flank regions of either side of the *cat* gene in pACYC184 so that it could be amplified using PCR:

Forward: 5' taaaaagtcttcaggagctaaggaagc 3'

Reverse: 5' cataaagtcttcctccttacgccccgccctgcc 3'

The resulting PCR product could then be inserted upstream of a plasmid containing repeats of *lacO.*

5.3.1.3: Confirmation of PCR product using agarose gel electrophoresis

The presence of the *cat* gene in the PCR mix was subsequently confirmed using agarose gel electrophoresis. Briefly, agarose gel electrophoresis is an analytical technique used to separate fragments of DNA by applying an electric field to move the negatively charged DNA through the pores of an agarose matrix. Shorter fragments move faster and migrate more quickly than larger fragments, therefore the DNA molecule of interest can be confirmed according to its size,

by running it alongside a pre-determined DNA ladder and then comparing band positions on the gel.

The PCR product was confirmed using agarose gel electrophoresis, with a 1% agarose gel in TAE buffer (1 % in distilled water), supplemented with 2.5 µl ethidium bromide. A DNA marker was added in 2 µl aliquots to the PCR product and they were then run alongside a 10 kb DNA ladder for 1 hour. Images of the gels were taken using trans UV light to confirm presence of gene products.

The *cat* gene is approximately 1 kb in length, so a band appearing alongside the 1 kb region of a DNA ladder would confirm PCR amplification. **Fig 5.3** shows the confirming agarose gel electrophoresis band of the amplified *cat* gene after running the PCR product alongside a 10 kb DNA ladder, which corresponds with the literature predicted values of approximately 1 kb[223].

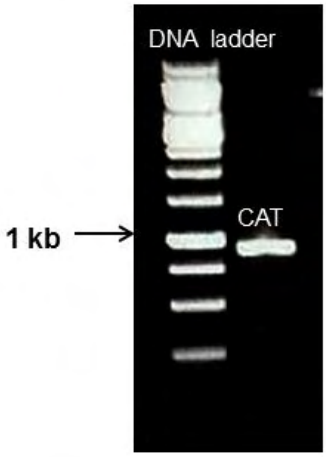

Fig 5.3 Agarose gel electrophoresis bands showing position of 1 kb *cat* gene next to 10 kb DNA ladder

The *cat* gene band was then cut out from the agarose gel and the DNA extracted using a gel purification kit (GE Healthcare).

5.3.2 Step 2: Ligating the antibiotic resistance marker to LacO

5.3.2.1: Overview

The plasmids containing the *lacO* genes were pUC18 derivatives designed by Lau *et al.*, 2004[176], and known as pLAU plasmids. The pUC18 vectors are small (2.6 kb), high copy number plasmids found in *E. coli*, and the main regions are the *bla* gene, which confers resistance to ampicillin by coding for a beta-lactamase, and the region of the *E. coli lac* operon containing the CAP binding site, the promoter *Plac*, the *lac* repressor binding site (*lacO*) and the *lacZ* gene encoding beta-galactosidase[224].

In order to visualise *lac* operators with GFP-LacI, it is theoretically beneficial to have more than one copy of the *lac* operator in the plasmid to allow many GFP-LacI molecules to bind, increasing the fluorescence signal given off by the foci. One of the main reasons for using pUC18 is that it contains a polylinker region, or multiple cloning site, in the *lacZ* gene. This polylinker region contains a series of unique restriction enzyme sites, found nowhere else in the plasmid, meaning that upon digestion with any of these enzymes a single cut will be formed in the plasmid (rather than being broken up into fragments), forming a linear molecule into which new DNA inserts can be ligated before re-circularising.

The pLAU plasmids used in this project were hence pUC18 derivatives that had been modified with multiple copies of the *lac* operons in the polylinker region. Three different plasmids were used: pLAU-07, pLAU-23 and pLAU-33 (with 28, 48 and 98 repeating units of *lac* operators respectively). **Fig 5.4 a** depicts the plasmid map of pLAU-07

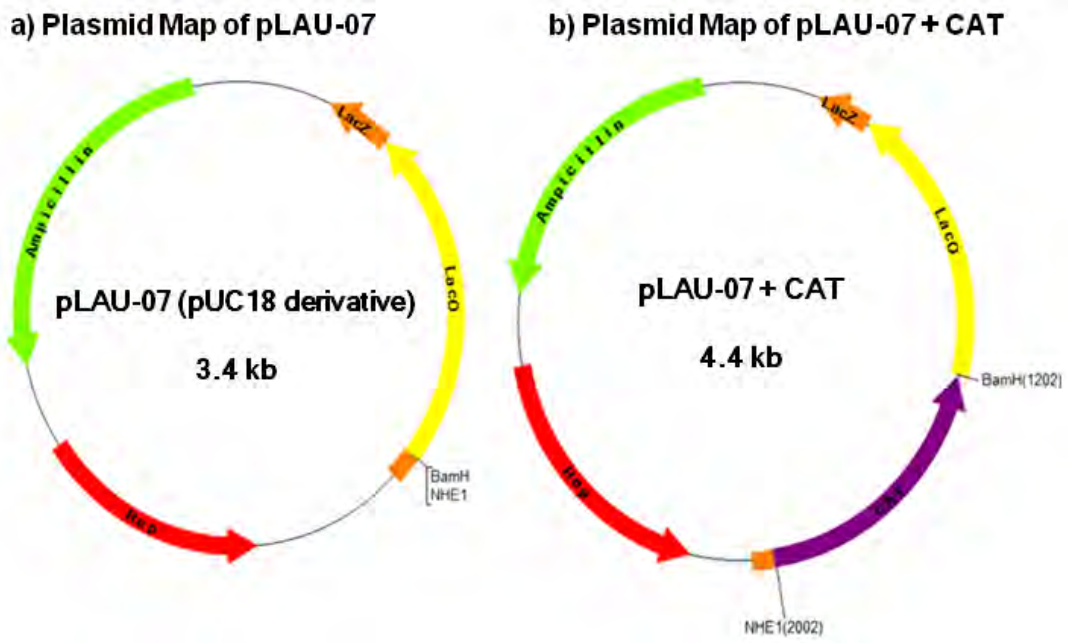

Fig 5.4 Map of pLAU-07, showing location of 800 bp repeating *lac*O region (yellow) and restriction enzymes BamH and NHe1 (**a**) and pLAU-07+ CAT (**b**) with the inserted *cat* gene (purple) upstream of the promoter for *lac*O.

5.3.2.2 Insertion of CAT gene into pLAU plasmids

The three pLAU plasmids (07, 23, 33) were extracted from cultures of *E. coli*. These plasmids were cut for 1.5 hours with restriction enzymes *Bam*H and *NHe*1 (sites located upstream of the *lac* operators) and the amplified *cat* gene was then ligated into the plasmids using DNA ligase, forming modified plasmids with repeating units of *lac* operators with chloramphenicol resistance (**Fig 5.4 b**). This was confirmed by running the ligation mix on an agarose gel, and comparing the modified plasmid bands with the original pLAU plasmids and the amplified *cat.*

Fig 5.5 shows the agarose gel electrophoresis bands of the pLAU-07 (28 *lac* operators), pLAU-23 (48 *lac* operators) and the pLAU-33 (98 *lac* operators) alongside the modified pLAU plasmids with the *cat* gene inserted. As expected, the unmodified pLAU plasmids are in the 3-4 kb region, with the pLAU-07 being the smallest at 3.4 kb. Each modified pLAU plasmid should therefore be 1 kb bigger than the original once the *cat* gene had been inserted, and the gel

confirms that we get a larger plasmid for all 3 types, with 1.8 kb for pLAU-07-*cat*; 2.6 kb for pLAU-23-*cat*; 4.2 kb for pLAU-33-*cat*. However, for the pLAU-07 there was one ligation mix that did not appear to have been successful, with two bands appearing instead of one. We therefore discarded this ligation mix and continued with the mix that had formed correctly.

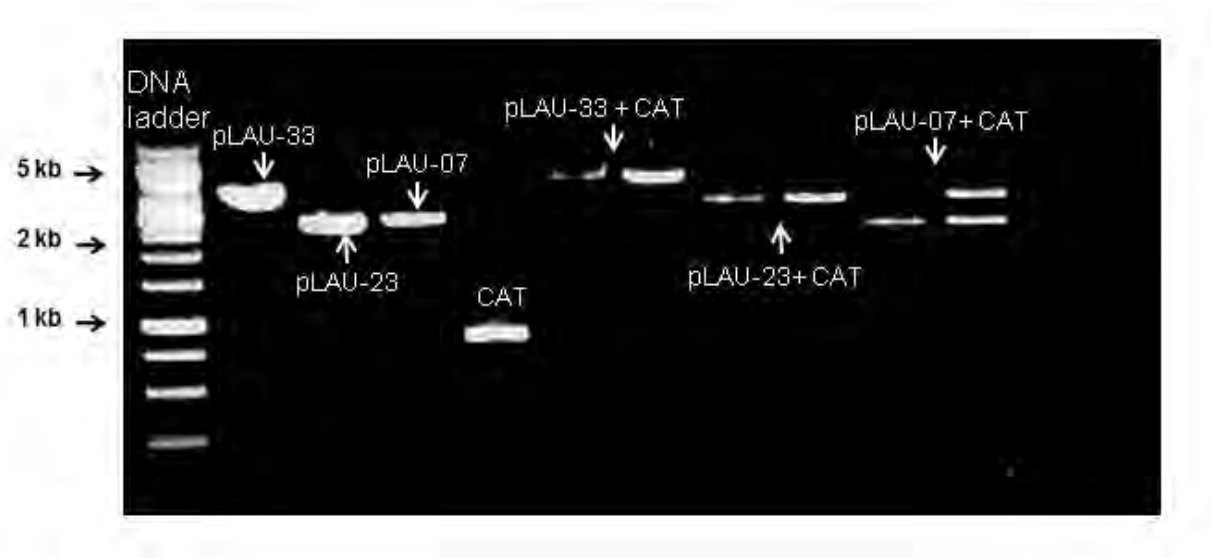

Fig 5.5 Agarose gel electrophoresis bands showing position of modified pLAU plasmids with the CAT gene next to 10 kb DNA ladder and the unmodified plasmids

5.3.2.3 Transformation of pLAU-*cat* plasmids into *E. coli*

The pLAU-*cat* plasmids were then introduced into competent DH5 α *E. coli* by transformation. Transformation involves binding the DNA to the outside of the bacteria, in the presence of Ca^{2+} ions and a short "heat shock" of the cells, which temporarily increases cell permeability to plasmid DNA. Competence is ensured by repeated rinsing of the cell suspension with calcium ions, which bind to the cell membrane and create channels for uptake of foreign DNA[225].

Pre-cultures of DH5α *E. coli* were grown at 37^{o}C with shaking at 200 rpm overnight in LB broth, and then re-inoculated in a 1:100 dilution the following morning, and grown for a further

two hours to bring the cells back to exponential phase. The cells were then pelleted at 5000 rpm, 4^{o}C for 7 minutes and re-suspended in 100mM pre-chilled $CaCl_2$ (2 ml per 5 ml culture). This was repeated twice, and then the cells were re-suspended in fresh 100mM pre-chilled $CaCl_2$ (0.5 ml per 5 ml culture), making them competent. The ligation mix (8 µl) of pLAU-*cat* plasmids was added to 100 µl of competent *E. coli* and placed on ice for 30 minutes. Subsequently, heat shock at 42^{o}C for 2 minutes caused the DNA to enter the cells. Addition of LB broth (1 ml) to the cells and then incubation at 37^{o}C for 1-2 hours enabled cell growth and plasmid activation. Cells successfully transformed were grown on selective media containing ampicillin (selecting for pLAU plasmids) and chloramphenicol (selecting for the *cat* gene).

5.3.3 Step 3: Insertion of *lacO-cat* into pUB307

5.3.3.1 Overview

The final step was to insert the *lacO-cat* fragments into pUB307. As pUB307 is a conjugative plasmid, it contains all of the machinery required for transfer and pilus formation in the *tra* loci; we therefore needed to find an insertion spot on the plasmid outside of these regions so its conjugative ability would remain intact. However, pUB307 has a lot fewer restriction sites than many other plasmids of similar size, and it was difficult to find an appropriate insertion site on the plasmid with a unique restriction enzyme that was not going to interfere with the transfer machinery if cut. The best option, therefore, was to "swap" the *lacO-cat* genes with a region of genes not required for transfer on pUB307, by using a homologous recombination method of fragment insertion via the enzyme red recombinase from bacteriophage lambda, found on the 'helper' plasmid pKD46 (**Fig 5.6 a**)

The Red operon encodes the nuclease inhibitor Redγ(*gam*) and the site specific recombinases Redα(*exo)* and Redβ(*bet)*, which mediate homologous recombination between fragments of DNA with complementary base pairs[226]. The procedure involves deletion of a region of plasmid

genes via recombination of the region of interest and a polymerase PCR product that contains flanking 'arms' (approx. 50bp) that are homologous to the target DNA[227], as depicted in **Fig 5.6 b**.

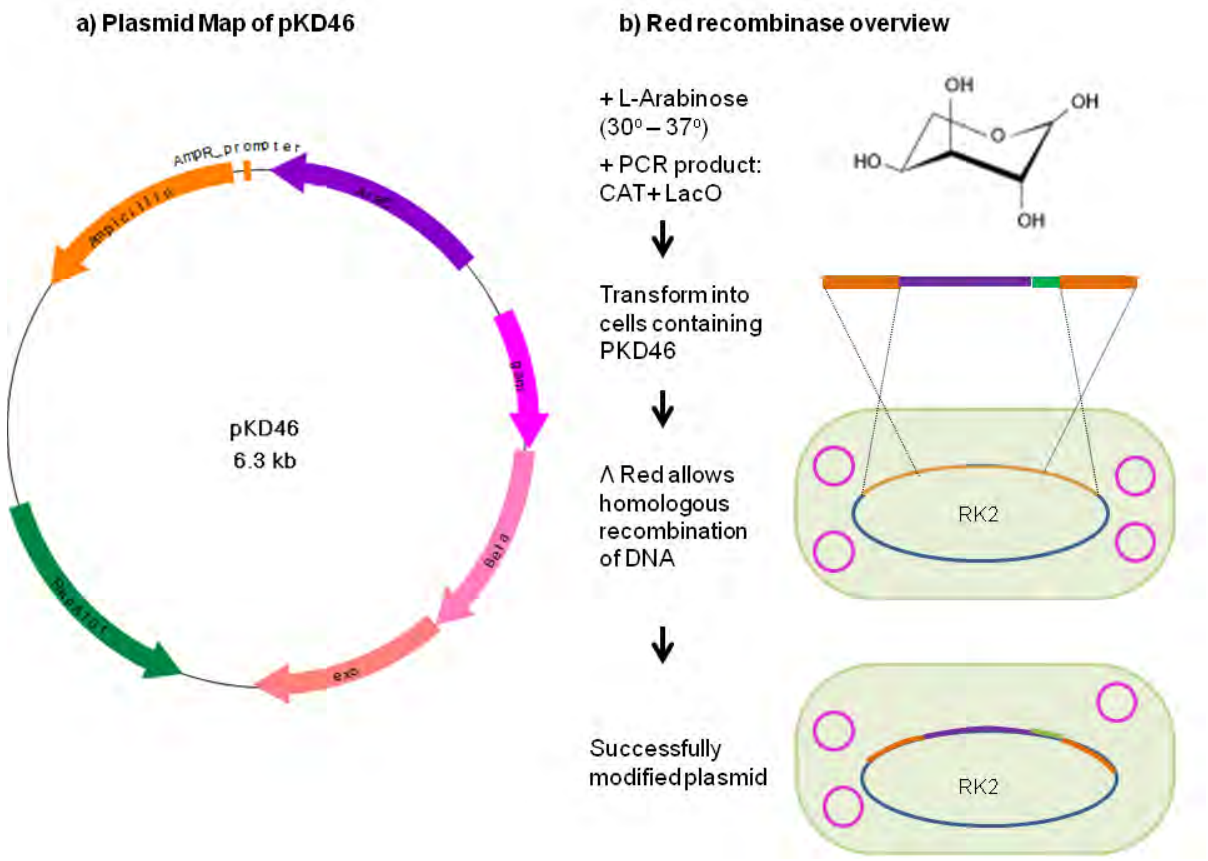

Fig 5.6 Map of pKD46, showing the *gam*, *beta* and *exo* genes required for red recombinase synthesis.The pKD46 plasmid replication is temperature specific (30°C) and the red recombinase requires the presence of arabinose to work[227].(**a**); and schematic representation of the homologous recombination of *lacO-cat* with the pUB307 plasmid (**b**)

Plasmid pUB307 has two antibiotic resistance genes conferring resistance to kanamycin and tetracycline. As the kanamycin resistance gene was located away from the transfer regions of the plasmid it was therefore the best site for homologous recombination with the *lacO-cat* fragment.

5.3.3.2 Extraction of and amplification of *lacO-cat* genes

Cultures of DH5α *E. coli* containing the modified pLAU plasmids were grown and the plasmids extracted. Subsequently, forward and reverse primers were designed to amplify *lacO-cat* regions of the modified pLAU plasmids by PCR, and including at the start of the primers regions homologous to the bases flanking the kanamycin gene of pUB307, to form the 'arms'. Primers were then designed to amplify the *LacO-cat* genes using PCR. Bases highlighted in blue form the pUB307 'arms' and bases highlighted in green amplify the *lacO-cat* genes:

Forward: 5' cgctgccgtgcccgagagca tggcggctca cgtgatggga tacaaatggg cgcgtg ccgtgcccgagagca tggcggctca cgtgatggga tacaaatggg cgcgtgta aaa cga cgg cca gtg cca agc 3'

Reverse: 5' gga aac agc tat gac cat gat tac Agg ggg cat cgc ctt aga aaa gtt cgt cca gca gga gat gaa att gca gc gcaagctgca atttcatctc ctgctggacg aacttttcta aggcgatgcc ccct 3'

This time, during PCR the annealing time was extended as the amplified DNA fragments were larger than the 1 kb *cat* fragment used previously (45 s for pLAU-07, 55 s for pLAU-23, 75 s for pLAU-33). **Fig 5.7** shows the results of the agarose gel bands of the PCR products, with the type of pLAU plasmid DNA run in each cycle (i-e boil preparation, or a 1:10, 1:100 dilution). It was important to dilute the DNA as too much plasmid DNA can sometimes cause incorrect recombination. **Fig 5.7 a** shows that for the pLAU-07 PCR fragment, we had five successful DNA bands between 1 and 2 kb that were cut out and extracted from the gel. The correct bands are those cut away from the gel. The pLAU-23 (**b**) and pLAU-33 (**c**) proved to be a lot more difficult to get right, as the pLAU-23 had PCR products that were of different sizes, and the pLAU-33 had to be repeated twice, and then we had only had two correct DNA bands.

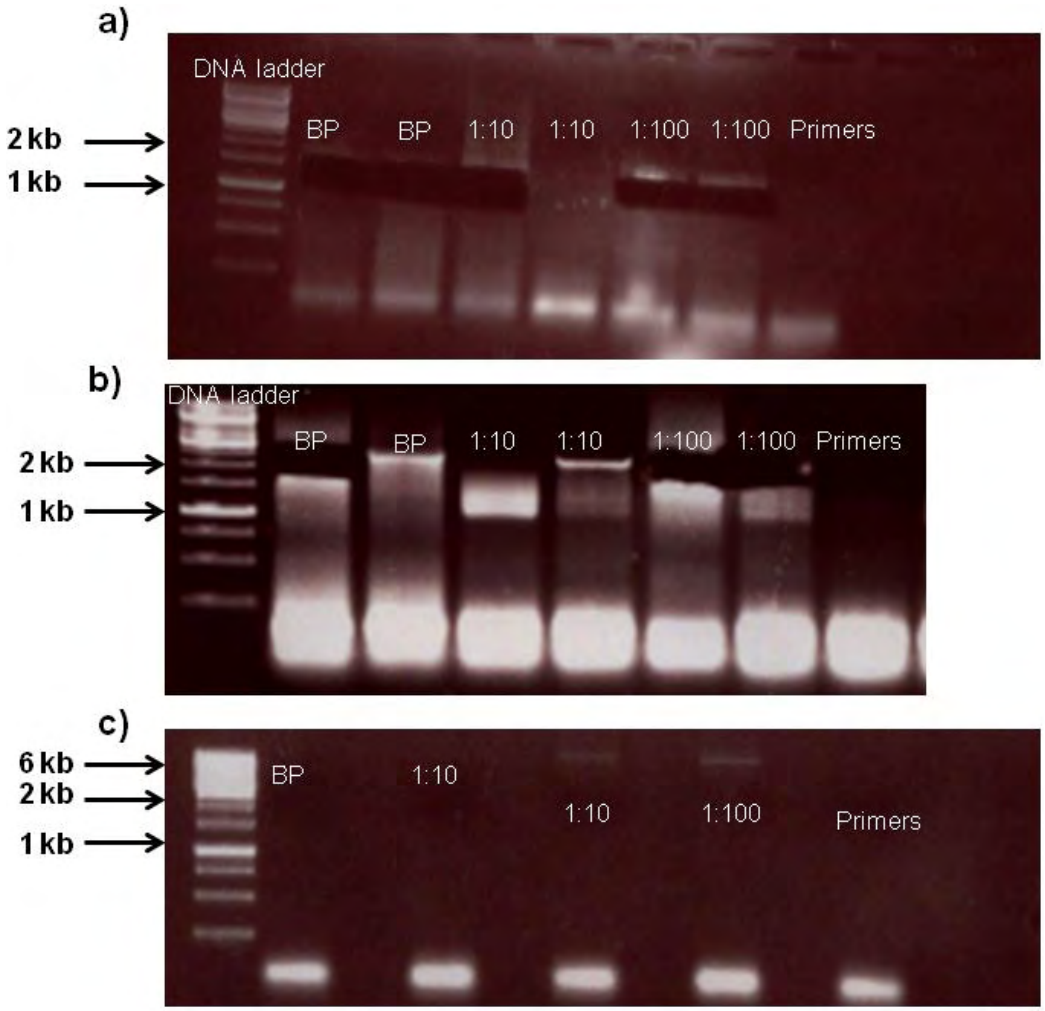

Fig 5.7 Agarose gel electrophoresis bands showing position of pLAU-*cat*- pUB307 arms PCR products of the pLAU-07 (correct bands cut away) (**a**), pLAU-23 (correct bands cut away) (**b**) and pLAU-33 (**c**)

5.3.3.3 Insertion of LacO-cat PCR product into pUB307

The final step was then to insert the three sized *lacO* gene sets into pUB307 along with their reporter genes, via homologous recombination with the kanamycin gene via red recombinase. The PCR products were electroporated into electro-competent cells containing the pUB307 plasmid and the helper plasmid pKD46. Electroporation involves subjecting cells to a short electric shock, which temporarily increases the permeability of the cell membrane and allows DNA to move into the cells. Cells are kept viable (electro-competent) by repeated pre-washing

with 10 % glycerol, and following electroporation they are re-suspended in a very nutritious media called Super Optimal broth with Catabolite repression (SOC solution).

pUB307 and pKD46 plasmids were thawed from frozen stocks and transformed into *E. coli* and plated onto selective media containing ampicillin (to select for pKD46) and tetracycline (to select for pUB307). (Colonies were grown at 30^{o}C instead of 37^{o}C as pKD46 is temperature sensitive). A colony of bacteria containing pKD46- pUB307 was then selected and grown as a pre-culture at 200 rpm overnight in LB broth at 30^{o}C, and then re-inoculated in a 1:50 suspension with 3 % arabinose (to induce red recombinase expression) to an OD at 600 nm of 0.6. The cells were then pelleted at 5000 rpm, 4^{o}C for 7 minutes and re-suspended in 10 % pre-chilled glycerol (0.4 ml per 5 ml culture). This was repeated three times, making the cells electro-competent.

Aliquots of 1µl of the amplified PCR products of *lacO-cat* genes were added to 40 µl of the electro-competent E. *coli* in pre-chilled electroporation cuvettes (0.2 cm electrode gap) and a 2.5 kV pulse was administered in the electroporator. Immediately afterwards, 1 ml of SOC medium (recipe in chapter 7) was added to the cell suspensions followed by incubation at 37^{o}C for three hours to allow homologous recombination.

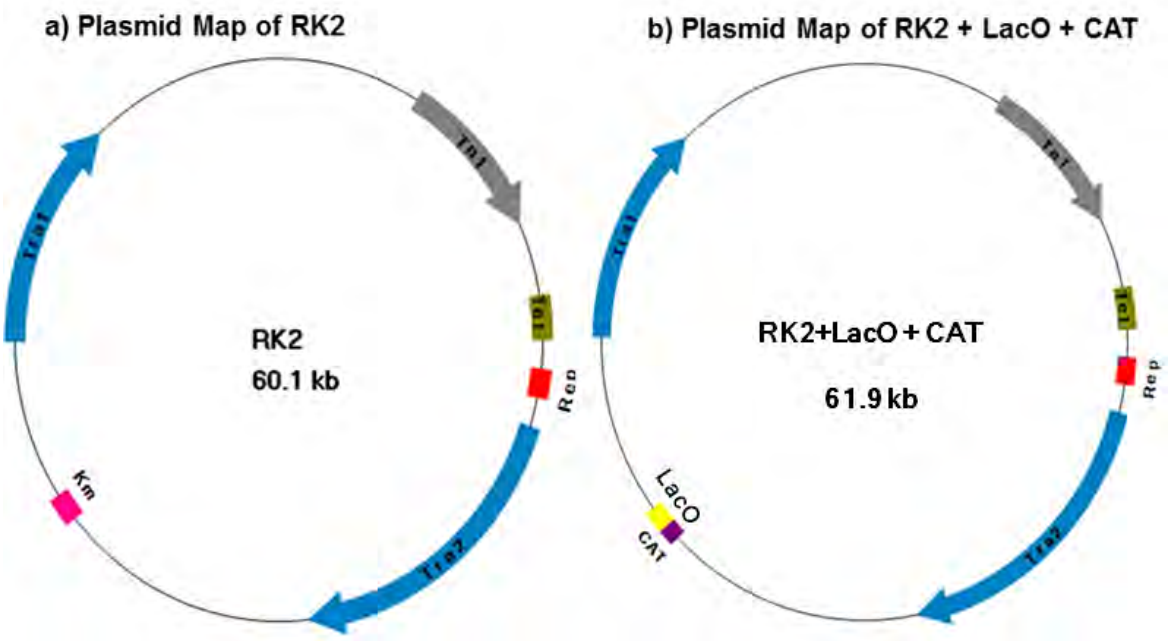

Fig 5.8 Plasmid Map of unmodified (**a**) and pUB307-*lacO* (**b**), showing the *tra* loci (blue), kanamycin resistance gene (pink) which is replaced with the *lacO-cat* fragment (yellow-purple)

Once the PCR product had been successfully electroporated into the bacteria, the presence of the red recombinase mediated the efficient homologous recombination between the PCR-product and pUB307, causing the l*acO-cat* fragment to replace the kanamycin gene (**Fig 5.8**). We selected for transformants using chloramphenicol and tetracycline, so that the growing cells would contain the *lacO-cat* genes on pUB307.

There were a lot of transformants from the smallest PCR product with the 28 *lac* operators, one or two transformants for the 48-mer and no transformants for the 98-mer. Electroporation is the standard transformation technique for large fragments of DNA[228]; however after two extra failed attempts to get the largest DNA fragments into the *E. coli* it was decided just to use the 28-mer and 48-mer due to time constraints.

Now that we had cells that were resistant to chloramphenicol and tetracycline, it was important to check whether they were sensitive to kanamycin. If the recombination had happened correctly, then technically the cells should be sensitive to kanamycin as the resistance gene in pUB307 was removed in the process. Selected colonies of transformants were therefore picked and streaked out into single colonies, and then re-streaked onto plates containing kanamycin. Most of the 28-mer *lacO* single colonies were sensitive to kanamycin, however, very few of the 48-mer colonies were sensitive. Therefore, it looked like re-combination may not have occurred correctly with the 48-mer PCR product, even though the *cat* gene had clearly inserted somewhere as the cells were resistant to chloramphenicol. However, the 48-mer PCR product may have inserted into a region of pUB307 that contained the transfer machinery, so a way to determine this would be to cut the plasmid with specific restriction enzymes, and then analyse the fragments by agarose gel electrophoresis. Fragments that are larger than they should be could indicate the position of the PCR product.

Considering, however, that it was likely that the 28-mer PCR fragment had recombined correctly with pUB307 as these cells were sensitive to kanamycin, it was decided to perform gene transfer studies with these cells, as other researchers have found fluorescent foci with just 5 tandem repeats of lac operons[229].

5.4 Conjugative transfer in micropatterned co-cultures

5.4.1 Control experiment with expression of foci in GFP-LacI recipients

Before using the pUB307-*lacO* to perform HGT experiments in the micro-patterned co-cultures, a simple control was employed to ensure that the presence of the *lacO* cassette inside the recipient cells would cause fluorescent foci to form. The pUB307-*lacO* was inserted into the recipient cells containing GFP-LacI and then grown to exponential phase; during growth the GFP-LacI should have bound the plasmids and cause fluorescent foci to form. **Fig 5.9** shows the confocal microscope images of a monolayer of recipient GFP-LacI with pUB307-LacO on MT-SAMs (**a**) compared with standard recipient GFP-LacI cells with no pUB307 (**b**). The fluorescent foci are highlighted with white arrows, and were primarily located at the ends of each individual cell. In the absence of conjugative plasmid, the GFP inside the recipient cells is spread out and the cells appear brighter. When foci are present, the GFP-LacI is sticking to the LacO cassette and therefore there is less GFP in the rest of the cells, so they appear duller.

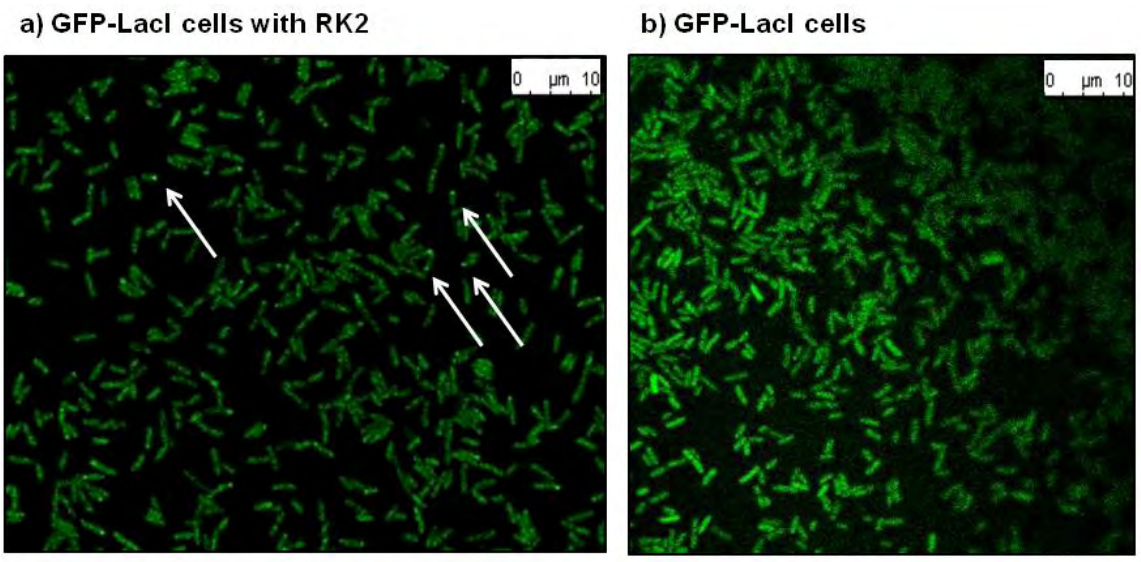

Fig 5.9: Confocal microscope images (x 63) of GFP-LacI *E. coli* on MT-SAMs transformed with pUB307-LacO to confirm induction of fluorescent foci (**a**) compared to GFP-LacI *E. coli* on MT-SAMs with no conjugative plasmid (**b**)

However, an important observation in this initial experiment was that the overall fluorescence signal emitted from the GFP-recipient cells was very poor compared to the DH5α *E. coli* cells with GFP used in chapters 3 and 4. The GFP cells used previously were detected using an emission spectra of 509 nm, whereas to pick up a signal from the GFP-LacI recipient cells the emission spectra had to be extended to 475-600 nm, right at the boundaries of the CFP and RFP spectra. Therefore, either there was not as much GFP being produced in the GFP-LacI cells or this particular GFP molecule was much more susceptible to photobleaching. Unfortunately, the GFP-LacI fusion protein was not under the control of any inducible promoters in the strains we were using; expression of some fluorescent molecules and proteins can be enhanced by using arabinose, glucose or isopropyl β-D-1-thiogalactopyranoside in the growth medium, but this was not the case here.

5.4.2 Conjugation in micro-patterned co-cultures

5.4.2.1 Confirmation of transfer ability by agar plate mating

Once the final pUB307 had been selected for, the retention of conjugative transfer ability was then confirmed by an agar plate mating of the GFP-LacI *E. coli* cells containing pUB307 and RFP cells that would become the donor strains in future experiments. Both cell types were mixed together on an antibiotic free agar plate for a number of hours to allow growth and transfer, and then they were re-streaked onto an agar plate containing ampicillin (to select for RFP) and chloramphenicol/tetracycline (to select for pUB307). The ampicillin would kill the GFP-LacI *E. coli* as it has no resistance gene for it.

5.4.2.2 Time-scale conjugation study in micropatterned co-cultures

Once the presence of foci had been confirmed, micropatterned co-cultures were formed on MT-SAMs. Briefly, donor RFP- pUB307-*lacO* bacteria were grown to an OD of 0.6 and then incubated at 37^{o}C onto MT-SAMs for two hours to allow attachment, followed by lift-off patterning with the 10 by 10 µm featured agarose stamps. Next, GFP-LacI recipients were incubated onto the single-strain patterns at 37^{o}C for one hour. Due to the fluorescence becoming duller once foci are formed, the GFP-LacI recipients were coated with a red membrane stain (FM4-64) to try and make the cells stand out. After recipient cell incubation, the patterned co-cultures were placed inside the flow cell, at a flow rate of 10 µl /min with pictures taken every hour for five hours.

Fig 5.10 shows the confocal images of the co-cultures taken once every hour over a four hour period. Unfortunately, although the patterns remained intact, no foci were observed at all over the four hours. Although **Fig 5.10** is only showing one image taken at each time point, the co-cultures looked the same across the whole substrate, with no foci. From the *E. coli* growth curve in single-strain patterns on MT-SAMs in Fig 4.21, we can see that the bacteria do not start to get into an exponential (high growth rate) until about four hours, therefore it is not surprising that between one and three hours there is a lack of foci, but between three and four hours we expected that gene transfer would have been occurring.

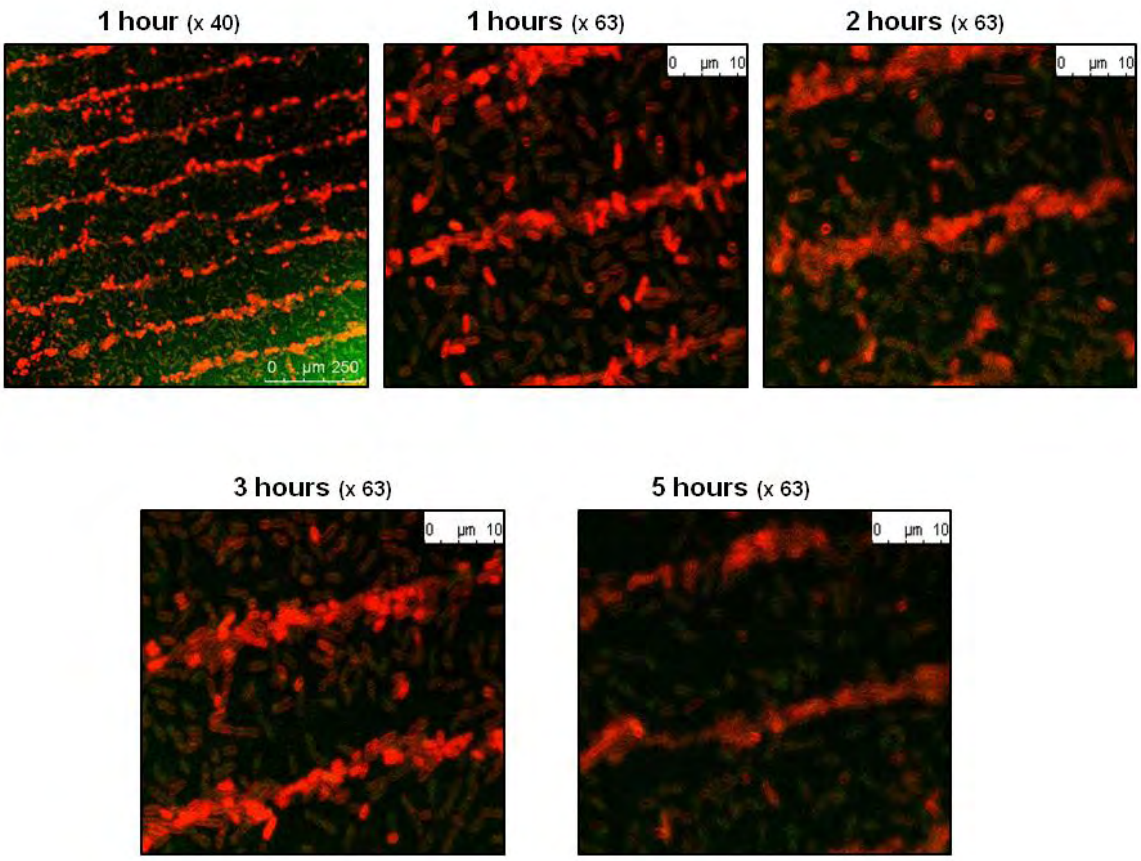

Fig 5.10: Confocal microscope images of micropatterned co-cultures of RFP donors containing pUB307-LacO and recipients of GFP-LacI on MT-SAMs. Substrates were placed inside the flow cell with a low flow rate of 10 µl/ min in M9 broth (with supplements)

However, the images also show that the GFP fluorescence of the recipient cells gets increasingly more photo-bleached after one hour on the surface, until the bacteria are barely visible after five hours. Therefore, it is likely that even if there were fluorescent foci being formed they would not show up anyway due to the poor fluorescence signal. We knew that the GFP in this strain of *E. coli* was not as robust as in the strain used for patterning, so the experiments were repeated by trying to optimise the confocal microscope to take this into account. We took care to minimise the laser exposure time to the cells; the size of the pinhole was increased to reduce the intensity of the laser; the shutter speed was adjusted and the cells were kept in the dark prior to experimentation but none of these things improved fluorescence integrity. Additionally, cells

were grown and maintained in a more nutritious media; using LB broth instead of minimal media, however the bleaching still occurred, and no foci were observed.

5.4.2.3 Improving fluorescence quenching using silane SAMs

One potential source of the photo-bleaching was the surface itself; studies have shown that metal surfaces such as gold can cause quenching of fluorescent molecules[230]. We therefore decided to test this theory by using COOH-terminated organosilanes to form MT-SAMs on glass slides. The SAMs were formed through vapour deposition of the COOH-silanes onto piranha cleaned glass substrates, with the coupling chemistry repeated in exactly the same way as with on the gold surfaces to attach the mannoside derivative to the surface. A monolayer of GFP-LacI recipients was then formed on the SAMs for 2 hours, and then the substrates were placed inside the flow cell as before. **Fig 5.11** shows the confocal microscopy images of the monolayers over a three hour period. After three hours as before, the GFP-LacI recipient cells were barely visible, suggesting that it was the robustness of the fluorescent molecules themselves, and not the surface that was the problem.

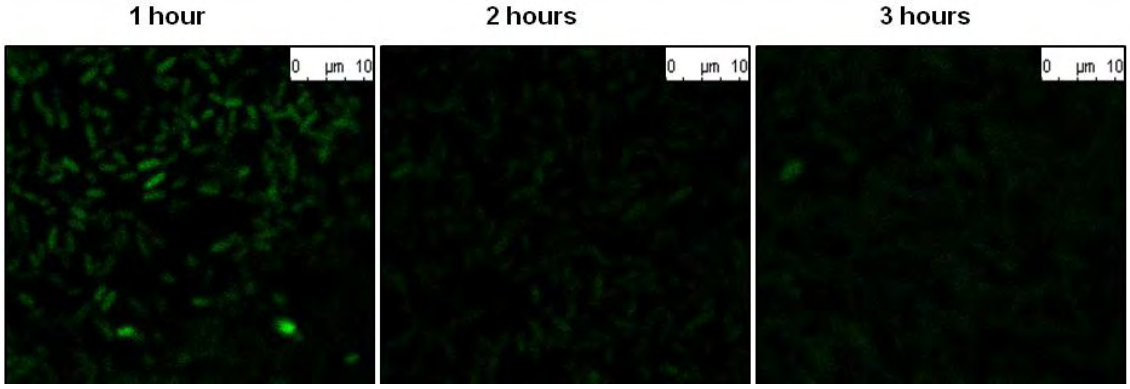

Fig 5.11: Confocal microscope images of GFP-LacI *E. coli* on MT-silane SAMs on glass. Substrates were placed inside the flow cell with a low flow rate of 10 µm/ min in M9 broth (with supplements)

5.4.2.4 Conjugation in un-patterned co-cultures

As a final test, HGT experiments were conducted in co-cultures on MT-SAMs and M9 agarose substrates without the patterning procedures. Donors and recipients were mixed together in a 1:100 ratio and subsequently deposited on top of the substrates and incubated for 2 hours to allow attachment. On the MT-SAMs, excess cells were rinsed away with 500 µl sterile PBS, and on the agarose substrates excess cells were rinsed with 200 µl sterile PBS (as they exhibit poor resistance to rinsing). In order to keep the conditions the same for both substrate types, the surfaces were then incubated at 37^{o}C with a thin covering of minimal media, and then confocal images were acquired every hour for 5 hours.

Fig 5.12 a shows that on MT-SAMs, the GFP-LacI recipient *E. coli* were marginally more resistant to photo-bleaching absent patterning procedures, however, there were still no fluorescent foci. However, on the agarose substrate foci (**Fig 5.12 b**) were observed after 3 hours incubation of donors and recipients and after 5 hours nearly all of the recipients appeared to have foci. With such a clear difference between the two substrates, the problem with the lack of foci was therefore attributed to the surface that co-cultures were growing on. The bacterial recovery experiment depicted in **Fig 4.21** showed that on M9 agarose, bacteria appear to divide rapidly at least an hour and a half before the bacteria on MT-SAMs. Even though bacteria in both substrate types are immersed in liquid media, the bacteria on the M9 agarose appear to have a shorter lag time . This means that conjugation is more likely to occur within this time frame, as it is a metabolic process. Additionally, the fluorescence emission was stronger in co-cultures incubated on M9 agarose, either due to increased synthesis of GFP-LacI (as cells were more metabolically active), or a reduction in production of fluorescence-quenching radicals inside the cells.

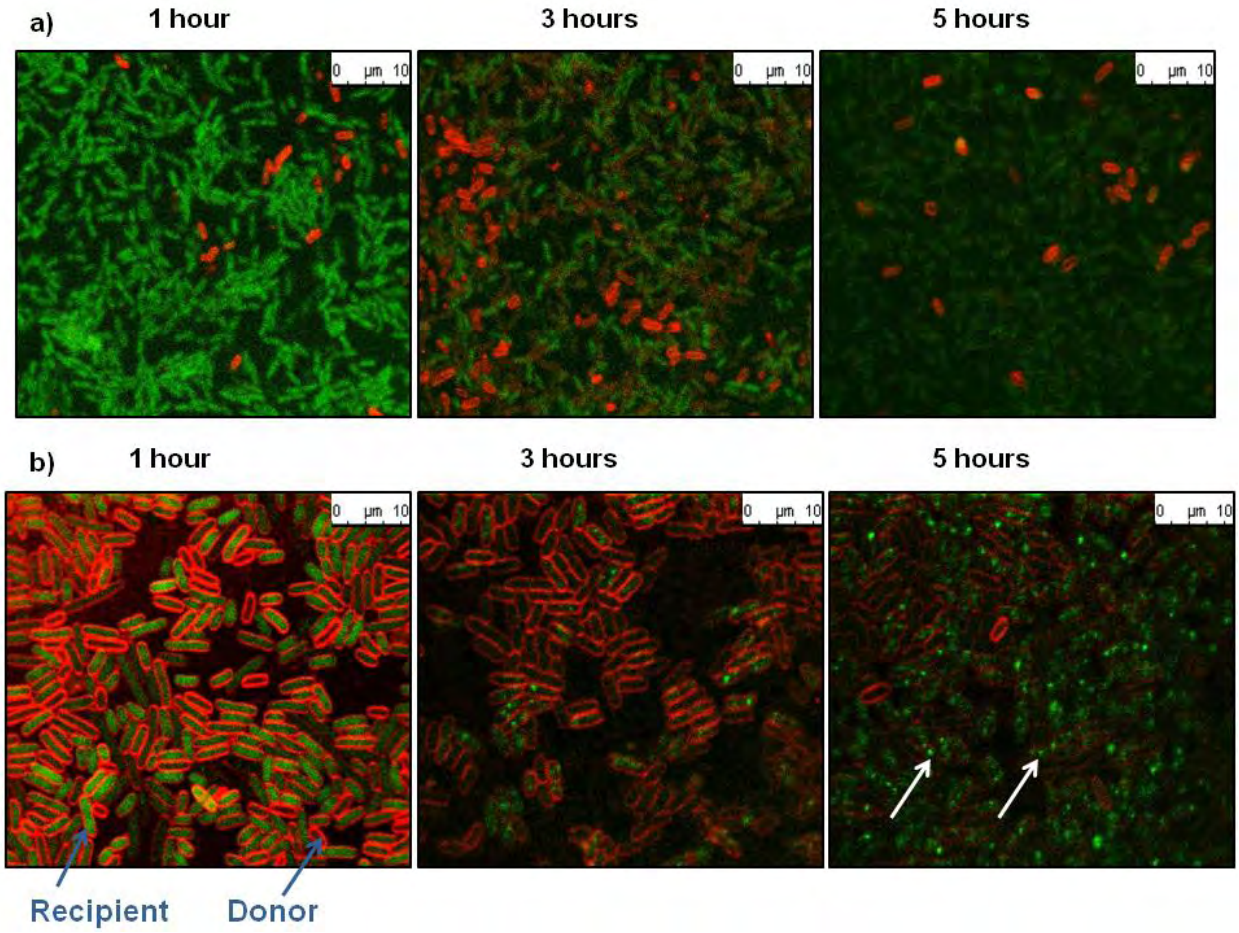

Fig 5.12: Confocal microscope images of a 1:100 ratio of RFP-donors containing pUB307-*LacO*, with GFP-LacI *E. coli* on MT-SAMs (**a**) and RFP-donors containing pUB307-*LacO*, with GFP-LacI *E. coli* with red membrane stain FM4-64 on M9 agarose (**b**), incubated at 37^{o}C over 5 hours.

5.4.2.5 Agar plate counting confirmation of HGT events

The final experiment performed was an agar plate counting experiment, using agar plates supplemented with antibiotics to select for donors, recipients and transconjugants. Patterned co-cultures on MT-SAMs were formed exactly as before, but instead of inserting the substrates into the flow cell for microscopy, they were incubated at 37^{o}C with either minimal media or LB broth for up to 3 hours. At each time point, the bacteria were removed from the surface by sonication then plated out onto media containing kanamycin (to select for recipients and transconjugants) and kanamycin, chloramphenicol and tetracycline (to select for

transconjugants). Additionally the same procedure (minus patterning) was performed on both LB-Agarose and M9-agarose substrates.

Fig 5.13 shows the results of the plating experiments. The results were expressed as the log number of transconjugants recovered from the surfaces and as a percentage of recipients that had been converted into transconjugants; this allows the *rate* of conjugation on each surface to be determined. **Fig 5.13a** shows that on all surfaces, the number of transconjugants irecovered increases on each surface type, however on both agarose surface types there appeared to be a dramatic increase in conjugation. After taking counting the number of GFP-lacI cells recovered from the plates we are able to calculate a percentage of recipients that had become transconjugants (**Fig 5.13b**). For both LB agarose and M9 agarose surfaces, 100 % of the recipients had become transconjugants after 2.5 hours, so all bacterial cells on the surface were carrying pUB307-*lacO*. There were differences observed between the type of media used; after one hour 20 % of the recipients had become transconjugants on the LB-agarose, compared with 6 % on the M9. This suggests that on the highly nutritious LB agarose, cells start to transfer very quickly after deposition onto the surface, whereas the cells on the M9 agarose have a longer lag time, thus it takes longer to assemble the machinery required for transfer. After two hours on an M9 agarose surface, the donor cells appear to start to transfer very rapidly, as indicated by the sharp increase in the linear slope of the curve, suggesting that they are moving into exponential phase.

There was very little conjugation on MT-SAMs when bacteria were incubated with both LB and M9 broth until 3 hours had passed, when the number of recipients increased to 11 % for LB broth, and 5 % for M9 broth. So this showed that conjugation can occur in micro-patterned co-cultures on MT-SAMs, however, it is very much dependent on the growth rate. As shown in chapter 4, the bacteria on MT-SAMs have a much longer lag phase compared to agarose, and

unfortunately by the time the cultures start to enter exponential phase (and hence start to transfer) the fluorescence has been bleached and we cannot visualise the fluorescent foci.

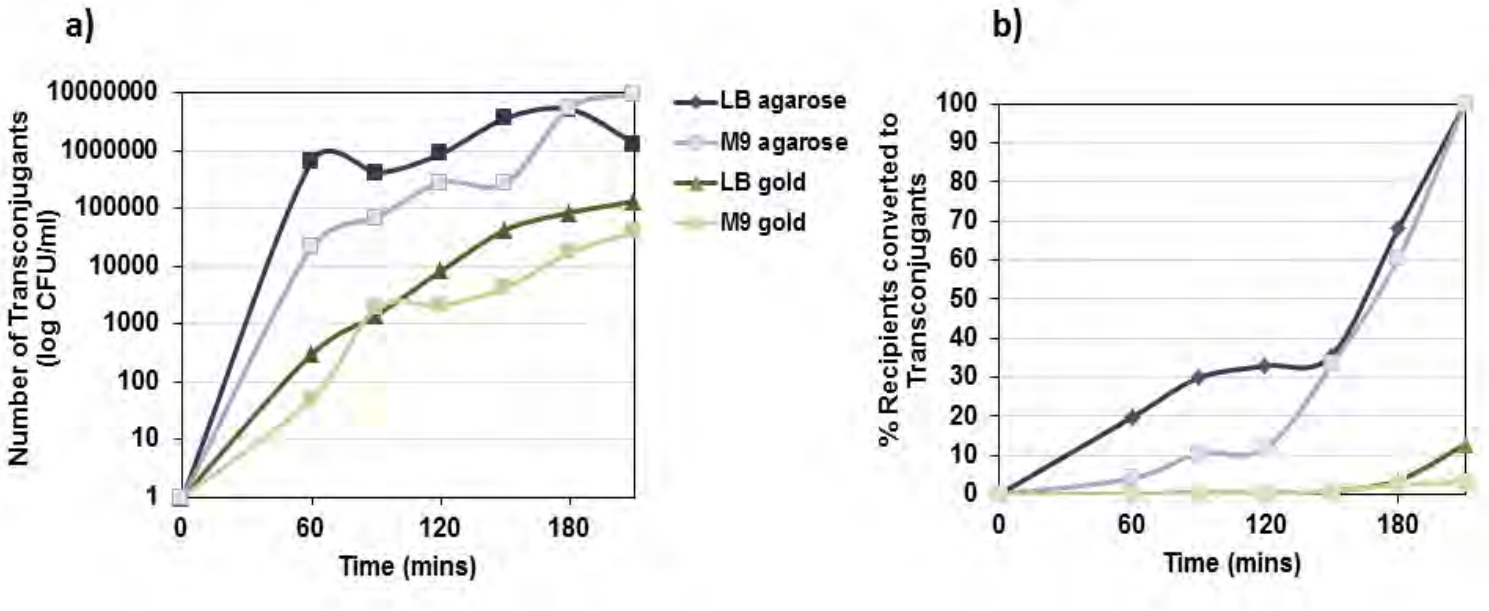

Fig 5.13: Gene transfer data showing the number of transconjugants recovered from surfaces (**a**) and the % recipients that are converted into transconjugants during mating experiments (**b**) in patterned co-cultures incubated with LB broth or M9 broth, and co-cultures on LB agarose and M9 agarose blocks.

5.5 Summary

In conclusion, we successfully managed to construct a conjugative plasmid that was capable of allowing real-time visualization of transformants via the formation of fluorescent foci, and we found that using a *lacO* cassette with 28 repeating units we were able to visualize fluorescent foci adequately when pUB307 was electroporated into recipient cells containing GFP-LacI, and through donor/ recipient matings on agarose blocks.

It was concluded that conjugation can occur in bacteria patterned and immobilized onto the MT-SAMs, but we were not able to visualize it happening. From the various controls employed to

test this, we found that conjugation is very much growth dependent – bacteria start to transfer on gold roughly after about 3-4 hours, at the same time that it takes for the bacteria to begin to multiply on MT-SAMs. By this point, however, the fluorescence in our cells had completely photo-bleached. It stands to reason, therefore, that the next step in this process would be to try and maintain the fluorescence in the cells for long enough, either by providing an anti-oxidant supplement to mop up the free radicals and free electrons that can quench the fluorescence, or by constructing new LacI recipients that are under the control of an inducible promoter, so that increased levels of GFP can be produced.

Chapter 6: Conclusions and Future Work

This project set out to adapt existing technologies available in the areas of surface chemistry and lithography, to create a micro-patterned functionalised surface that would support the spatial adhesion of two bacterial strains of *E. coli*, and as such could be used to visualize conjugation in real-time.

We have created a MT-SAM that can support the adhesion of *E. coli* for prolonged periods under fluid flow conditions. We found that bacteria fully adhered to MT-SAMs after two hours, and subsequently became resistant to rinsing at rates of up to 50 µl /min, due to the shear-enhanced catch bond mechanism of the FimH-mannose bond. In contrast, bacteria on agarose substrates were very susceptible to rinsing procedures as they do not form specific adhesive bonds with the surface.

The importance of bacterial adhesion has shown that patterning techniques must be tailored to their future uses; a lot of researchers have described various methods for patterning bacteria without any attempts to use them for studying cell behavior beyond looking at how cells grow where they are placed. In fact, many of the patterning procedures in the literature are thus far unsuitable for co-culture formation and studying conjugation. For studying conjugation in patterned co-cultured environments, we have shown that the patterning techniques must not inhibit bacterial adhesion to the surface, as to have two bacterial types on the same surface they must be added separately to prevent mixing, and as they are in liquid medium the cells will always be at risk of dislodgement. Therefore, the surface properties are perhaps the most important factors in the sustained patterning of co-cultures, which is why this lead onto lift-off patterning, which allows for an appropriate adhesion time so that cells will not be dislodged during rinsing.

We have also demonstrated that conjugation can occur in the micro-patterned co-cultures on MT-SAMs, although real-time fluorescent foci were unfortunately not observed. However, the results have established that conjugation is very much dependent on microbial growth rates, and perhaps with recipient GFP-LacI bacteria that are more resistant to photobleaching the conjugation experiments could be extended for longer periods of time, and fluorescent foci could be observed. We have also verified that conjugation occurs rapidly on agarose substrates and fluorescent foci are easily visualized. However, we cannot maintain our co-cultured patterns on agarose due to poor adhesion and susceptibility to rinsing. It seems logical, therefore, for a future step to attempt to make the agarose surfaces more "sticky" so that pattern formation is improved. For example, perhaps by supplementing the agarose gel with mannan (a tri-mannose molecule) it would encourage *E. coli* adhesion via the same catch bond mechanism exhibited on MT-SAMs[231].

Chapter 7: Materials and Methods

7.1 Materials

7.1.1 Chemicals

All materials and reagents were used as received. O-(2-Carboxyethyl)-O'-(2-mercaptoethyl) heptaethylene glycol, 4-Aminophenyl α-D-mannopyranoside, Concanavalin A type 1V, 1-ethyl-3(3-dimethylaminopropyl) carbodiimide (EDC), N-hydroxysuccinimide (NHS), Luria (LB) broth/agar, M9 broth, trifluoroacetic acid (TFA), agarose (type I-A, low EEO), and phosphate buffered saline (PBS: 10 mM phosphate containing KH_2PO_4 and $Na_2HPO_4 \bullet 2\ H_2O$, 138 mM NaCl, and 2.7 mM KCl), EDTA disodium salt , kanamycin, ampicillin sodium salts, chloramphenicol, tetracycline, valine, arginine, thiamine, D-glucose, D-mannose, and membrane stain FM4-64 were from Sigma-Aldrich. PDMS 184 Elastomer Base and 184 Curing Agent were from Sylgard. UHQ (ultra high quality) H_2O (resistivity >18 Ω cm^{-1}, TOC reading of < 3 ppb) was purified by using a Millipore-Q Integral 5 water purification system. HPLC ethanol, Sulfuric acid (H_2SO_4) and hydrogen peroxide (H_2O_2) were from Fisher. Restriction enzymes *BamH, EcoR1 and NHe1* and DNA polymerase velocity Taq were from Invitrogen. Primers were ordered and constructed at the University of Birmingham.

7.1.2 Gold substrates

Polycrystalline gold substrates were purchased from George Albert PVD., Germany and consisted of a 50 nm gold layer deposited onto glass covered with a thin layer (5 nm) of chromium as the adhesion layer. For ellipsometry, 100 nm gold layers were deposited onto silicon wafers.

7.1.3 DNA kits

For plasmid extraction from bacterial suspensions: Accuprep® plasmid extraction kit, from Bioneer. For DNA extraction from agarose gels: Gel purification kit (GE Healthcare)

7.1.4 Consumables

Glass cover slips were purchased from VWR international with an area of 22 x 32 mm and thickness: No.1. Petri dishes, plastic spreaders and 50 ml centrifuge tubes were from Fisher.

7.1.5 Bacterial strains and plasmids

7.1.5.1 Bacterial Strains

The *E. coli* strains for initial cell patterning used in this study were K-12 DH5α strains expressing GFP from the plasmid pUA66pacpP (*kmR*), under the control of the promoter acpP (from Dr. N. Burton, Biosciences, University of Birmingham); and mCherry (*ampR*) from the plasmid pJet1.2, expressed constitutively (from Yanina Sevastsyanovich, Biosciences, University of Birmingham). For gene cloning of *LacO* arrays into pUB307, plasmids were transformed using *E. coli* K12 DH5 α. GFP-LacI recipients were in MG1665 (*kmR*), from Maritoni Sanchez-Romero, Biosciences.

7.1.5.2 Plasmids:

The following plasmids were used in this project:

Name	Function	Source
pUA66pacpP	The parent vector was pUA66 into which the *pacpP* promoter was cloned upstream of GFP*mut2*. This vector also contains the *aph* gene coding for kanamycin resistance	Dr Neil Burton, Biosciences, University of Birmingham
pJet1.2	A pUC19 derivative with a multiple cloning site used for	Yanina Sevastsyanovich, Biosciences, University of

	positive selection, mCherry produced due to the read-through from the vector promoter that just happens to be upstream. Also encodes resistance to ampicillin	Birmingham
pACYC184	Carries a gene encoding resistance to tetracycline and a gene encoding resistance to chloramphenicol	NEB
pLAU07	pUC18 derivatives with 28-repeating lac operators cloned into the MCS. Resistant to ampicillin	David Sherratt, University of Oxford
pKD46	Temperature sensitive replication (repA101ts), encodes lambda Red genes (*exo*, *bet*, *gam*); native terminator (tL3) after *exo* gene; arabinose-inducible promoter for expression (P_{araB}); encodes *araC* for repression of P_{araB} promoter; Ampicillin resistant.	Dr Maritoni Sanchez-Romero, Biosciences, University of Birmingham
pUB307	Conjugative RK2 derivative. Chloramphenicol and tetracycline resistant.	Professor Christopher Thomas, Biosciences, University of Birmingham

7.2 Methods

7.2.1 Formation of MT-SAMs for bacterial attachment

7.2.1.1 Substrate cleaning

Au substrates were cut to approximately 1 cm x 1 cm using a diamond tipped scriber. The substrates were then rinsed with ethanol to clear the surface of any dust that was produced from the cutting process. The cut silicon was then immersed into piranha solution (3:1, H_2SO_4 : 30%

H_2O_2) for 10 min. The piranha solution was then rinsed off the substrate with UHQ water, and then then HPLC grade EtOH thoroughly for 1 min. The substrates were then stored in HPLC grade EtOH and used within 2 days[232].

7.2.1.2 Formation of MT-SAMs

Solutions of the O-(2-Carboxyethyl)-O'-(2-mercaptoethyl) heptaethylene glycol (0.1 mM) were prepared in HPLC EtOH, with the addition of 3% (v/v) trifluoroacetic acid to prevent the formation of hydrogen bonds between the carboxylic acid groups of the bound thiolate on the Au surface, and that of free thiol in the bulk solution. The clean Au substrates were immersed in the thiol solutions for 24 h to form the COOH-SAMs, and then the substrates were rinsed with HPLC EtOH with NH_4OH and dried with argon.

COOH-SAMs were immersed in a solution of (0.05 M) NHS and (0.2 M) EDC in UHQ water for 10 minutes. In the presence of EDC, the surface carboxylic acid groups are converted into NHS esters. Excess NHS and EDC was rinsed away with UHQ water for 1 minute, followed by immersion of the substrates in a solution of 4-Aminophenyl α-D-mannopyranoside (2mg/ml in PBS, pH 8) for 60 minutes to form MT-SAMs[124].

7.2.2 Surface Characterisation of SAMs

7.2.2.1 X-ray Photoelectron Spectroscopy (XPS).

XPS spectra were obtained on the Scienta ESCA300 instrument based at the Council for the Central Laboratory of the Research Councils (CCLRC) in The National Centre for Electron Spectroscopy and Surface Analysis (NCESS) facility at Daresbury, UK. XPS experiments were carried out using a monochromatic Al K_α X-ray source (1486.7 eV) and a takeoff angle of 15^o. High-resolution scans of N1s and S2p were recorded using a pass energy of 150 eV at a step size of 0.05 eV. Fitting of XPS peaks was performed using the *Avantage* V*2.2* processing software.

7.2.2.2 Ellipsometry

Ellipsometry measurements were taken using a Jobin-Yvon UVISEL ellipsometer with a He-Ne laser light source at an angle of incidence of 70 °C using a wavelength range of 280–800 nm. The ellipsometric parameters, Δ and ψ, were recorded for both the bare, clean substrates and for the substrates on which SAMs were formed. DeltaPsi software was used to determine the film thickness

The angle of incidence between the analyser and the polariser was set to 70^{o} and was maintained for all subsequent measurements. All measurements were made under conditions of ambient temperature, pressure and humidity. SAM thicknesses are averages of a minimum of six measurements, each made at a different location on the substrate.

7.2.2.3 Contact Angle

Contact angle of substrates were determined using the sessile drop method, using a home built contact angle apparatus equipped with a charge coupled device (CCD) video camera linked to a computer for image capture. All data was collected at room temperature and pressure under ambient humidity conditions. A 1μL gastight syringe was used for changing the volume of the droplet for all measurements, allowing volume adjustments of ~ 1 μL to be performed manually. The droplet was released onto the sample surface from a blunt-ended needle of ~ 1 mm diameter. The advancing and receding contact angles were taken as the volume of a water drop on the substrate surface was increased and decreased using the 1 μL syringe. Analysis was carried out using software from FTA. A minimum of six measurements were performed for each sample. All errors presented are the standard error of the mean advancing or receding contact angle.

7.2.2.4 Surface Plasmon Resonance (SPR).

SPR experiments were performed with a Reichert SR7000DC Dual Channel Spectrometer (Buffalo, NY, USA) at 25 °C. Prior to the mannose binding studies, a baseline for the COOH-SAMs was established by running degassed PBS pH 7.4 through the machine at a flow rate of 100 µl/min. Solutions of 1ml EDC/NHS, mannose and ConA were subsequently injected over the sensor chip surface for 10 secs at 1500 µl/min and for 10 min at 100 µl/min (NHS/EDC) and 30 min at 8 µl/min mannose and 30 min at 8 µl ConA. The decrease in flow rate from 1500 to 8 µl/min ensures that sufficient exposure time was provided for binding to occur between the COOH-SAMs on the surface and molecules in solution. In order to remove any unbound molecules from the surface of the SAMs, the sensor chips were washed with degassed PBS for 10 secs at a flow rate of 1500 µl/min, followed by 5 min at a flow rate of 100 µl/min.

7.2.3 Bacterial Microarray Fabrication

7.2.3.1 Bacterial Growth Conditions for cell patterning

Unless otherwise stated, all cultures of *E. coli* were initially inoculated as a pre-culture and grown overnight in LB or M9 minimal media at 37^{o}C, with the appropriate antibiotics to select for plasmids and/or fluorescence. The next day, the pre-culture was diluted 10 fold into fresh media (the same as the pre-culture) and grown to an exponential phase OD_{600} of 0.6 (approximately 2-3 h further growth). The cultures were then spun down using a centrifuge at 5000 rpm for 7 min, followed by re-suspension in fresh media and further dilution as required. After re-suspension and dilution, cells were used immediately, to prevent overgrowth and cell stress. M9 minimal media was made as directed (10 g/l) and supplemented with D-glucose (20 ml of 1M solution); arginine, thiamine, valine (100 mg/l each), $CaCO_3$ (15 mg/l) and $MgSO_4$ (20 mg/l).

7.2.3.2 Silicon master preparation

Silicon masters containing a negative relief of the PDMS stamp mold were manufactured by Jonathan Bramble, University of Leeds. A silicon wafer was prepared by ultrasonic cleaning for 5 mins in Decon 90 detergent, UHQ water, acetone and UHQ water. The wafer was subsequently cleaned in piranha etch solution for 20 mins and rinsed thoroughly in UHQ water. The wafer was dried with nitrogen, dehydrated in an oven at 150 ^{o}C for 1 h and left to cool slowly. The negative tone photoresist SU8 2000 (MicroChem Corp) was used to fabricate the stamp masters. SU8 2000 was spin coated onto the wafer and patterned using standard UV lithography following the standard procedures described by MicroChem. Firstly, the wafer was baked at 65^{o}C for 1 min followed by a further bake at 95 ^{o}C for 2 min, then cooled slowly to room temperature. An exposure dose of 80 mJ/cm^{2}(measured at 365 nm) was found to give the best results. A post-exposure bake at 55 ^{o}C for 1 h was performed to crosslink the SU8 material. The wafer was allowed to cool slowly to room temperature, developed for 1 min using SU8 developer, rinsed with iso-propanol (IPA) and dried with nitrogen.

7.2.3.3 Preparation of stamps for cell patterning

Firstly, a PDMS mold was fabricated by casting a 10:1 (v: v) mixture of PDMS-Sylgard 184 Silicone Elastomer Base and 184 Sylgard Curing Agent onto a micropatterned silicon master. After allowing the PDMS to degas at ambient conditions for 1 h, the PDMS was cured for 2 h at 60°C to promote the cross-linking. The solidified PDMS mold was then carefully peeled from the master and sonicated in EtOH for 30 minutes for sterilization. Subsequently, the stamps were rinsed with UHQ water and dried with argon. For agarose stamps, a replica of the PDMS mold was made by casting a hot de-gassed (4% w/v) solution of high-strength agarose in M9 over the patterned stamps. The agarose was cooled and solidified at room temperature, then carefully peeled away from the PDMS, and cut up into individual stamps (approximately 1cm by 1 cm).

7.2.3.4 Formation of a Bacterial Monolayer on MT-SAMs

The MT-SAMs were immersed in a suspension of *E. coli* grown to an OD 0.6 (approximately 100 µl of a 10^8 cells/ml in M9 broth and 3% glycerol) for 2 h at 37^{o}C, forming a monolayer of *E. coli* on the surface. Unattached cells were rinsed off the surface with sterile PBS.

7.2.3.5 Formation of Patterned Microarray via Direct Printing

PDMS stamps were placed feature-side-up and inked with a suspension of bacteria (100 µl *E. coli*) for 1 hour at 37^{o}C. The excess liquid was then drained using a sterile tissue, and the stamp was then brought into conformal contact with the MT-SAMs and lifted off, leaving a pattern of cells on the surface.

7.2.3.5 Formation of Patterned Microarray via Lift-Off Patterning

Monolayers of *E. coli* were formed as in **7.2.3.4**. Patterned agarose stamps were then placed feature side down onto the MT-SAMs and lifted off again, leaving a pattern of bacteria on the surface. Various pressures were investigated to ascertain the optimal pressure required for patterning (between 0.96 and 36.3 Pa) and it was found to be 13.9 Pa. Stamps were then lowered feature-side-down onto the substrate using the micromanipulator, until the optimal pressure signal was given off by the load cell. The stamps were then removed, leaving a patterned monolayer of cells on the surface.

7.2.3.6 Micro-patterned Co-Cultures

The patterned substrate was then immersed in a second strain of *E. coli* for 1 hr at an optimal OD of 0.4 at 600 nm, allowing the cells to adhere to the MT-SAMS in unpatterned regions. The rinsing procedure was then repeated, and the substrates were then immersed in 20µl of M9 broth to keep the cells viable during microscopy and further experimentation.

7.2.3.7 Fluorescence Microscopy

Fluorescence images were collected using two microscopes - a Zeiss SM-LUX fluorescent microscope and a Leica SPE scanning confocal microscope. The Zeiss was equipped with a Canon Powershot G5 monochrome camera using a mercury lamp as the light source. Pictures were acquired using software remote capture with identical exposure parameters and analysed using *Image J 1.40g* (NIH).

7.2.4 Preparation of Donor and Recipient Bacterial Strains

Throughout this work we used a derivative of *E. coli* K-12 strain MG1655 that had been constructed by the gene doctoring method of Lee *et al.*[233] to fuse the *gfp* gene to the 3'end of the *lacI* gene.

7.2.4.1 Extraction of chloramphenicol resistance gene (*cat* gene) and *lacO* Genes

A DH5α *E. coli* strain containing pLAU plasmids with *lac* operons (28 repeating units) and a DH5α *E. coli* strain containing plasmid pACYC184 (with *cat* gene) were grown at 37^{o}C with shaking at 200rpm overnight in LB broth. Cells were then pelleted by centrifugation at 8000 rpm for 1 minute, and the supernatant disposed off. Accuprep® plasmid extraction kits were used to isolate plasmid DNA from the cultures. Extracted plasmid DNA was then kept on ice until needed

7.2.4.2 Amplification of *cat* gene

Primers were designed to amplify the *cat* gene present in the pACYC184.

Forward: 5' taaaaagtcttcaggagctaaggaagc 3'

Reverse: 5' cataaagtcttcctccttacgccccgccctgcc 3'

A PCR mix with the following chemicals was made up:

Solution	Volume (µl)
Plasmid DNA	1
5 x Hifi Buffer	10
DNTPs	5
DMSO	1.5
Forward Primer	2
Reverse Primer	2
DNA polymerase (Velocity Taq)	0.5
Distilled H_2O	27

Velocity Taq was added to the mix immediately before PCR to prevent premature polymerisation. The following PCR set up was employed:

Stage	Temperature (^oC)	Time
Initial	**94**	**5 min**
PCR (30 cycles)		
Denaturing	94	45s
Annealing	55	30s
Extending	72	1 min 30s
Final Step	**72**	**10 min**

Amplified DNA was then stored at -20^{o}C until needed.

7.2.4.3 Confirmation of amplified *cat* gene via agarose gel electrophoresis

A 1% agarose gel solution was produced by adding 1 g agarose to TAE buffer. TAE buffer is made by mixing 100 ml of 0.5 M EDTA (EDTA disodium salt 200 g/l, pH 8 TAE buffer), 242 g Tris base, 57.1 ml glacial acid and 750 mL deionized water. Final concentration was adjusted to

1% in distilled water. The agarose was heated and then cooled to 50^{o}C followed by addition of 2.5 µl ethidium bromide to the gel. After gentle mixing, the gel was poured into a gel plate with well markers. Once the gel had set, it was loaded onto the electrophoresis plate with fresh 1% TAE Buffer and the well markers removed. A DNA marker (TOP) was added in 2 µl aliquots to the amplified *cat* gene and centrifuged briefly to mix, before loading the samples into the wells in the agarose gel alongside a DNA ladder. Electrophoresis was run at 100 V for 1 hour. Images of the gels were taken using trans UV light to confirm presence of gene products.

7.2.4.4 Extraction of amplified *cat* gene from agarose gel

The agarose containing the *cat* gene band was cut out using a scalpel, and weighed. Capture buffer (potassium iodide, 100 µl per 100mg) was added to dissolve the agarose and release the DNA, and the gel purification kit from GE healthcare was used to collect the DNA in a binding column.

7.2.4.5 Restriction digestion of pLAU plasmids

The pLAU plasmids were cut with restriction enzymes on one side of the 28-mer *lacO* cassette to allow subsequent insertion of the *cat* gene. The following mixture was set up and incubated at 37^{o}C for 1.5 hours:

Solution	**Volume (µl)**
Diluted Bovine Serum Albumen	4
Plasmid DNA	10
Restriction enzyme BamH1	2
Restriction enzyme NHE1	2
Buffer NEB2	4
Sterile distilled water	18

After digestion, the restriction enzymes were inactivated by heat shock for 20 minutes.

7.2.4.6 Ligation of *cat* gene to digested pLAU plasmids

Competent Cells

E. coli strains were grown at 37^{o}C with shaking at 200 rpm overnight in LB broth and then re-inoculated in a 1:100 dilution the following morning, and grown for a further two hours to bring the cells back to exponential phase. The cells were then pelleted at 5000 rpm, 4^{o}C for 7 minutes and re-suspended in 100mM pre-chilled $CaCl_2$ (2 ml per 5 ml culture). The cells were incubated on ice for 20 min, and then pelleted at 5000 rpm, 4^{o}C for 7 minutes. The supernatant was removed, and re-suspended in fresh 100 mM $CaCl_2$ (0.5 ml per 5 ml culture), making them competent.

Ligation of PCR products to plasmid DNA

A solution of digested plasmid DNA (5 µl), PCR product (2 µl), ligase buffer (2 µl) and ligase (1 µl) was added to a sterile eppendorf tube and left for 12 hours to ligate at RT.

Cell Transformation

Ligation mix (8 µl) was added to 100 µl of competent *E. coli* cells and placed on ice for 30 minutes. Subsequently, heat shock at 42^{o}C for 2 minutes caused the DNA to enter the cells. Addition of LB broth (1 ml) to the cells and then incubation at 37^{o}C for 1-2 hours enabled cell growth and plasmid activation. The cells were then streaked on selective LB agar plates containing antibiotics using glass beads to select colonies containing both sets of resistance genes (ampicillin: 50 µg/ml to select pLAU plasmids; chloramphenicol 36 µg/ml to select for the *cat* gene) .

7.2.4.7 Extraction of and amplification of *lacO-cat* genes

Pre-cultures of DH5α *E. coli* containing the modified pLAU plasmids were grown and the plasmids extracted**.** Primers were then designed to amplify the *LacO-cat* genes using PCR:

Forward: 5' cgctgccgtgcccgagagca tggcggctca cgtgatggga tacaaatggg cgcgtg ccgtgcccgagagca tggcggctca cgtgatggga tacaaatggg cgcgtgta aaa cga cgg cca gtg cca agc 3'

Reverse: 5' gga aac agc tat gac cat gat tac agg ggg cat cgc ctt aga aaa gtt cgt cca gca gga gat gaa att gca gc gcaagctgca atttcatctc ctgctggacg aacttttcta aggcgatgcc ccct 3'

The following PCR mix was set up:

Solution	**Volume (µl)**
Plasmid DNA	1
5 x Hifi Buffer	10
DNTPs	5
DMSO	1.5
Forward Primer	2
Reverse Primer	2
DNA polymerase (Velocity Taq)	0.5
Distilled H_2O	27

Velocity Taq was added to the mix immediately before PCR to prevent premature polymerisation. The following PCR set up was employed:

Stage	**Temperature (^oC)**	**Time**
Initial	**94**	**5 min**
PCR (25 cycles)		

Denaturing	94	45s
Annealing	55	30s
Extending	72	1 min 45s
Final Step	**72**	**10 min**

Amplified DNA was then stored at -20^{o}C until needed.

7.2.4.8 Insertion of *lac-cat* genes into pUB307 plasmids via electroporation

pUB307 and pKD46 plasmids were thawed from frozen stocks and co-transformed into *E. coli* as in **7.2.4.6,** and plated onto selective media containing ampicillin (to select for pKD46) and tetracycline (to select for pUB307). Colonies were grown at 30^{o}C instead of 37^{o}C as pKD46 is temperature sensitive. A colony of bacteria containing pKD46- pUB307 was then selected and grown as a pre-culture at 200 rpm overnight in LB broth at 30^{o}C, and then re-inoculated in a 1:50 suspension with 3 % arabinose (to induce red recombinase expression) to an OD at 600 nm of 0.6. The cells were then pelleted at 5000 rpm, 4^{o}C for 7 minutes and re-suspended in 10 % pre-chilled glycerol (0.4 ml per 5 ml culture). This was repeated three times, making the cells electro-competent.

Aliquots of 1 µl of the amplified PCR products of *lacO-cat* genes were added to 40 µl of the electro-competent *E. coli* in pre-chilled electroporation cuvettes (0.2 cm electrode gap) and a 2.5 kV pulse was administered in the electroporator. Immediately afterwards, 1 ml of SOC medium was added to the cell suspensions followed by incubation at 37^{o}C for three hours to allow homologous recombination. The cells were then streaked on selective LB agar plates containing chloramphenicol (35 µg/ml) and tetracycline (50 µg/ml) to select colonies containing both sets of resistance genes.

SOC medium

SOC medium contains bacto-tryptone (2 % w/v), 0.5% w/v bacto-yeast extract (5 g), 8.56mM NaCl, 2.5mM KCl, $_{dd}H_2O$ to 1000 mL, 10 mM $MgCl_2$ and 20 mM glucose (3.603 g)[234]

7.2.5 Conjugation in co-cultures

7.2.5.1 Conjugation control with pUB307-*lacO* in GFP-LacI recipients

GFP-LacI cells were made electro-competent as in **6.2.4.8**, and the pUB307-*lacO* was electroporated into recipient GFP-LacI cells by adding aliquots of 1µl plasmid DNA 40 µl of the electro-competent *E. coli* in pre-chilled electroporation cuvettes (0.2 cm electrode gap). Then, a 2.5 kV pulse was administered in the electroporator. Immediately afterwards, 1 ml of SOC medium was added to the cell suspensions followed by incubation at 37^{o}C for 1.5 hours. Cell suspensions were then streaked onto selective agar plates and containing chloramphenicol (35 µg/ml), tetracycline (50 µg/ml) and kanamycin (50 µg/ml) to select for GFP-LacI cells containing the pUB307-*lacO*. Once the colonies had grown, a colony of *E. coli* was picked and grown to exponential phase with the same antibiotics. Cells were then incubated onto a MT-SAM for 2 hours at 37^{o}C to form a monolayer, and then imaged using confocal fluorescence microscopy.

7.2.5.2 Conjugation experiment in micro-patterned co-cultures

RFP-cells were converted into donor cells by electroporating the pUB307-*lacO* into them in the same manner as in **7.2.5.1**, but the selective media was now chloramphenicol (35 µg/ml), tetracycline (50 µg/ml) and ampicillin (100 µg/ml). RFP donors were then patterned using lift-off patterning as in **7.2.3.5**, and then the GFP-LacI recipients were incubated onto the single-strain patterns at 37^{o}C for one hour, then the whole substrate was placed inside the flow cell at a flow rate of 10 µm/min with pictures taken every hour for five hours.

7.2.5.3 Agar plate counting confirmation of HGT events

Patterned co-cultures on MT-SAMs were formed exactly as in **7.2.3.2**, but instead of inserting the substrates into the flow cell for microscopy, they were incubated at 37^{o}C with either minimal media or LB broth for up to 3 hours. At each time point, the bacteria were removed from the surface by sonication and following serial dilutions they were plated out onto media containing kanamycin (to select for recipients and transconjugants) and kanamycin, chloramphenicol and tetracycline (to select for transconjugants). Additionally the same procedure (minus patterning) was performed on both LB-Agarose and M9-agarose substrates. The results were expressed as the % recipients that had become transconjugants.

Chapter 8: References

(1) van Elsas, J. D.; Bailey, M. J., The ecology of transfer of mobile genetic elements *Fems Microbiology Ecology* **2002**, *42*, 187-197.

(2) Canchaya, C.; Fournous, G.; Chibani-Chennoufi, S.; Dillmann, M. L.; Brussow, H., Phage as agents of lateral gene transfer *Current Opinion in Microbiology* **2003**, *6*, 417-424.

(3) Jiang, S. C.; Paul, J. H., Gene transfer by transduction in the marine environment *Applied and Environmental Microbiology* **1998**, *64*, 2780-2787.

(4) Susskind, M. M.; Botstein, D., Molecular genetics of Bacteriophage-P22 *Microbiological Reviews* **1978**, *42*, 385-413.

(5) Dale, J., Molecular genetics of bacteria *John Wiley and Sons* **2004**, *4*.

(6) Thomas, C. M.; Nielsen, K. M., Mechanisms of, and barriers to, horizontal gene transfer between bacteria *Nature Reviews Microbiology* **2005**, *3*, 711-721.

(7) Chen, I.; Dubnau, D., DNA uptake during bacterial transformation *Nature Reviews Microbiology* **2004**, *2*, 241-249.

(8) Friedlander, A. M., DNA release as a direct measure of microbial killing by phagocytes *Infection and Immunity* **1978**, *22*, 148-154.

(9) Lorenz, M. G.; Gerjets, D.; Wackernagel, W., Release of transforming plasmid and chromosomal DNA from 2 cultured soil bacteria *Archives of Microbiology* **1991**, *156*, 319-326.

(10) Achtman, M.; Schwuchow, S.; Helmuth, R.; Morelli, G.; Manning, P. A., Cell-cell interactions in conjugating *Escherichia-coli* - con-mutants and stabilization of mating aggregates *Molecular & General Genetics* **1978**, *164*, 171-183.

(11) Grossman, T. H.; Silverman, P. M., Structure and function of conjugative Pili - induced synthesis of functional F-Pili by *Escherichia-coli* K-12 containing a LAC-TRA operon fusion *Journal of Bacteriology* **1989**, *171*, 650-656.

(12) Frost, L. S.; Ippenihler, K.; Skurray, R. A., Analysis of the sequence and gene-products of the transfer region of the F-sex factor *Microbiological Reviews* **1994**, *58*, 162-210.

(13) Sorensen, S. J.; Bailey, M.; Hansen, L. H.; Kroer, N.; Wuertz, S., Studying plasmid horizontal transfer in situ: A critical review *Nature Reviews Microbiology* **2005**, *3*, 700-710.

(14) Llosa, M.; Gomis-Ruth, F. X.; Coll, M.; de la Cruz, F., Bacterial conjugation: a two-step mechanism for DNA transport *Molecular Microbiology* **2002**, *45*, 1-8.

(15) Ochman, H.; Lawrence, J. G.; Groisman, E. A., Lateral gene transfer and the nature of bacterial innovation *Nature* **2000**, *405*, 299-304.

(16) del Solar, G.; Giraldo, R.; Ruiz-Echevarria, M. J.; Espinosa, M.; Diaz-Orejas, R., Replication and control of circular bacterial plasmids *Microbiology and Molecular Biology Reviews* **1998**, *62*, 434-464.

(17) Takeshita, S.; Sato, M.; Toba, M.; Masahashi, W.; Hashimotogotoh, T., High-copy-number and low-copy-number plasmid vectors for LACZ-Alpha-complementation and chloramphenicol-resistance or Kanamycin-resistance selection *Gene* **1987**, *61*, 63-74.

(18) Williams, D. R.; Thomas, C. M., ACtive partitioning of bacterial plasmids *Journal of General Microbiology* **1992**, *138*, 1-16.

(19) Thomas, C. M.; Smith, C. A., Incompatibility group-P plasmids - genetics, evolution, and use in gentic manipulation *Annual Review of Microbiology* **1987**, *41*, 77-101.

(20) Nathans, D.; Smith, H. O., Restriction endonucleases in analysis and restructuring of DNA-nolecules. *Annal Review of Biochemistry* **1975**, *44*, 273-293.

(21) Davey, R. B.; Pittard, J., Endonuclease fingerprinting of plasmids mediating Gentamicin resistance in an outbreak of hospital infections *Australian Journal of Experimental Biology and Medical Science* **1980**, *58*, 331-338.

(22) Clowes, R. C., Molecular structure of bacterial plasmids *Bacteriological Reviews* **1972**, *36*, 361-405.

(23) Schroder, G.; Lanka, E., The mating pair formation system of conjugative plasmids - A versatile secretion machinery for transfer of proteins and DNA *Plasmid* **2005**, *54*, 1-25.

(24) Wang, Y. A.; Yu, X.; Silverman, P. M.; Harris, R. L.; Egelman, E. H., The Structure of F-Pili *Journal of Molecular Biology* **2009**, *385*, 22-29.

(25) Harris, R. L.; Sholl, K. A.; Conrad, M. N.; Dresser, M. E.; Silverman, P. M., Interaction between the F plasmid TraA (F-pilin) and TraQ proteins *Molecular Microbiology* **1999**, *34*, 780-791.

(26) Clarke, M.; Maddera, L.; Harris, R. L.; Silverman, P. M., F-pili dynamics by live-cell imaging *Proceedings of the National Academy of Sciences of the United States of America* **2008**, *105*, 17978-17981.

(27) Silverman, P. M.; Clarke, M. B., New insights into F-pilus structure, dynamics, and function *Integrative Biology* **2010**, *2*, 25-31.

(28) Boyd, E. F.; Hill, C. W.; Rich, S. M.; Hartl, D. L., Mosaic structure of plasmids from natural populations of *Escherichia coli Genetics* **1996**, *143*, 1091-1100.

(29) Thomas, C. M., Molecular-genetics of broad host range plasmid RK2 *Plasmid* **1981**, *5*, 10-19.

(30) Adamczyk, M.; Jagura-Burdzy, G., Spread and survival of promiscuous IncP-1 plasmids *Acta Biochimica Polonica* **2003**, *50*, 425-453.

(31) Meyer, R. J.; Shapiro, J. A., Genetic organization of the broad-host-range INCP-1 plasmid R751 *Journal of Bacteriology* **1980**, *143*, 1362-1373.

(32) Meyer, R.; Figurski, D.; Helinski, D. R., Molecular vehicle properties of broad host range plasmid-RK2 *Science* **1975**, *190*, 1226-1228.

(33) Guiney, D. G.; Helinski, D. R., DNA-protein relaxation complex of the plasmid RK2 - location of the site-specific nick in the region of the proposed origin of transfer *Molecular & General Genetics* **1979**, *176*, 183-189.

(34) Larbig, K. D.; Christmann, A.; Johann, A.; Klockgether, J.; Hartsch, T.; Merkl, R.; Wiehlmann, L.; Fritz, H. J.; Tummler, B., Gene islands integrated into tRNA(Gly) genes confer genome diversity on a Pseudomonas aeruginosa clone *Journal of Bacteriology* **2002**, *184*, 6665-6680.

(35) Gogarten, J. P.; Townsend, J. P., Horizontal gene transfer, genome innovation and evolution *Nature Reviews Microbiology* **2005**, *3*, 679-687.

(36) Boto, L., Horizontal gene transfer in evolution: facts and challenges *Proceedings of the Royal Society B-Biological Sciences* **2010**, *277*, 819-827.

(37) Weinberg, S. R.; Stotzky, G., Conjugation and genetic recombination of *Escherichia-coli* soil *Soil Biology and Biochemistry* **1972**, *4*, 171-180.

(38) Lawrence, J. G.; Ochman, H., Amelioration of bacterial genomes: Rates of change and exchange *Journal of Molecular Evolution* **1997**, *44*, 383-397.

(39) Avrain, L.; Vernozy-Rozand, C.; Kempf, I., Evidence for natural horizontal transfer of tetO gene between Campylobacter jejuni strains in chickens *Journal of Applied Microbiology* **2004**, *97*, 134-140.

(40) Kreft, J. U.; Booth, G.; Wimpenny, J. W. T., BacSim, a simulator for individual-based modelling of bacterial colony growth *Microbiology-Uk* **1998**, *144*, 3275-3287.

(41) Lardon, L. A.; Merkey, B. V.; Martins, S.; Doetsch, A.; Picioreanu, C.; Kreft, J.-U.; Smets, B. F., iDynoMiCS: next-generation individual-based modelling of biofilms *Environmental Microbiology*, *13*, 2416-2434.

(42) Hausner, M.; Wuertz, S., High rates of conjugation in bacterial biofilms as determined by quantitative in situ analysis *Applied and Environmental Microbiology* **1999**, *65*, 3710-3713.

(43) Babic, A.; Lindner, A. B.; Vulic, M.; Stewart, E. J.; Radman, M., Direct visualization of horizontal gene transfer *Science* **2008**, *319*, 1533-1536.

(44) Lawley, T. D.; Taylor, D. E., Bacterial conjugative transfer: Visualization of successful mating pairs and plasmid establishment in live *Escherichia coli Plasmid* **2002**, *48*, 263-264.

(45) Gordon, G. S.; Sitnikov, D.; Webb, C. D.; Teleman, A.; Straight, A.; Losick, R.; Murray, A. W.; Wright, A., Chromosome and low copy plasmid segregation in E-coli: Visual evidence for distinct mechanisms *Cell* **1997**, *90*, 1113-1121.

(46) Lawley, T. D.; Gordon, G. S.; Wright, A.; Taylor, D. E., Bacterial conjugative transfer: visualization of successful mating pairs and plasmid establishment in live *Escherichia coli Molecular Microbiology* **2002**, *44*, 947-956.

(47) Babic, A.; Berkmen, M. B.; Lee, C. A.; Grossman, A. D., Efficient Gene Transfer in Bacterial Cell Chains *Mbio* **2011**, *2*.

(48) Dunne, W. M., Bacterial adhesion: Seen any good biofilms lately? *Clinical Microbiology Reviews* **2002**, *15*, 155-166.

(49) Costerton, J. W.; Lewandowski, Z.; Caldwell, D. E.; Korber, D. R.; Lappinscott, H. M., Microbial Biofilms *Annual Review of Microbiology* **1995**, *49*, 711-745.

(50) Bruinsma, G. M.; van der Mei, H. C.; Busscher, H. J., Bacterial adhesion to surface hydrophilic and hydrophobic contact lenses *Biomaterials* **2001**, *22*, 3217-3224.

(51) Schmidt, D. L.; Brady, R. F.; Lam, K.; Schmidt, D. C.; Chaudhury, M. K., Contact angle hysteresis, adhesion, and marine biofouling *Langmuir* **2004**, *20*, 2830-2836.

(52) Fux, C. A.; Costerton, J. W.; Stewart, P. S.; Stoodley, P., Survival strategies of infectious biofilms *Trends in Microbiology* **2005**, *13*, 34-40.

(53) Donlan, R. M., Biofilms: Microbial life on surfaces *Emerging Infectious Diseases* **2002**, *8*, 881-890.

(54) Davey, M. E.; O'Toole, G. A., Microbial biofilms: from ecology to molecular genetics *Microbiology and Molecular Biology Reviews* **2000**, *64*, 847-867.

(55) Jefferson, K. K., What drives bacteria to produce a biofilm? *Fems Microbiology Letters* **2004**, *236*, 163-173.

(56) Busscher, H. J.; Weerkamp, A. H., Specific and Nonspecific ineractions in bacterial adhesion to solid substrata *Fems Microbiology Reviews* **1987**, *46*, 165-173.

(57) Bos, R.; van der Mei, H. C.; Busscher, H. J., Physico-chemistry of initial microbial adhesive interactions - its mechanisms and methods for study *Fems Microbiology Reviews* **1999**, *23*, 179-230.

(58) Rutter, P. R.; Vincent, B. In *Marshall, K. C.* 1985, p 21-38.

(59) van Oss, C. J., Long-range and short-range mechanisms of hydrophobic attraction and hydrophilic repulsion in specific and aspecific interactions *Journal of Molecular Recognition* **2003**, *16*, 177-190.

(60) Busscher, H. J.; Weerkamp, A. H.; Vandermei, H. C.; Vanpelt, A. W. J.; Dejong, H. P.; Arends, J., Measurement of the surface free-energy of bacterial-cell surfaces and its relevance for adhesion *Applied and Environmental Microbiology* **1984**, *48*, 980-983.

(61) An, Y. H.; Friedman, R. J., Concise review of mechanisms of bacterial adhesion to biomaterial surfaces *Journal of Biomedical Materials Research* **1998**, *43*, 338-348.

(62) Morra, M.; Cassinelli, C., Bacterial adhesion to polymer surfaces: A critical review of surface thermodynamic approaches *Journal of Biomaterials Science-Polymer Edition* **1997**, *9*, 55-74.

(63) Cunliffe, D.; Smart, C. A.; Alexander, C.; Vulfson, E. N., Bacterial adhesion at synthetic surfaces *Applied and Environmental Microbiology* **1999**, *65*, 4995-5002.

(64) Li, B. K.; Logan, B. E., Bacterial adhesion to glass and metal-oxide surfaces *Colloids and Surfaces B-Biointerfaces* **2004**, *36*, 81-90.

(65) Hultgren, S. J.; Abraham, S.; Caparon, M.; Falk, P.; Stgeme, J. W.; Normark, S., Pilus and nonpilus bacterial adhesins - assembly and function in cell recognition *Cell* **1993**, *73*, 887-901.

(66) Soto, G. E.; Hultgren, S. J., Bacterial adhesins: Common themes and variations in architecture and assembly *Journal of Bacteriology* **1999**, *181*, 1059-1071.

(67) Kuehn, M. J.; Heuser, J.; Normark, S.; Hultgren, S. J., P Pili in uropathogenic Escherichia-Coli are composite fibers with distinct fibrillar adhesive tips *Nature* **1992**, *356*, 252-255.

(68) Krogfelt, K. A., Bacterial adhesion - genetics, biogenesis, and role in pathogenesis of fibrial adhesins of Escherichia-Coli *Reviews of Infectious Diseases* **1991**, *13*, 721-735.

(69) Klemm, P., Fimbrial adhesins of Escherichia-Coli *Reviews of Infectious Diseases* **1985**, *7*, 321-340.

(70) Falkow, S.; Isberg, R. R.; Portnoy, D. A., The interaction of bacteria with mammalian-cells *Annual Review of Cell Biology* **1992**, *8*, 333-363.

(71) Chhatwal, G. S., Anchorless adhesins and invasins of Gram-positive bacteria: a new class of virulence factors *Trends in Microbiology* **2002**, *10*, 205-208.

(72) Degraaf, F. K.; Mooi, F. R., The fimbrial adhesins of Escherichia-Coli *Advances in Microbial Physiology* **1986**, *28*, 65-143.

(73) Houwink, A. L.; Vaniterson, W., Electron microscopical observations on bacterial cytology. 2. A study on flagellation *Biochimica Et Biophysica Acta* **1950**, *5*, 10-44.

(74) Knight, S.; Bouckaert, J.; Lindhorst, T. K., Oscarson, S., Eds.; Springer Berlin / Heidelberg: 2009; Vol. 288, p 67-107.

(75) Dempsey, M. J., MARINE BACTERIAL FOULING - A SCANNING ELECTRON-MICROSCOPE STUDY *Marine Biology* **1981**, *61*, 305-315.

(76) Mol, O.; Oudega, B., Molecular and structural aspects of fimbriae biosynthesis and assembly in *Escherichia coli Fems Microbiology Reviews* **1996**, *19*, 25-52.

(77) Ottow, J. C. G., Ecology, physiology, and genetics of fimbriae and Pili *Annual Review of Microbiology* **1975**, *29*, 79-108.

(78) Johnson, J. R., Virulence factors in *Escherichia-coli* urinary-tract infection *Clinical Microbiology Reviews* **1991**, *4*, 80-128.

(79) Bell, G. I., Models for specific and adhesion of cells to cells *Science* **1978**, *200*, 618-627.

(80) Forero, M.; Yakovenko, O.; Sokurenko, E. V.; Thomas, W. E.; Vogel, V., Uncoiling mechanics of *Escherichia coli* type I fimbriae are optimized for catch bonds *Plos Biology* **2006**, *4*, 1509-1516.

(81) Aprikian, P.; Tchesnokova, V.; Kidd, B.; Yakovenko, O.; Yarov-Yarovoy, V.; Trinchina, E.; Vogel, V.; Thomas, W.; Sokurenko, E., Interdomain interaction in the FimH adhesin of *Escherichia coli* regulates the affinity to mannose *Journal of Biological Chemistry* **2007**, *282*, 23437-23446.

(82) Patti, J. M.; Allen, B. L.; McGavin, M. J.; Hook, M., Mscramm-media adherence of microorganisms to host tissues *Annual Review of Microbiology* **1994**, *48*, 585-617.

(83) Premkumar, J. R.; Lev, O.; Marks, R. S.; Polyak, B.; Rosen, R.; Belkin, S., Antibody-based immobilization of bioluminescent bacterial sensor cells *Talanta* **2001**, *55*, 1029-1038.

(84) Meyer, R. L.; Zhou, X.; Tang, L.; Arpanaei, A.; Kingshott, P.; Besenbacher, F., Immobilisation of living bacteria for AFM imaging under physiological conditions *Ultramicroscopy*, *110*, 1349-1357.

(85) Colville, K.; Tompkins, N.; Rutenberg, A. D.; Jericho, M. H., Effects of Poly(L-lysine) Substrates on Attached *Escherichia coli* Bacteria *Langmuir*, *26*, 2639-2644.

(86) Fendler, J. H., Chemical self-assembly for electronic applications *Chemistry of Materials* **2001**, *13*, 3196-3210.

(87) Whitesides, G. M.; Mathias, J. P.; Seto, C. T., Molecular self-assembly and nanochemistry - A chemical strategy for the synthesis of nanostructures *Science* **1991**, *254*, 1312-1319.

(88) De Feyter, S.; De Schryver, F. C., Self-assembly at the liquid/solid interface: STM reveals *Journal of Physical Chemistry B* **2005**, *109*, 4290-4302.

(89) Mendes, P. M.; Chen, Y.; Palmer, R. E.; Nikitin, K.; Fitzmaurice, D.; Preece, J. A., Nanostructures from nanoparticles *Journal of Physics-Condensed Matter* **2003**, *15*, S3047-S3063.

(90) Whitesides, G. M.; Grzybowski, B., Self-assembly at all scales *Science* **2002**, *295*, 2418-2421.

(91) Jeremy M Berg, J. L. T., and Lubert Stryer., Biochemistry, *W. H. Freeman and Company* **2002**, *5th edition*.

(92) Zhang, S. G., Fabrication of novel biomaterials through molecular self-assembly *Nature Biotechnology* **2003**, *21*, 1171-1178.

(93) Whitesides, G. M.; Boncheva, M., Beyond molecules: Self-assembly of mesoscopic and macroscopic components *Proceedings of the National Academy of Sciences of the United States of America* **2002**, *99*, 4769-4774.

(94) Stang, P. J.; Olenyuk, B., Self-assembly, symmetry, and molecular architecture: Coordination as the motif in the rational design of supramolecular metallacyclic polygons and polyhedra *Accounts of Chemical Research* **1997**, *30*, 502-518.

(95) Ulman, A., Formation and structure of self-assembled monolayers *Chemical Reviews* **1996**, *96*, 1533-1554.

(96) Prime, K. L.; Whitesides, G. M., Self-assembled organic monolayers - model systems for studying adsorption of proteins at surfaces *Science* **1991**, *252*, 1164-1167.

(97) Mrksich, M., Using self-assembled monolayers to understand the biomaterials interface *Current Opinion in Colloid & Interface Science* **1997**, *2*, 83-88.

(98) Fang, J. Y.; Knobler, C. M., Phase-separated two-component self-assembled organosilane monolayers and their use in selective adsorption of a protein *Langmuir* **1996**, *12*, 1368-1374.

(99) Gao, W.; Dickinson, L.; Grozinger, C.; Morin, F. G.; Reven, L., Self-assembled monolayers of alkylphosphonic acids on metal oxides *Langmuir* **1996**, *12*, 6429-6435.

(100) Poirier, G. E.; Pylant, E. D., The self-assembly mechanism of alkanethiols on Au(111) *Science* **1996**, *272*, 1145-1148.

(101) Schreiber, F., Structure and growth of self-assembling monolayers *Progress in Surface Science* **2000**, *65*, 151-256.

(102) Love, J. C.; Estroff, L. A.; Kriebel, J. K.; Nuzzo, R. G.; Whitesides, G. M., Self-assembled monolayers of thiolates on metals as a form of nanotechnology *Chemical Reviews* **2005**, *105*, 1103-1169.

(103) Choy, K. L., Chemical vapour deposition of coatings *Progress in Materials Science* **2003**, *48*, 57-170.

(104) Fendler, J. H., Self-assembled nanostructured materials *Chemistry of Materials* **1996**, *8*, 1616-1624.

(105) Delamarche, E.; Michel, B.; Biebuyck, H. A.; Gerber, C., Golden interfaces: The surface of self-assembled monolayers *Advanced Materials* **1996**, *8*, 719-729.

(106) Wink, T.; vanZuilen, S. J.; Bult, A.; vanBennekom, W. P., Self-assembled monolayers for biosensors *Analyst* **1997**, *122*, R43-R50.

(107) Dubois, L. H.; Nuzzo, R. G., Synthesis, structure, and properties of model organic-surfaces *Annual Review of Physical Chemistry* **1992**, *43*, 437-463.

(108) Nuzzo, R. G.; Zegarski, B. R.; Dubois, L. H., Fundamental-studies of the chemisorption of organofulfur compounds on Au(111) - implications for molecular self-assembly on gold surfaces *Journal of the American Chemical Society* **1987**, *109*, 733-740.

(109) Patel, N.; Davies, M. C.; Hartshorne, M.; Heaton, R. J.; Roberts, C. J.; Tendler, S. J. B.; Williams, P. M., Immobilization of protein molecules onto homogeneous and mixed carboxylate-terminated self-assembled monolayers *Langmuir* **1997**, *13*, 6485-6490.

(110) Tam-Chang, S. W.; Iverson, I., Applications of self-assembled monolayers (SAMs) of alkanethiolates on gold *Adsorption and Its Applications in Industry and Environmental Protection, Vol I: Applications in Industry* **1999**, *120*, 917-950.

(111) Ostuni, E.; Yan, L.; Whitesides, G. M., The interaction of proteins and cells with self-assembled monolayers of alkanethiolates on gold and silver *Colloids and Surfaces B-Biointerfaces* **1999**, *15*, 3-30.

(112) Arendt, A.; Kolodziejczyk, A. M., O-Acylureas and N-Acylureas in peptide-synthesis by DCC method - New observations *Tetrahedron Letters* **1978**, *40*, 3867-3868.

(113) Nakajima, N.; Ikada, Y., Mechanism of amide formation by carbodiimide for bioconjugation in aqueous-media *Bioconjugate Chemistry* **1995**, *6*, 123-130.

(114) Williams, A.; Ibrahim, I. T., Carbodiimide chemistry - recent advances *Chemical Reviews* **1981**, *81*, 589-636.

(115) Fischer, M. J. E. In *Surface Plasmon Resonance: Methods and Protocols*; DeMol, N. J. F. M. J. E., Ed. 2010; Vol. 627, p 55-73.

(116) Lewis, A. L., Phosphorylcholine-based polymers and their use in the prevention of biofouling *Colloids and Surfaces B-Biointerfaces* **2000**, *18*, 261-275.

(117) Wisniewski, N.; Reichert, M., Methods for reducing biosensor membrane biofouling *Colloids and Surfaces B-Biointerfaces* **2000**, *18*, 197-219.

(118) Lee, D. H.; Kim, D.; Oh, T.; Cho, M., Phase state effect on adhesion behavior of self-assembled monolayers *Langmuir* **2004**, *20*, 8124-8130.

(119) Prime, K. L.; Whitesides, G. M., Adsorption of proteins onto surfaces containing end-attached oligo(ethylene oxide) - A model system using self-assembled monolayers *Journal of the American Chemical Society* **1993**, *115*, 10714-10721.

(120) Harder, P.; Grunze, M.; Dahint, R.; Whitesides, G. M.; Laibinis, P. E., Molecular Conformation in Oligo(ethylene glycol)-Terminated Self-Assembled Monolayers on Gold and Silver Surfaces Determines Their Ability To Resist Protein Adsorption *The Journal of Physical Chemistry B* **1998**, *102*, 426-436.

(121) Parreira, P.; Magalhaes, A.; Goncalves, I. C.; Gomes, J.; Vidal, R.; Reis, C. A.; Leckband, D. E.; Martins, M. C. L., Effect of surface chemistry on bacterial adhesion, viability, and morphology *Journal of Biomedical Materials Research Part A* **2011**, *99A*, 344-353.

(122) Sousa, C.; Teixeira, P.; Bordeira, S.; Fonseca, J.; Oliveira, R., Staphylococcus epidermidis adhesion to modified polyearbonate surfaces: Gold and SAMs coated *Journal of Adhesion Science and Technology* **2008**, *22*, 675-686.

(123) Terrettaz, S.; Ulrich, W. P.; Vogel, H.; Hong, Q.; Dover, L. G.; Lakey, J. H., Stable self-assembly of a protein engineering scaffold on gold surfaces *Protein Science* **2002**, *11*, 1917-1925.

(124) Qian, X. P.; Metallo, S. J.; Choi, I. S.; Wu, H. K.; Liang, M. N.; Whitesides, G. M., Arrays of self-assembled monolayers for studying inhibition of bacterial adhesion *Analytical Chemistry* **2002**, *74*, 1805-1810.

(125) Liang, M. N.; Smith, S. P.; Metallo, S. J.; Choi, I. S.; Prentiss, M.; Whitesides, G. M., Measuring the forces involved in polyvalent adhesion of uropathogenic *Escherichia coli* to mannose-presenting surfaces *Proceedings of the National Academy of Sciences of the United States of America* **2000**, *97*, 13092-13096.

(126) Whitesides, G. M.; Ostuni, E.; Takayama, S.; Jiang, X. Y.; Ingber, D. E., Soft lithography in biology and biochemistry *Annual Review of Biomedical Engineering* **2001**, *3*, 335-373.

(127) Kane, R. S.; Takayama, S.; Ostuni, E.; Ingber, D. E.; Whitesides, G. M., Patterning proteins and cells using soft lithography *Biomaterials* **1999**, *20*, 2363-2376.

(128) Nie, Z.; Kumacheva, E., Patterning surfaces with functional polymers *Nature Materials* **2008**, *7*, 277-290.

(129) Xia, Y. N.; Whitesides, G. M., Soft lithography *Annual Review of Materials Science* **1998**, *28*, 153-184.

(130) Michel, B.; Bernard, A.; Bietsch, A.; Delamarche, E.; Geissler, M.; Juncker, D.; Kind, H.; Renault, J. P.; Rothuizen, H.; Schmid, H.; Schmidt-Winkel, P.; Stutz, R.; Wolf, H., Printing meets lithography: Soft approaches to high-resolution printing *Ibm Journal of Research and Development* **2001**, *45*, 697-719.

(131) Cerf, A.; Cau, J.-C.; Vieu, C., Controlled assembly of bacteria on chemical patterns using soft lithography *Colloids and Surfaces B-Biointerfaces* **2008**, *65*, 285-291.

(132) Rowan, B.; Wheeler, M. A.; Crooks, R. M., Patterning bacteria within hyperbranched polymer film templates *Langmuir* **2002**, *18*, 9914-9917.

(133) Weibel, D. B.; DiLuzio, W. R.; Whitesides, G. M., Microfabrication meets microbiology *Nature Reviews Microbiology* **2007**, *5*, 209-218.

(134) Xu, L.; Robert, L.; Qi, O.; Taddei, F.; Chen, Y.; Lindner, A. B.; Baigl, D., Microcontact printing of living bacteria arrays with cellular resolution *Nano Letters* **2007**, *7*, 2068-2072.

(135) Weibel, D. B.; Lee, A.; Mayer, M.; Brady, S. F.; Bruzewicz, D.; Yang, J.; DiLuzio, W. R.; Clardy, J.; Whitesides, G. M., Bacterial printing press that regenerates its ink: Contact-printing bacteria using hydrogel stamps *Langmuir* **2005**, *21*, 6436-6442.

(136) Balaban, N. Q.; Merrin, J.; Chait, R.; Kowalik, L.; Leibler, S., Bacterial persistence as a phenotypic switch *Science* **2004**, *305*, 1622-1625.

(137) Unger, M. A.; Chou, H. P.; Thorsen, T.; Scherer, A.; Quake, S. R., Monolithic microfabricated valves and pumps by multilayer soft lithography *Science* **2000**, *288*, 113-116.

(138) Takayama, S.; Ostuni, E.; LeDuc, P.; Naruse, K.; Ingber, D. E.; Whitesides, G. M., Selective chemical treatment of cellular microdomains using multiple laminar streams *Chemistry & Biology* **2003**, *10*, 123-130.

(139) Sirringhaus, H.; Kawase, T.; Friend, R. H.; Shimoda, T.; Inbasekaran, M.; Wu, W.; Woo, E. P., High-resolution inkjet printing of all-polymer transistor circuits *Science* **2000**, *290*, 2123-2126.

(140) Tekin, E.; Smith, P. J.; Schubert, U. S., Inkjet printing as a deposition and patterning tool for polymers and inorganic particles *Soft Matter* **2008**, *4*, 703-713.

(141) Merrin, J.; Leibler, S.; Chuang, J. S., Printing Multistrain Bacterial Patterns with a Piezoelectric Inkjet Printer *Plos One* **2007**, *2*.

(142) Eun, Y.-J.; Weibel, D. B., Fabrication of Microbial Biofilm Arrays by Geometric Control of Cell Adhesion *Langmuir* **2009**, *25*, 4643-4654.

(143) Ingham, C.; Bomer, J.; Sprenkels, A.; van den Berg, A.; de Vos, W.; Vlieg, J. v. H., High-resolution microcontact printing and transfer of massive arrays of microorganisms on planar and compartmentalized nanoporous aluminium oxide *Lab on a Chip*, *10*, 1410-1416.

(144) Seah, M. P., A review of the analysis of surfaces and thin films by AES and XPS *Vacuum* **1984**, *34*, 463-478.

(145) Moulder, J. *Handbook of X-ray Photoelectron Spectroscopy*; Perkin-Elmer Corporation, 1992.

(146) Hirose, K.; Nohira, H.; Azuma, K.; Hattori, T., Photoelectron spectroscopy studies of SiO2/Si interfaces *Progress in Surface Science* **2007**, *82*, 3-54.

(147) Venezia, A. M., X-ray photoelectron spectroscopy (XPS) for catalysts characterization *Catalysis Today* **2003**, *77*, 359-370.

(148) de Groot, F., Multiplet effects in X-ray spectroscopy *Coordination Chemistry Reviews* **2005**, *249*, 31-63.

(149) Theeten, J. B.; Aspnes, D. E., Ellipsometry in thin-film analysis *Annual Review of Materials Science* **1981**, *11*, 97-122.

(150) Pedrotti, F. L. P., L.S., Introduction to Optics *2nd ed., Prentice Hall:New Jersey*, **1993**.

(151) Goncalves, D.; Irene, E. A., Fundamentals and applications of spectroscopic ellipsometry *Quimica Nova* **2002**, *25*, 794-800.

(152) Schubert, M., Generalized ellipsometry and complex optical systems *Thin Solid Films* **1998**, *313*, 323-332.

(153) Schubert, M., Another century of ellipsometry *Annalen Der Physik* **2006**, *15*, 480-497.

(154) Gottesfeld, S., Ellipsometry - Principles and recent applications in electrochemistry *Electroanalytical Chemistry* **1989**, *15*, 143-265.

(155) Kim, S. H.; Ock, K. S.; Im, J. H.; Kim, J. H.; Koh, K. N.; Kang, S. W., Photoinduced refractive index change of self-assembled spiroxazaine monolayer based on surface plasmon resonance *Dyes and Pigments* **2000**, *46*, 55-62.

(156) Bonn, D.; Eggers, J.; Indekeu, J.; Meunier, J.; Rolley, E., Wetting and spreading *Reviews of Modern Physics* **2009**, *81*, 739-805.

(157) Feng, B.; Weng, J.; Yang, B. C.; Qu, S. X.; Zhang, X. D., Characterization of surface oxide films on titanium and adhesion of osteoblast *Biomaterials* **2003**, *24*, 4663-4670.

(158) Bowen, J., Pettitt, M. E., Kendall, K., Leggett, G. J., Preece, J. A., Callow, M. E., Callow, J. A., The influence of surface lubricity on the adhesion of Navicula perminuta and Ulva linza to alkanethiol self-assembled monolayers *J. R. Soc. Interface* **2007**, *4*, 473-477.

(159) Chen W., F. A. Y., Hsieh M C.,Oner D.,; Youngblood J., M. T. J., Ultrahydrophobic and Ultralyophobic Surfaces: Some Comments and Examples *Langmuir* **1999**, *15*, 3395-3399.

(160) Mrksich, M.; Sigal, G. B.; Whitesides, G. M., Surface-Plasmon Resonance permits in-situ measurement of protein adsorption on self-assembled monolayers of alkanethiolates on Gold *Langmuir* **1995**, *11*, 4383-4385.

(161) Barnes, W. L.; Dereux, A.; Ebbesen, T. W., Surface plasmon subwavelength optics *Nature* **2003**, *424*, 824-830.

(162) Raether, H., Influence of roughness on optical-properties of surfaces - plasma resonance emission and plasmon dispersion-relation *Thin Solid Films* **1975**, *28*, 119-124.

(163) Brockman, J. M.; Nelson, B. P.; Corn, R. M., Surface plasmon resonance imaging measurements of ultrathin organic films *Annual Review of Physical Chemistry* **2000**, *51*, 41-63.

(164) Homola, J., Present and future of surface plasmon resonance biosensors *Analytical and Bioanalytical Chemistry* **2003**, *377*, 528-539.

(165) Kretschm.E; Raether, H., Radiative decay of non radiative surface plasmons excited by light *Zeitschrift Fur Naturforschung Part a-Astrophysik Physik Und Physikalische Chemie* **1968**, *A 23*, 2135.

(166) Ritchie, R. H., Plasma losses by fast electrons in thin films *Physical Review* **1957**, *106*, 874-881.

(167) Homola, J.; Koudela, I.; Yee, S. S., Surface plasmon resonance sensors based on diffraction gratings and prism couplers: sensitivity comparison *Sensors and Actuators B-Chemical* **1999**, *54*, 16-24.

(168) Joseph R, L., Fluorescence spectroscopic investigations of the dynamic properties of proteins, membranes and nucleic acids *Journal of Biochemical and Biophysical Methods*, *2*, 91-119.

(169) Stryer, L., Fluorescence spectroscopy of proteins *Science* **1968**, *162*, 526-533.

(170) Ntziachristos, V., Fluorsecence molecular imaging *Annual Review of Biomedical Engineering* **2006**, *8*, 1-33.

(171) Ballou, B.; Lagerholm, B. C.; Ernst, L. A.; Bruchez, M. P.; Waggoner, A. S., Noninvasive imaging of quantum dots in mice *Bioconjugate Chemistry* **2004**, *15*, 79-86.

(172) Kerppola, T. K., Visualization of molecular interactions by fluorescence complementation *Nature Reviews Molecular Cell Biology* **2006**, *7*, 449-456.

(173) Tsien, R. Y., The green fluorescent protein *Annual Review of Biochemistry* **1998**, *67*, 509-544.

(174) Patterson, G. H.; Knobel, S. M.; Sharif, W. D.; Kain, S. R.; Piston, D. W., Use of the green fluorescent protein and its mutants in quantitative fluorescence microscopy *Biophysical Journal* **1997**, *73*, 2782-2790.

(175) Chalfie, M.; Tu, Y.; Euskirchen, G.; Ward, W. W.; Prasher, D. C., Green fluorescent protein as a marker for gene-expression *Science* **1994**, *263*, 802-805.

(176) Lau, I. F.; Filipe, S. R.; Soballe, B.; Okstad, O. A.; Barre, F. X.; Sherratt, D. J., Spatial and temporal organization of replicating *Escherichia coli* chromosomes *Molecular Microbiology* **2003**, *49*, 731-743.

(177) Lichtman, J. W.; Conchello, J. A., Fluorescence microscopy *Nature Methods* **2005**, *2*, 910-919.

(178) Young, M. R., Principles and technique of fluorescence microscopy *Quarterly Journal of Microscopical Science* **1961**, *102*, 419.

(179) Minsky, M., Memoir on inventing the confocal scanning microscope *Scanning* **1988**, *10*, 128-138.

(180) Paddock, S. W., Principles and practices of laser scanning confocal microscopy *Molecular Biotechnology* **2000**, *16*, 127-149.

(181) Laurent, M.; Johannin, G.; Leguyader, H.; Fleury, A., Confocal scanning of optical microscopy and 3-dimensional imaging *Biology of the Cell* **1992**, *76*, 113-124.

(182) Connell, H.; Agace, W.; Klemm, P.; Schembri, M.; Marild, S.; Svanborg, C., Type 1 fimbrial expression enhances *Escherichia coli* virulence for the urinary tract *Proceedings of the National Academy of Sciences of the United States of America* **1996**, *93*, 9827-9832.

(183) Suo, Z. Y.; Avci, R.; Yang, X. H.; Pascual, D. W., Efficient immobilization and patterning of live bacterial cells *Langmuir* **2008**, *24*, 4161-4167.

(184) Yakovenko, O.; Sharma, S.; Forero, M.; Tchesnokova, V.; Aprikian, P.; Kidd, B.; Mach, A.; Vogel, V.; Sokurenko, E.; Thomas, W. E., FimH forms catch bonds that are enhanced by mechanical force due to allosteric regulation *Journal of Biological Chemistry* **2008**, *283*, 11596-11605.

(185) Mrksich, M.; Chen, C. S.; Xia, Y. N.; Dike, L. E.; Ingber, D. E.; Whitesides, G. M., Controlling cell attachment on contoured surfaces with self-assembled monolayers of alkanethiolates on gold *Proceedings of the National Academy of Sciences of the United States of America* **1996**, *93*, 10775-10778.

(186) Myrskog, A.; Anderson, H.; Aastrup, T.; Ingemarsson, B.; Liedberg, B., Esterification of Self-Assembled Carboxylic-Acid-Terminated Thiol Monolayers in Acid Environment: A Time-Dependent Study *Langmuir* **2010**, *26*, 821-829.

(187) Wang, H.; Chen, S. F.; Li, L. Y.; Jiang, S. Y., Improved method for the preparation of carboxylic acid and amine terminated self-assembled monolayers of alkanethiolates *Langmuir* **2005**, *21*, 2633-2636.

(188) Revell, D. J.; Knight, J. R.; Blyth, D. J.; Haines, A. H.; Russell, D. A., Self-assembled carbohydrate monolayers: Formation and surface selective molecular recognition *Langmuir* **1998**, *14*, 4517-4524.

(189) Homola, J., Surface plasmon resonance sensors for detection of chemical and biological species *Chemical Reviews* **2008**, *108*, 462-493.

(190) Yamamoto, Y.; Takashima, T., Friction and wear of water lubricated PEEK and PPS sliding contacts *Wear* **2002**, *253*, 820-826.

(191) Wang, Z.; Shi, Y. L.; Li, H. L., Investigation of two-component mixed self-assembled monolayers on gold *Canadian Journal of Chemistry-Revue Canadienne De Chimie* **2001**, *79*, 328-336.

(192) Whelan, C. M.; Smyth, M. R.; Barnes, C. J.; Brown, N. M. D.; Anderson, C. A., An XPS study of heterocyclic thiol self-assembly on Au(111) *Applied Surface Science* **1998**, *134*, 144-158.

(193) Mendoza, S. M.; Arfaoui, I.; Zanarini, S.; Paolucci, F.; Rudolf, P., Improvements in the characterization of the crystalline structure of acid-terminated alkanethiol self-assembled monolayers on Au(111) *Langmuir* **2007**, *23*, 582-588.

(194) Marc, H., An application of ellipsometry: Assessment of polysaccharide and glycoprotein interaction with lectin at a liquid/solid interface *Biochimica et Biophysica Acta (BBA) - General Subjects* **1980**, *632*, 298-309.

(195) Adiciptaningrum, A. M.; Blomfield, I. C.; Tans, S. J., Direct observation of type 1 fimbrial switching *Embo Reports* **2009**, *10*, 527-532.

(196) Choi, C. H.; Lee, J. H.; Hwang, T. S.; Lee, C. S.; Kim, Y. G.; Yang, Y. H.; Huh, K. M., Preparation of bacteria microarray using selective patterning of polyelectrolyte multilayer and poly(ethylene glycol)-poly(lactide) diblock copolymer *Macromolecular Research* **2010**, *18*, 254-259.

(197) Cerf, A.; Cau, J. C.; Vieu, C., Controlled assembly of bacteria on chemical patterns using soft lithography *Colloids and Surfaces B-Biointerfaces* **2008**, *65*, 285-291.

(198) Rozhok, S.; Shen, C. K. F.; Littler, P. L. H.; Fan, Z. F.; Liu, C.; Mirkin, C. A.; Holz, R. C., Methods for fabricating microarrays of motile bacteria *Small* **2005**, *1*, 445-451.

(199) Rozhok, S.; Fan, Z. F.; Nyamjav, D.; Liu, C.; Mirkin, C. A.; Holz, R. C., Attachment of motile bacterial cells to prealigned holed microarrays *Langmuir* **2006**, *22*, 11251-11254.

(200) Suh, K. Y.; Khademhosseini, A.; Yoo, P. J.; Langer, R., Patterning and separating infected bacteria using host-parasite and virus-antibody interactions *Biomedical Microdevices* **2004**, *6*, 223-229.

(201) Krsko, P.; Kaplan, J. B.; Libera, M., Spatially controlled bacterial adhesion using surface-patterned poly(ethylene glycol) hydrogels *Acta Biomaterialia* **2009**, *5*, 589-596.

(202) Koh, W. G.; Revzin, A.; Simonian, A.; Reeves, T.; Pishko, M., Control of mammalian cell and bacteria adhesion on substrates micropatterned with poly(ethylene glycol) hydrogels *Biomedical Microdevices* **2003**, *5*, 11-19.

(203) Xu, T.; Petridou, S.; Lee, E. H.; Roth, E. A.; Vyavahare, N. R.; Hickman, J. J.; Boland, T., Construction of high-density bacterial colony arrays and patterns by the ink-jet method *Biotechnology and Bioengineering* **2004**, *85*, 29-33.

(204) Xu, L. P.; Robert, L.; Qi, O. Y.; Taddei, F.; Chen, Y.; Lindner, A. B.; Baigl, D., Microcontact printing of living bacteria arrays with cellular resolution *Nano Letters* **2007**, *7*, 2068-2072.

(205) Li, H. W.; Muir, B. V. O.; Fichet, G.; Huck, W. T. S., Nanocontact printing: A route to sub-50-nm-scale chemical and biological patterning *Langmuir* **2003**, *19*, 1963-1965.

(206) Ehlers, R. U.; Strauch, O., Improvement of the dessication and temperature tolerance of heterorhabditis bacteriophora *Journal of Nematology* **2003**, *35*, 336.

(207) Chaudhury, M. K.; Whitesides, G. M., Direct measurement of interfacial interactions between semispherical lenses and flat sheets of poly(dimethylsiloxane) and their chemical derivatives *Langmuir* **1991**, *7*, 1013-1025.

(208) Sadhu, V. B.; Perl, A.; Peter, M.; Rozkiewicz, D. I.; Engbers, G.; Ravoo, B. J.; Reinhoudt, D. N.; Huskens, J., Surface modification of elastomeric stamps for microcontact printing of polar inks *Langmuir* **2007**, *23*, 6850-6855.

(209) Kartalov, E. P.; Anderson, W. F.; Scherer, A., The analytical approach to polydimethylsiloxane microfluidic technology and its biological applications *Journal of Nanoscience and Nanotechnology* **2006**, *6*, 2265-2277.

(210) Gou, H.-L.; Xu, J.-J.; Xia, X.-H.; Chen, H.-Y., Air plasma assisting microcontact deprinting and printing for gold thin film and PDMS patterns *ACS Appl Mater Interfaces* **2010**, *2*, 1324-30.

(211) Seguin, C.; McLachlan, J. M.; Norton, P. R.; Lagugne-Labarthet, F., Surface modification of poly(dimethylsiloxane) for microfluidic assay applications *Applied Surface Science* **2010**, *256*, 2524-2531.

(212) Kim, B.; Peterson, E. T. K.; Papautsky, I.; ieee In *Proceedings of the 26th Annual International Conference of the Ieee Engineering in Medicine and Biology Society, Vols 1-7* 2004; Vol. 26, p 5013-5016.

(213) Efimenko, K.; Wallace, W. E.; Genzer, J., Surface modification of Sylgard-184 poly(dimethyl siloxane) networks by ultraviolet and ultraviolet/ozone treatment *Journal of Colloid and Interface Science* **2002**, *254*, 306-315.

(214) Berdichevsky, Y.; Khandurina, J.; Guttman, A.; Lo, Y. H., UV/ozone modification of poly(dimethylsiloxane) microfluidic channels *Sensors and Actuators B-Chemical* **2004**, *97*, 402-408.

(215) Nejadnik, M. R.; Olsson, A. L. J.; Sharma, P. K.; van der Mei, H. C.; Norde, W.; Busscher, H. J., Adsorption of Pluronic F-127 on Surfaces with Different Hydrophobicities Probed by Quartz Crystal Microbalance with Dissipation *Langmuir* **2009**, *25*, 6245-6249.

(216) Delamarche, E.; Donzel, C.; Kamounah, F. S.; Wolf, H.; Geissler, M.; Stutz, R.; Schmidt-Winkel, P.; Michel, B.; Mathieu, H. J.; Schaumburg, K., Microcontact printing using poly(dimethylsiloxane) stamps hydrophilized by poly(ethylene oxide) silanes *Langmuir* **2003**, *19*, 8749-8758.

(217) Stevens, M. M.; Mayer, M.; Anderson, D. G.; Weibel, D. B.; Whitesides, G. M.; Langer, R., Direct patterning of mammalian cells onto porous tissue engineering substrates using agarose stamps *Biomaterials* **2005**, *26*, 7636-7641.

(218) Miller, M. C.; Nesmelova, I. V.; Platt, D.; Klyosov, A.; Mayo, K. H., The carbohydrate-binding domain on galectin-1 is more extensive for a complex glycan than for simple saccharides: implications for galectin-glycan interactions at the cell surface *Biochemical Journal* **2009**, *421*, 211-221.

(219) Smith, C. G.; Hinman, J. W., Chloramphenicol *Progress in industrial microbiology* **1963**, *4*, 137-63.

(220) Shaw, W. V., Chloramphenicol acetyltransferase - Enzymology and molecular-biology *Crc Critical Reviews in Biochemistry* **1983**, *14*, 1-46.

(221) Erlich, H. A.; Gelfand, D.; Sninsky, J. J., Recent advances in the polymerase chain-reaction *Science* **1991**, *252*, 1643-1651.

(222) Jackson, D. P.; Payne, J.; Bell, S.; Lewis, F. A.; Taylor, G. R.; Peel, K. R.; Sutton, J.; Quirke, P., Extraction of DNA from exfoliative cytology specimens and its suitability for analysis by the polymerase chain reaction *Cytopathology : official journal of the British Society for Clinical Cytology* **1990**, *1*, 87-96.

(223) Close, T. J.; Rodriguez, R. L., Construction and characterization of the chloramphenicol-resistance gene cartridge: A new approach to the transcriptional mapping of extrachromosomal elements *Gene* **1982**, *20*, 305-316.

(224) Martinez, E.; Bartolome, B.; Delacruz, F., PACYC 184-derived cloning vectors containing the multiple cloning site and LACZ-ALPHA reporter gene of PUC 18/19 plasmids *Gene* **1988**, *68*, 159-162.

(225) Chen, I.; Christie, P. J.; Dubnau, D., The ins and outs of DNA transfer in bacteria *Science* **2005**, *310*, 1456-1460.

(226) Lee, D. J.; Bingle, L. E. H.; Heurlier, K.; Pallen, M. J.; Penn, C. W.; Busby, S. J. W.; Hobman, J. L., Gene doctoring: a method for recombineering in laboratory and pathogenic *Escherichia coli* strains *Bmc Microbiology* **2009**, *9*.

(227) Datsenko, K. A.; Wanner, B. L., One-step inactivation of chromosomal genes in *Escherichia coli* K-12 using PCR products *Proceedings of the National Academy of Sciences of the United States of America* **2000**, *97*, 6640-6645.

(228) Dower, W. J.; Miller, J. F.; Ragsdale, C. W., High-efficiency transformation of *Escherichia-coli* by high-voltage electroporation *Nucleic Acids Research* **1988**, *16*, 6127-6145.

(229) Grainger, D. C.; Lee, D. J.; Busby, S. J. W., Direct methods for studying transcription regulatory proteins and RNA polymerase in bacteria *Current Opinion in Microbiology* **2009**, *12*, 531-535.

(230) Pagnot, T.; Barchiesi, D.; VanLabeke, D.; Pieralli, C., Use of a scanning near-field optical microscope architecture to study fluorescence and energy transfer near a metal *Optics Letters* **1997**, *22*, 120-122.

(231) Nilsson, L. M.; Thomas, W. E.; Trintchina, E.; Vogel, V.; Sokurenko, E. V., Catch bond-mediated adhesion without a shear threshold - Trimannose versus monomannose interactions with the FimH adhesin of *Escherichia coli Journal of Biological Chemistry* **2006**, *281*, 16656-16663.

(232) Kang, J.; Rowntree, P. A., Gold film surface preparation for self-assembled monolayer studies *Langmuir* **2007**, *23*, 509-516.

(233) Lee, D.; Bingle, L.; Heurlier, K.; Pallen, M.; Penn, C.; Busby, S.; Hobman, J., Gene doctoring: a method for recombineering in laboratory and pathogenic *Escherichia coli* strains *Bmc Microbiology* **2009**, *9*, 252.

(234) Kim, J.; Seo, S. Y., Optimization for electroporation of *Escherichia coli Korean Journal of Genetics* **1996**, *18*, 275-283.